

# tekstilec

4/2023 • vol. 66 • 249–350

ISSN 0351-3386 (tiskano/printed)

ISSN 2350 - 3696 (elektronsko/online)

UDK 677 + 687 (05)



Univerza v Ljubljani  
Naravoslovnolehniška fakulteta





<http://www.tekstilec.si>

Časopisni svet/*Publishing Council*

**Barbara Simončič**, predsednica/*President*

**Katja Burger**, Univerza v Ljubljani

**Manja Kurečič**, Univerza v Mariboru

**Tatjana Kreže**, Univerza v Mariboru

**Gašper Lesjak**, Predilnica Litija, d. o. o.

**Nataša Peršuh**, Univerza v Ljubljani

**Petra Prebil Bašin**, Gospodarska zbornica Slovenije

**Melita Rebič**, Odeja, d. o. o.

**Tatjana Rijavec**, Univerza v Ljubljani

**Zoran Stjepanović**, Maribor, SI

**Helena Zidarič Kožar**, Inplet pletiva, d. o. o.

**Vera Žlabravec**, Predilnica Litija, d. o. o.

Glavna in odgovorna urednica/*Editor-in-Chief*

*Editor-in-Chief*

**Tatjana Rijavec**

Namestnica glavne in odgovorne

urednice/*Assistant Editor*

**Tatjana Kreže**

Področni uredniki/*Associate Editors*

**Matejka Bizjak**, **Katja Burger**, **Andrej Demšar**,

**Mateja Kos Koklič**, **Alenka Pavko Čuden**,

**Andreja Rudolf**, **Barbara Simončič**, **Dunja**

**Šajn Gorjanc**, **Sonja Šterman**, **Brigita Tomšič**

Izvršna urednica za podatkovne baze/*Executive Editor for Databases*

*Executive Editor for Databases*

**Irena Sajovic**

Mednarodni uredniški odbor/*International Editorial Board*

*International Editorial Board*

Arun Aneja, Greenville, US

Andrea Ehrmann, Bielefeld, DE

Aleš Hladnik, Ljubljana, SI

Petra Forte Tavčer, Ljubljana, SI

Darinka Fakin, Maribor, SI

Jelka Geršak, Maribor, SI

Karl Gotlih, Maribor, SI

Memon Hafeezullah, Shanghai, CN

Abu Naser Md. Ahsanul Haque, Daka, BD;

Geelong, AU

Ilda Kazani, Tirana, AL

Svjetlana Janjić, Banja Luka, BA

Igor Jordanov, Skopje, MK

Petra Komarkova, Liberec, CZ

Mirjana Kostić, Beograd, RS

Manja Kurečič, Maribor, SI

Rimvydas Milasius, Kaunas, LT

Olga Paraska, Khmelnytskyi, UA

Irena Petrinić, Maribor, SI

Željko Penava, Zagreb, HR

Tanja Pušić, Zagreb, HR

Zenun Skenderi, Zagreb, HR

Snežana Stanković, Beograd, RS

Jovan Stepanović, Leskovac, RS

Zoran Stjepanović, Maribor, SI

Simona Strnad, Maribor, SI

Jani Toroš, Ljubljana, SI

Mariana Ursache, Iai, RO

Antoneta Tomljenović, Zagreb, HR

Dušan Trajković, Leskovac, RS

Hidekazu Yasunaga, Kyoto, JP

**tekstilec** (ISSN: 0351-3386 tiskano, 2350-3696 elektronsko) je znanstvena revija, ki podaja temeljne in aplikativne znanstvene informacije v fizikalni, kemijski in tehnološki znanosti, vezani na tekstilno in oblačilno tehnologijo, oblikovanje in trženje tekstilij in oblačil. V prilogah so v slovenskem jeziku objavljeni strokovni članki in prispevki o novostih v tekstilni tehnologiji iz Slovenije in sveta, prispevki s področja oblikovanja tekstilij in oblačil, informacije o raziskovalnih projektih ipd.

**tekstilec** (ISSN: 0351-3386 printed, 2350-3696 online) the scientific journal gives fundamental and applied scientific information in the physical, chemical and engineering sciences related to the textile and clothing industry, design and marketing. In the appendices written in Slovene language, are published technical and short articles about the textile-technology novelties from Slovenia and the world, articles on textile and clothing design, information about research projects etc.

Dosegljivo na svetovnem spletu/*Available Online at*  
[www.tekstilec.si](http://www.tekstilec.si)



Tekstilec je indeksiran v naslednjih bazah/*Tekstilec is indexed in*  
**Emerging Sources Citation Index – ESCI (by Clarivate Analytics) za 2022: Journal Impact Factor (JIF): 0.7; Journal Citation Indicator (JCI): 0.25**  
**Leiden University's Center for Science & Technology Studies: 2021: SNIP 0.777**  
**SCOPUS/Elsevier za 2022: Q3, SJR 0.2, Cite Score 1.8, H Index 14**  
Ei Compendex  
DOAJ  
WTI Frankfurt/TEMA® Technology and Management/TOGA® Textile Database  
World Textiles/EBSCO Information Services  
Textile Technology Complete/EBSCO Information Services  
Textile Technology Index/EBSCO Information Services  
Chemical Abstracts/ACS  
ULRICHWEB – global serials directory  
LIBRARY OF THE TECHNICAL UNIVERSITY OF LODZ  
dLIB  
**SICRIS: 1A3 (Z, A', A1/2); Scopus (d)**

# tekstilec

## Ustanovitelj / Founded by

- Zveza inženirjev in tehnikov tekstilcev Slovenije /  
*Association of Slovene Textile Engineers and Technicians*
- Gospodarska zbornica Slovenije – Združenje za tekstilno,  
oblačilno in usnjarsko predelovalno industrijo /  
*Chamber of Commerce and Industry of Slovenia – Textiles,  
Clothing and Leather Processing Association*

## Revijo sofinancirajo / Journal is Financially Supported

- Javna agencija za raziskovalno dejavnost Republike Slovenije /  
*Slovenian Research Agency*
- Univerza v Ljubljani, Naravoslovnotehniška fakulteta /  
*University of Ljubljana, Faculty of Natural Sciences and Engineering*
- Univerza v Mariboru, Fakulteta za strojništvo /  
*University of Maribor, Faculty for Mechanical Engineering*

## Sponsor / Sponsor

Predilnica Litija, d. o. o.

## Izdajatelj / Publisher

Univerza v Ljubljani, Naravoslovnotehniška fakulteta /  
*University of Ljubljana, Faculty of Natural Sciences and Engineering*

Revija Tekstilec izhaja šestkrat letno  
(štirje znanstveni zvezki in dve strokovni prilogi)

*Journal Tekstilec appears six times a year (four  
scientific issues and two professional supplements)*

Revija Tekstilec izhaja pod okriljem Založbe Univerze v Ljubljani /  
*The journal Tekstilec is published by the University of Ljubljana Press*

Revija je pri Ministrstvu za kulturo vpisana v  
razvid medijev pod številko 583.  
Letna naročnina za člane Društev inženirjev in  
tehnikov tekstilcev je vključena v članarino.  
Letna naročnina za posameznike 38 € za  
študente 22 €  
za mala podjetja 90 € za velika podjetja 180 €  
za tujino 110 €

## Naslov uredništva / Editorial Office Address:

Uredništvo Tekstilec, Snežniška 5, SI-1000 Ljubljana  
Tel. / Tel.: + 386 1 200 32 00, +386 1 200 32 24  
Faks / Fax: + 386 1 200 32 70

E-pošta / E-mail: [tekstilec@ntf.uni-lj.si](mailto:tekstilec@ntf.uni-lj.si)

Spletni naslov / Internet page: <http://www.tekstilec.si>;  
<https://journals.uni-lj.si/tekstilec>

Cena posamezne številke 10 €

## Lektor za slovenščino / Slovenian Language Editor

Milojka Mansoor

## Lektor za angleščino / English Language Editor

Glen Champagne, Barbara Luštek Preskar

Na podlagi Zakona o davku na dodano vrednost  
sodi revija Tekstilec med proizvode, od katerih se  
obračunava DDV po stopnji 5 %.

## Oblikovanje platnice / Design of the Cover

Tanja Nuša Kočevar

## Oblikovanje / Design

ENOOKI Kraft, Mitja Knapič s.p.

## Oblikovanje spletnih strani / Website Design

Jure Ahtik

## Imetnik računa / Account holder:

Univerza v Ljubljani,  
Naravoslovnotehniška fakulteta,  
Askerceva 12, 1000 Ljubljana, SI-Slovenija

## Tisk / Printed by

DEMAT d.o.o.

## Transakcijski račun / Bank Account:

SI56 01100-6030708186, Banka Slovenije,  
Slovenska 35, 1000 Ljubljana, SI-Slovenija  
SWIFT / SWIFT Code: BSLJSI2X

## Copyright © 2023 by Univerza v Ljubljani, Naravoslovnotehniška fakulteta,

Oddelek za tekstilstvo, grafiko in oblikovanje

Noben del revije se ne sme reproducirati brez predhodnega pisnega dovoljenja  
izdajatelja / No part of this publication may be reproduced without the prior written  
permission of the publisher.

SCIENTIFIC ARTICLES/

Znanstveni članki

- 252** *M. Saravanan*  
**Casein and Banana Peel-Loaded Bacterial-Resistant Surgical Textiles S kazeinom in bananinim olupkom obdelana tekstilija za dosego protibakterijske aktivnosti za medicinske namene**
- 263** *Jan Lukas Storck, Bjarte Alexander Feldmann, Johannes Fiedler, Yordan Kyosev*  
**Numerical Optimization of Polygon Tessellation for Generating Machine-producible Crochet Patterns**  
*Numerična optimizacija teselacije z mnogokotniki za generiranje strojno izdelanih kvačkanih vzorcev*
- 285** *Mohammad Ehsan Momeni Heravi, Mohammad Hossein Moattar*  
**Carpet Back Sizing Quality Assessment by Measuring the Amount of Resin Using Image Processing and Machine Learning Approaches**  
*Ocenjevanje kakovosti utrjevanja hrbtne strani preproge z določanjem količine zamreževala s pomočjo obdelave slik in strojnega učenja*
- 299** *Volodymyr Dvorzhak, Mykola Rubanka, Alla Rubanka, Oleh Polishchuk*  
**Computer Modelling of Yarn Winding on Conical Bobbins**  
*Računalniško modeliranje navijanja preje na stožčaste navitke*
- 307** *Marwa A. Ali, Khaled Mohamed Seddik*  
**Effect of Blending Cotton/Bamboo on UV Protection and Functional Purposes of Trilobal Polyester Microfibers Knitted Fabrics Using Different Structures**  
*Učinek mešanja preje iz bombaža oziroma bambusove viskoze s filamentno prejo iz poliestrskih mikrovlačen s trilobalnim prečnim prerezom na UV-zaščito in funkcionalne lastnosti pletiv različnih struktur*
- 321** *Brigita Tomšič, Nika Savnik, Elena Shapkova, Laura Cimperman, Lara Šoba, Marija Gorjanc, Barbara Simončič*  
**Green In-situ Synthesis of TiO<sub>2</sub> in Combination with *Curcuma longa* for the Tailoring of Multifunctional Cotton Fabric**  
*Zelena in situ sinteza TiO<sub>2</sub> v prisotnosti ekstrakta kurkume za izdelavo večfunkcionalne bombažne tkanine*
- 339** *Arzu Marmarali, Mehmet Sevgi*  
**Study on the Comfort Properties of Knitted Fabrics Produced from Conventional and Sustainable Cotton and Polyester Fibres**  
*Študija udobnosti pletiv, izdelanih iz konvencionalnega in trajnostnega bombaža in poliestrskih vlaken*

M. Saravanan

Department of Textile Technology, Kumaraguru College of Technology, Coimbatore-641049,  
Tamil Nadu, India

---

# Casein and Banana Peel-Loaded Bacterial-Resistant Surgical Textiles

*S kazeinom in bananinim olupkom obdelana tekstilija za dosego protibakterijske aktivnosti za medicinske namene*

**Original scientific article/Izvirni znanstveni članek**

Received/Prispelo 2-2022 • Accepted/Sprejeto 9-2023

Corresponding author/Korespondenčni avtor:

**Dr. M. Saravanan, Assistant Professor**

E-mail: saravanan.m.txt@kct.ac.in

ORCID ID: 0000-0002-1678-8993

---

## Abstract

Today, the need for fabrics that resist the growth of microorganisms is rising rapidly, as bacteria and other microbes are resistant to any clean room environment. In particular, health care and hygiene textile products must be more bacterial resistant. This study thus concentrated on developing antibacterial surgical textile products using eco-friendly material, such as casein and banana peel, which were used to coat fabric using cyclodextrin as a cross-linking agent. In this research work, fabric was treated with banana peel, casein, and a combination of banana peel and casein, without cyclodextrin, while cyclodextrin-loaded fabric treated samples were tested for antimicrobial resistance (AATCC100-2004). The treated samples initially studied using FTIR showed a peak point at  $3,278.99\text{ cm}^{-1}$ , which infers the presence of an O-H group for banana peel extract, and at  $3,340.71\text{ cm}^{-1}$ , which infers the presence of an N-H group for casein. Antimicrobial tests against *E. coli* showed a bacterial reduction of 81.44%, while a reduction of 52.80% was recorded for *S. aureus*. An analysis of untreated and treated samples showed that treatment with extracts of an agent through the pad-dry-cure process did not have a significant effect on the tensile and air permeability characteristics of the samples.

Keywords: banana peel, casein, antibacterial resistance, colony-forming units, natural agents

## Izvleček

V današnjem času potreba po medicinskih in higienskih tekstilijah s protimikrobnim delovanjem izjemno hitro narašča, ker bakterije in drugi mikroorganizmi tudi v aseptičnih prostorih postajajo čedalje bolj odporni. Glede na to je bil namen raziskave razviti protibakterijske tekstilije za medicinske namene z uporabo okolju prijaznega materiala, kot sta kazein in bananin olupke, ki sta bila nanesena na tkanino v kombinaciji s ciklodekstrinom kot zamreževalnim sredstvom. V eksperimentalnem delu so bili vzorci tkanine obdelani z bananinim olupkom, kazeinom, kombinacijo bananinega olupka in kazeina s ciklodekstrinom in brez njega. Protibakterijska aktivnost vzorcev je bila testirana v skladu s standardno metodo AATCC 100-2004. Rezultati analize FTIR obdelanega vzorca so pokazali prisotnost absorpcijskega traku pri  $3278,99\text{ cm}^{-1}$ , ki nakazuje na prisotnost skupine O-H ekstrakta bananinega olupka,

in absorpcijskega traku pri  $3340,71\text{ cm}^{-1}$ , ki nakazuje na prisotnost skupine N-H kazeina. Rezultati protibakterijske aktivnosti so pokazali 81,44-odstotno redukcijo rasti bakterije *E. coli* in 52,80-odstotno redukcijo rasti *S. aureus*. Pri merjava neobdelanih in obdelanih vzorcev je pokazala, da nanos proučevanih sredstev z impregnirnim postopkom nima bistvenega vpliva na natezne lastnosti in zračno prepustnost tkanine.

*Ključne besede:* bananin olupek, kazein, protibakterijska odpornost, število bakterijskih celic, ki na gojišču tvorijo kolonije, naravna sredstva

## 1 Introduction

Currently, natural agents [1–10] are used for multifunctional application [4–12] in many alternate treatments. These natural agents can also be treated in textile substrates for the development of protective, medical and hygienic products. Surgical clothing is mainly classified as reusable and decomposable textiles. In reusable textiles, cotton/cotton-viscose are widely used, and the clothing is laundered and reused. The risk of contamination with bacteria is much higher. On the other hand, disposable textiles solve the problem of contamination to a large extent, but are not eco-friendly. To overcome this problem, cotton woven textile material can be treated with anti-microbial agents and used for several washes with a lower percentage of contamination.

We chose two natural agents, i.e. casein [6–13] and banana peel [10–16], for application on cotton fabric. The work also included cyclodextrin [17–21] as a cross-linking agent to enhance the durability of cotton fabric. These natural agents thus transfer a microbial resistance property to cotton fabric.

## 2 Materials and methods

### 2.1 Materials

Specifications of the fabric used in this study are summarized in Table 1, while basic properties were determined using standard instruments and procedures.

Table 1: Cotton fabric details

Seq. no.	Parameters	Values
1.	Yarn count: warp/weft	16.9 (35 <sup>a</sup> )/21.9 (27 <sup>a</sup> )
2.	Fabric mass (g/m <sup>2</sup> )	100
3.	Warp density (ends/cm)	28.35
4.	Weft density (picks/cm)	24.41
5.	Cover factor	18.91
6.	Stiffness (mgcm)	15.73
7.	Thickness (mm)	0.21

a) Ne, cotton (English)

Peels from ripening green bananas (*Musa sapientum*) were gathered from the local market in Coimbatore, India. Peels were sliced into small pieces after drying for 15 days. Casein (Hi-Media M-Protein, vitamin free) (Precision & Scientific, Coimbatore, India) and  $\beta$ -cyclodextrin with a molecular weight of 1,134.98 g/mol (Sigma-Aldrich, USA) were used in this research work. The above-mentioned natural agents were then extracted using the Soxhlet apparatus method.

### Aqueous extraction of banana peel

A total of 100 g of natural agent, i.e. banana peel (*Musa sapientum*), was taken and placed inside the Soxhlet apparatus in the presence of a universal solvent water for aqueous extraction. The extraction was carried out for 10 siphoning cycles at 40 °C. The obtained extracts were sealed with aluminium foil and refrigerated at 4 °C until required for fabric finishing treatment using the pad-dry-cure process. The prepared fabric samples were then subjected to strength and anti-microbial tests, and Fourier transform infrared spectroscopy (FTIR) analysis.

### Fabric pretreatment and padding process

The fabric was pre-treated using a standard detergent (pH of 7–8) soap solution (10 g/l) at 90 °C with a liquor to material ratio (L:M) of 50:1 for 90 minutes, followed by hot and cold washes (five times each) and drying in ambient conditions.

As seen in Table 2, the pre-treated cotton fabric was padded with an aqueous herbal extract with cyclodextrin (2% on the weight of the material, OWM) and without the aid of cyclodextrin using a laboratory scale padding mangle machine with a working width of 450 mm (manufactured by RB

Electronics, Maharashtra, India) following the padding-drying-curing sequence. A 60% wet pick-up was achieved during padding, followed by drying at 80 °C for five minutes and curing at 120 °C for three minutes. The quantity of herbal extract present in the fabric after drying was tabulated in Table 2 as a percentage of the weight of the material (OWM). The treated samples were then washed under standard wash conditions. Both the treated (unwashed) and washed samples were taken for antibacterial testing. The detailed experimental methodology used in this study is shown in Figure 1.

Table 2: Sample details and percentage of weight add-on (% OWM) after the pad-dry-cure process

Sample no.	Peel : casein ratio (%)	OMW <sup>a)</sup> (%)	Cyclodextrin in solution (%)	OWM after PDPCP <sup>b)</sup> (%)
1	10 : 90	5	0	4
2	10 : 90	10	0	8
3	10 : 90	5	2	4
4	10 : 90	10	2	9.5
5	25 : 75	5	0	4.5
6	25 : 75	10	0	7
7	25 : 75	5	2	5
8	25 : 75	10	2	9
9	50 : 50	5	0	3.5
10	50 : 50	10	0	7.5
11	50 : 50	5	2	4.5
12	50 : 50	10	2	10
13	75 : 25	5	0	4
14	75 : 25	10	0	9
15	75 : 25	5	2	5
16	75 : 25	10	2	9
17	90 : 10	5	0	3.5
18	90 : 10	10	0	8.5
19	90 : 10	5	2	6
20	90 : 10	10	2	9
21	100 : 0	5	0	5
22	100 : 0	10	0	9.5
23	100 : 0	5	2	5.5
24	100 : 0	10	2	9
25	0 : 100	5	0	5
26	0 : 100	10	0	9
27	0 : 100	5	2	4.5
28	0 : 100	10	2	10
29	0 : 0	0	0	0

a) On the weight of the material; b) Weight add-on of the material after the pad-dry-cure process

## 2.2 Methodology

Figure 1 illustrates the methodology used in the experiment.

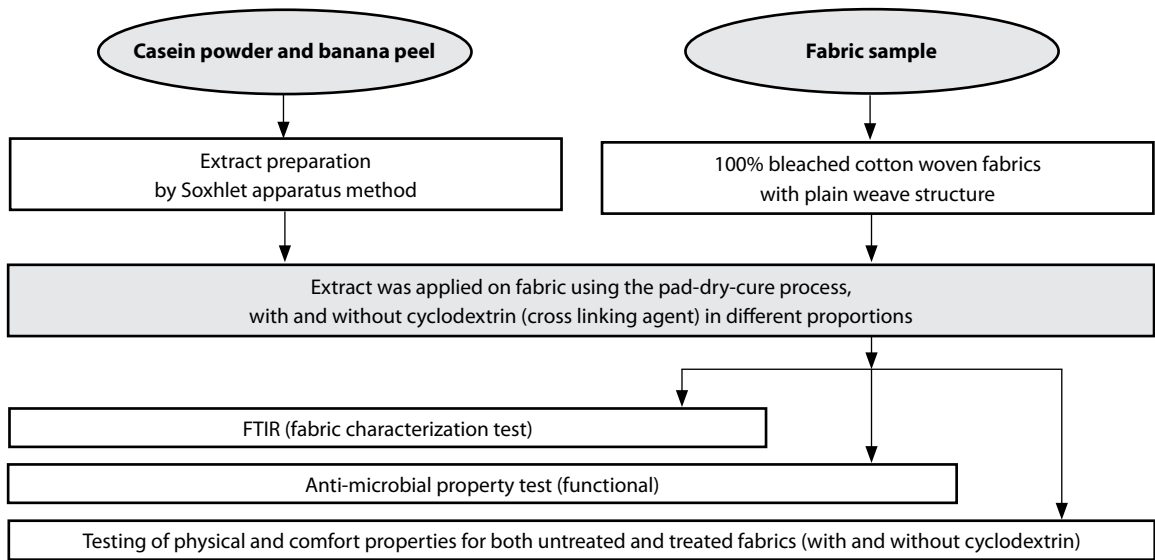


Figure 1: Methodology chart

## 2.3 Testing methods

### Testing of anti-microbial activity

The cotton samples, both coated and untreated, were put in separate glass jars in accordance with the AATCC 100 [22] test methodology, and 1 ml of test bacterial inoculum was added. The jars were shaken vigorously 10 times after being diluted with distilled water. Following serial dilution, the solution was plated on nutrient agar and incubated for 24 hours at 37.2 °C. The number of colony-forming units (CFU) was determined by counting the colonies. This result determined the number of colonies in the zero contact period. A similar procedure was carried out for an 18 hour contact period of cotton and bacteria, and the number of colonies were counted. In order to determine the percentage reduction of bacteria (R) (equation 1), colonies of bacteria recovered on the agar plate for both untreated and treated materials were counted before and after washing.

$$R = \frac{(B-A)}{B} \times 100 (\%) \quad (1)$$

where B represents the number of bacterial colonies from the untreated control specimen after

inoculation at zero contact time and A represents the number of bacterial colonies from the treated specimen after inoculation throughout an 18 hour contact period.

### Wash fastness test

The AATCC 124 [23] test methodology, proposed in literature reference [24], was used to perform the wash fastness test. The test results indicated the bio efficacy of the bound chitosan to cotton fabrics and the number of washes it can withstand in the textile.

The treated fabrics were washed using an AATCC standard reference detergent without a bleaching agent in accordance with the AATCC 124 test methodology [23], as presented in Table 3, to determine how long the antibacterial effect would last. Five normal, careful hand washings at a temperature of 40 °C ± 3 °C were equivalent to one cycle of washing using this method. All of the treated samples underwent three consecutive cycles of washing. The samples were rinsed with warm water at the conclusion of the third cycle, allowed to air dry, and then tested for antibacterial activity using the AATCC 100 methodology [22] (mentioned above).

Table 3: Washing conditions AATCC 124 test methodology

Details	Conditions
Cycle	Normal/sturdy cotton
Wash water temperature (°C)	60 ± 3
Rinse water temperature (°C)	< 29
Water level (l)	68.14 ± 3.785
Agitation speed (rotations/min)	179 ± 2
Wash time (min)	12
Spin speed (rotations/min)	630–660
Final spin cycle (min)	6

#### Fourier transform infrared spectroscopy (FTIR)

A Fourier transform infrared spectrometer (Shimadzu, Japan) was used. An FTIR spectrogram was obtained at a spectral range of 4000–400 cm<sup>-1</sup> at a resolution of 0.9–1 cm.

#### Physical and comfort properties of fabrics

The physical and comfort properties of 100% cotton

woven fabrics, such as the thickness [25], tensile properties (ASTM D 5035) [26], air permeability (ASTM D737) [27], wickability [28] and wettability [29] of both untreated and treated samples were evaluated using standard testing procedures and equipment after conditioning the samples at 65% relative humidity and 27 °C ± 1 °C for 24 hours to bring them to approximate moisture equilibrium in standard atmospheric conditions for preconditioning textile as directed by ASTM D 1776 in an environmental chamber [30].

### 3 Results and discussion

#### 3.1 Antimicrobial test

An antimicrobial test applying the AATCC 100 [22] standard was performed for two strains, i.e. *E. coli* and *S. aureus*. The results obtained are presented below in Figure 2 and Table 4.

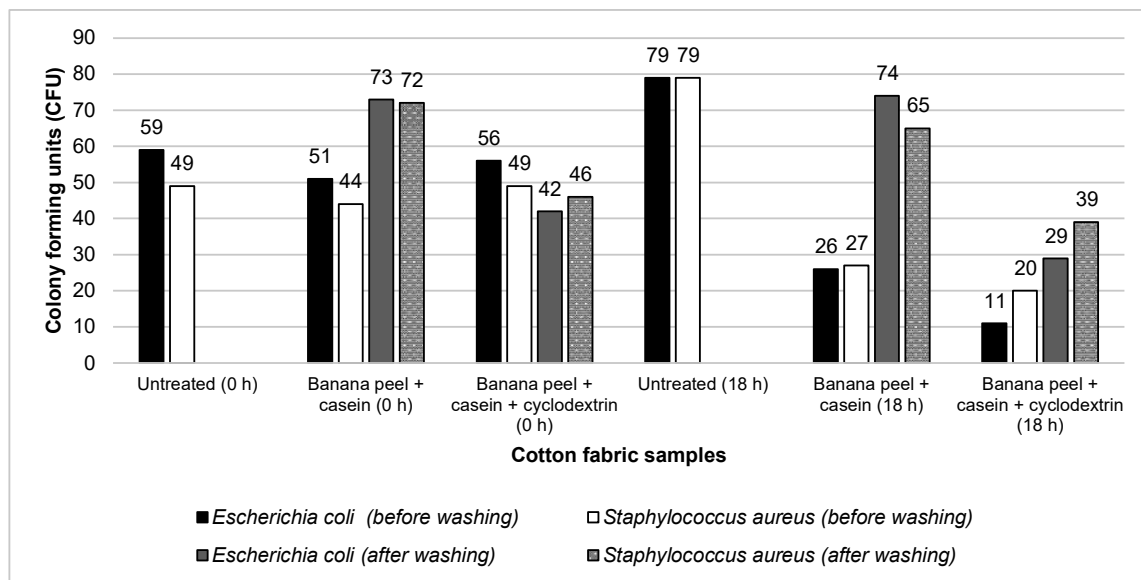


Figure 2: Growth of tested bacteria on treated and washed samples

Table 4: Growth rate of the tested bacteria on the samples

Bacteria	Washing	Fabric	Time (h)	Number of colonies					
				10 <sup>-2</sup>	10 <sup>-3</sup>	10 <sup>-4</sup>	10 <sup>-5</sup>	10 <sup>-6</sup>	10 <sup>-7</sup>
<i>Escherichia coli</i>	No	Untreated CO	0	TNTC	TNTC	TNTC	92	59	46
			18	TNTC	TNTC	TNTC	TNTC	79	53
		Banana peel- and casein-treated CO	0	TNTC	TNTC	TNTC	89	51	43
			18	82	71	57	40	26	14
		Banana peel-, casein- and cyclodextrin-treated CO	0	TNTC	TNTC	TNTC	94	56	39
			18	64	43	32	19	11	7
<i>Staphylococcus aureus</i>	No	Untreated CO	0	TNTC	TNTC	TNTC	81	49	30
			18	TNTC	TNTC	TNTC	TNTC	79	53
		Banana peel- and casein-treated CO	0	TNTC	TNTC	TNTC	74	44	21
			18	117	84	69	44	27	16
		Banana peel-, casein- and cyclodextrin-treated CO	0	TNTC	TNTC	TNTC	68	49	29
			18	97	78	56	34	20	11
<i>Escherichia coli</i>	After first washing	Banana peel- and casein-treated CO	0	TNTC	TNTC	TNTC	109	73	59
			18	TNTC	TNTC	89	60	42	29
		Banana peel-, casein- and cyclodextrin-treated CO	0	TNTC	TNTC	TNTC	123	74	46
			18	TNTC	TNTC	79	47	29	18
<i>Staphylococcus aureus</i>	After first washing	Banana peel- and casein-treated CO	0	TNTC	TNTC	TNTC	98	72	46
			18	TNTC	TNTC	TNTC	69	46	29
		Banana peel-, casein- and cyclodextrin-treated CO	0	TNTC	TNTC	TNTC	93	65	51
			18	TNTC	TNTC	TNTC	61	39	27

Table 5: Overall performance on treated material and washed material

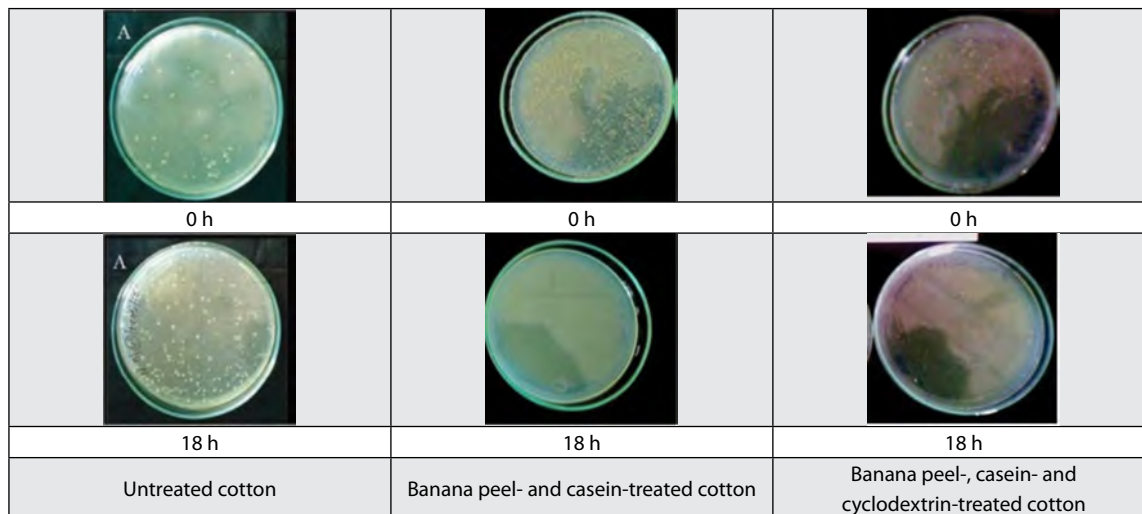
Seq. no.	Bacteria	Sample description	Washing specification	Bacterial growth reduction (10 <sup>-7</sup> inoculation) (%)
1.	<i>Escherichia coli</i>	Untreated	×	-15.21
2.	<i>Escherichia coli</i>	Banana peel and casein	×	67.44
3.	<i>Escherichia coli</i>	Banana peel, casein and cyclodextrin	×	82.05
4.	<i>Staphylococcus aureus</i>	Untreated	×	-76.66
5.	<i>Staphylococcus aureus</i>	Banana peel and casein	×	23.8
6.	<i>Staphylococcus aureus</i>	Banana peel, casein and cyclodextrin	×	62.06
7.	<i>Escherichia coli</i>	Banana peel and casein	✓	50.84
8.	<i>Escherichia coli</i>	Banana peel, casein and cyclodextrin	✓	60.86
9.	<i>Staphylococcus aureus</i>	Banana peel and casein	✓	36.95
10.	<i>Staphylococcus aureus</i>	Banana peel, casein and cyclodextrin	✓	47.05

Positive and negative values in bacterial growth reduction indicate that the inoculation of serial dilution effectiveness, i.e. at zero hours and at 18 hours of serial dilution of inoculates; if the CFU value (number of colonies) at 18 hours exceeds the CFU value at 0 hours, the resultant bacterial growth reduction

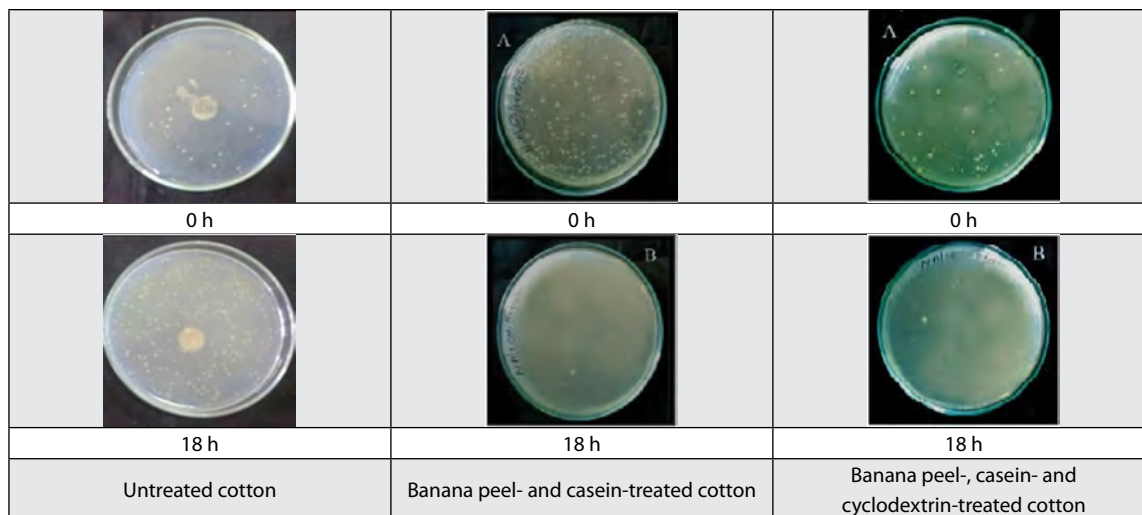
is negative, otherwise the bacterial growth reduction value will be positive. A positive value indicates that the bacteria multiplication factor fell sharply, while a negative value indicates the bacteria multiplied in increasing rather than decreasing order. Thus, an additional dilution might be needed for evaluation.

It is evident from Table 5 and Figures 3 and 4 that the treated and washed samples have traces of the applied natural extracts, which helps explain why the tested samples demonstrated antibacterial activity against both strains of *E. coli* and *S. aureus*.

$\beta$ -cyclodextrins used as cross-linking agent acted as a reservoir in treated samples and leached key components of applied natural extracts after each washing cycles to contribute to the antibacterial activity of treated samples.

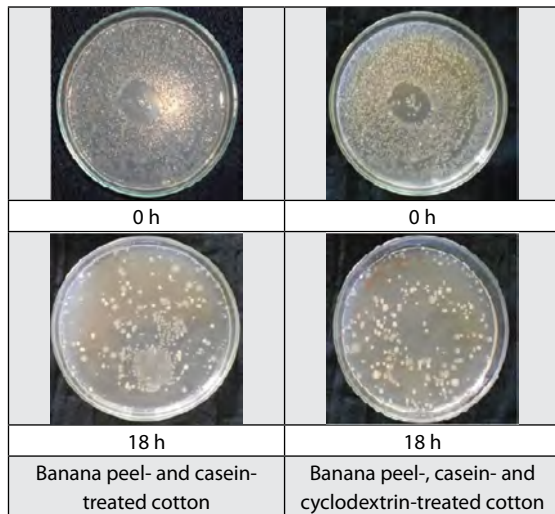


a) Antimicrobial activity against *Escherichia coli* (without washing)

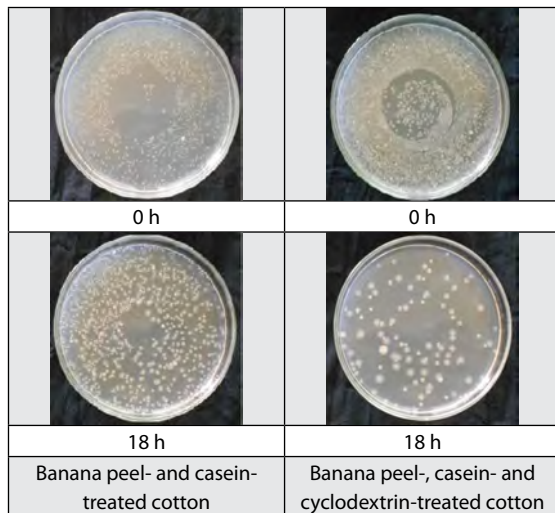


b) Antimicrobial activity against *Staphylococcus aureus* (without washing)

Figure 3: Antimicrobial activity of untreated and treated cotton (without washing)



a) Antimicrobial activity against *Escherichia coli* (first wash)



b) Antimicrobial activity against *Staphylococcus aureus* (first wash)

Figure 4: Antimicrobial activity of the treated cotton (after washing)

### 3.3 FTIR

FTIR curves were obtained and the wavelength in each individual FTIR of extracts applied fabric sample infers that the natural agents became affixed to the fabric during the pad-dry-cure process. The treated sample characterized by FTIR showed distinguished peak point at various wavelengths, notably at  $3,278.99\text{ cm}^{-1}$  and  $3,340.71\text{ cm}^{-1}$ . It is evident from

Figures 5 and 6 that the peak point is achieved at  $3,348.42\text{ cm}^{-1}$ , which infer the presence of an N-H group of amines for casein, while the peak point at  $3,217.27\text{ cm}^{-1}$  infer the presence of an O-H group of phenols for banana peel.

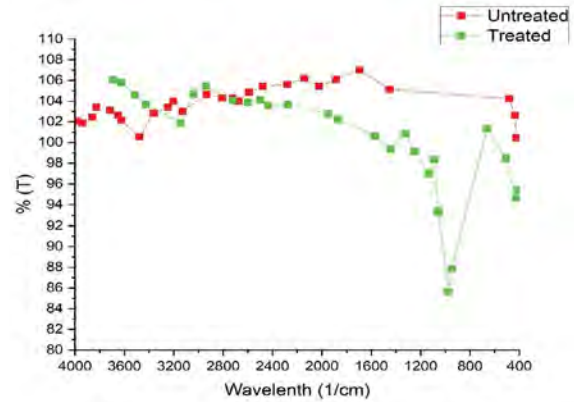


Figure 5: FTIR graph of untreated and banana peel-casein combination treated fabrics

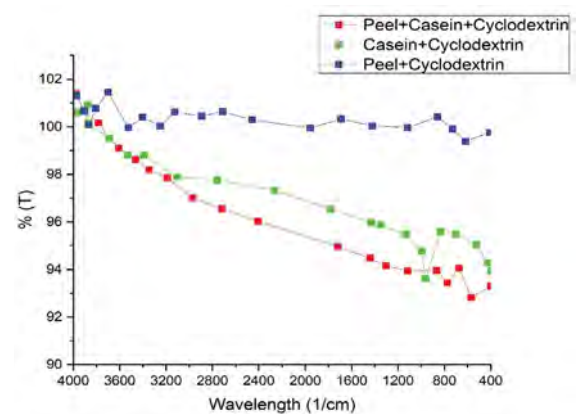


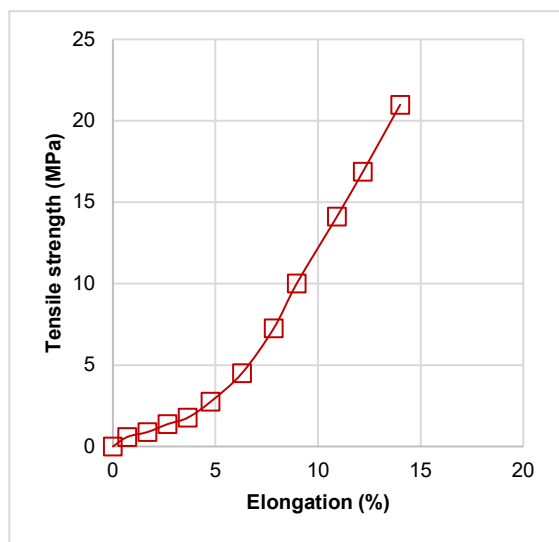
Figure 6: FTIR graph of untreated and treated fabrics (banana peel-casein combination with cyclodextrin)

Figures 5 and 6 illustrate FTIR curves, and an analysis of those curves shows that the following points can be observed in a precise manner: the peaks at  $3,348.42\text{ cm}^{-1}$  and  $2,785.21\text{ cm}^{-1}$  are due the O-H stretching vibration of primary alcoholic groups in glucose units and the C-H stretching vibration of residual wax, respectively, which are present in the untreated cotton fabric. In the case of banana-peel extract and casein-finished materials, peaks at  $1,366.60\text{ cm}^{-1}$ ,  $3,278.99\text{ cm}^{-1}$ , and  $3,340.71\text{ cm}^{-1}$  can be

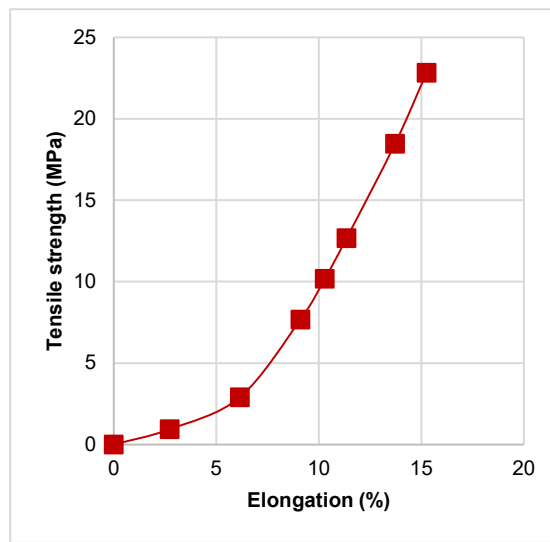
attributed to the O-H bending of active phenolic content of banana peels and N-H stretching of amines in casein, respectively. To summarize, FTIR analyses revealed the presence of the key chemical component of both banana peel and casein on treated samples at peak wavelengths of  $3,278.99\text{ cm}^{-1}$  (phenolic group) and  $3,340.71\text{ cm}^{-1}$  (amines group), respectively.

### 3.4 Instron tensile strength tester

When comparing untreated sample and treated sample strength, as presented in Figures 7 and 8, it can be inferred that there is an increase in tensile strength characteristic of 9.08% with respect to individual evaluations of the tensile strength of untreated samples of 21.31 MPa and the tensile strength of treated sample of 23.24 MPa.



a) Untreated fabric sample



b) Treated fabric sample

Figure 7: Tensile trend of untreated fabric and treated (combination of peel, casein and cyclodextrin) fabrics

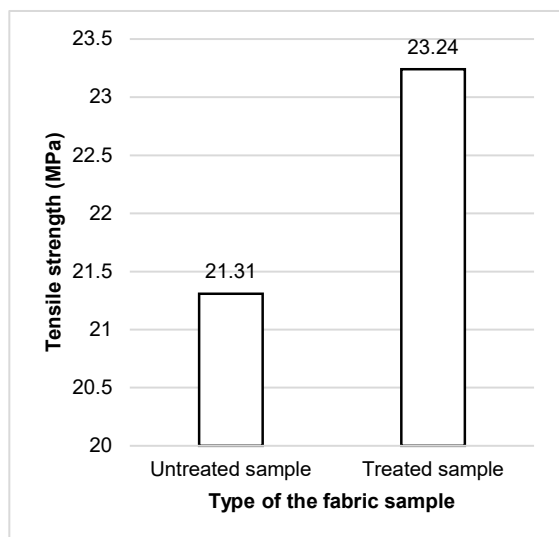


Figure 8: Tensile strength of untreated fabric and treated fabrics

### 3.5 Air permeability

The air permeability of untreated samples was  $16.3\text{ cm}^3\text{cm}^{-2}\text{s}^{-1}$  (rotometer reading of 590 litre/cm<sup>3</sup>), while the air permeability of treated samples was  $15.5\text{ cm}^3\text{cm}^{-2}\text{s}^{-1}$  (rotometer reading of 560 litre/cm<sup>3</sup>). Thus, the permeability value of treated samples was slightly lower due to the application of natural agents. This clearly indicates, however, that comfort aspects do not under go significant changes due to the finishing process.

## 4 Conclusion

The study resulted in the following important conclusions:

- From the physical properties of control (untreated and treated samples), it can be concluded that treatments with the extracts of a natural agent through the pad-dry-cure process did not have a significant effect on physical properties, such as air permeability, wettability and wickability.
- Antibacterial activity showed that the natural agents of banana peel and casein extracts demonstrated a satisfactory and good activity against bacteria, such as *Escherichia coli* and *Staphylococcus aureus*.
- Both the properties investigated in the study were well-supported by the cross-linking agent  $\beta$ -cyclodextrin in the form retention of both agents, and responded well, even after the treated sample were washed applying standard washing procedures
- The development of natural agent-finished garments was designed especially for medical textiles, such as face masks and surgical gowns.

## References

1. MOKBEL, M.S., HASHINAGA, F. Antibacterial and antioxidant activities of banana (*Musa*, AAA cv. Cavendish) fruits peel. *American Journal of Biochemistry and Biotechnology*, 2005, **1**(3), 125–131, doi:10.3844/ajbbsp.2005.125.131.
2. SINGH, C.R., KATHIRESAN, K., BOOPATHY, N.S., ANANDHAN, S., GOVINDAN, T. Evaluation of microbial potential of different colored banana peels. *International Journal of Preclinical & Pharmaceutical Research*, 2013, **4**(2), 62–64.
3. SARAVANAN, M., BHAARATHI, D. Necessity of a safe antibacterial finish for kitchen textiles. *Ecology Environment and Conservation*, 2018, **24**, 400–404.
4. KUMAR, K.P.S., BHOWMIK, D., DURAIVEL, S., UMADEVI, M. Traditional and medicinal uses of banana. *Journal of Pharmacognosy and Phytochemistry*, 2012, **1**(3), 51–63.
5. SARAVANAN, M. Herbals in home textiles. *Colourage*, 2014, **61**(12), 92–95.
6. TAHA, F.T., ELSAADANY, S.S., ABO-EYTA, A.M., WAHDAN, K.M.M. Proximate compositions, phytochemical constituents and antimicrobial activities of peels extracts of bitter orange and banana, *Zagazig Journal of Agricultural Biochemistry and its Application*, 2015, **42**(6), 1–9.
7. SARAVANAN, M. A study on the influence of natural agents on the absorption properties of cotton fabrics – part 1. *Journal of Testing and Evaluation*, 2022, **50**(4), 1994–2008, doi: 10.1520/JTE20210740.
8. ALSULA, K.C.L., BULLECER, L.A.A., CALO, R.C.M., CLAROS, M.M., LOMONGO, R.F.O., MAMA, N.M.M. Antibacterial properties of cavendish banana peel (yellow and green) on pathogens *Escherichia coli* and *Staphylococcus aureus*. *Asian Scientific Journals*, 2013, **1**(1), 1521–1532.
9. SARAVANAN, M. Effect of natural agents on the mechanical and flame retardant properties of cotton fabric – dyeing technique. *Journal of Testing and Evaluation*, 2022, **50**(4), 2009–2020, doi: 10.1520/JTE20210773.
10. HELLEMANS, Alexander. Milk proteins protect fabrics from fire. *Chemical & Engineering News*, March 11, 2014. [accessed 29. 9. 2023]. Available on World Wide Web: <<https://cen.acs.org/articles/92/web/2014/03/Milk-Proteins-Protect-Fabrics-Fire.html>>.
11. PHADUNGATH, C. Casein micelle structure: a concise review. *Songklanakarin Journal of Science and Technology*, 2005, **27**(1), 201–212.
12. SARAVANAN, M. An attempt to develop antibacterial fabric for foodborne bacteria. *Journal of Testing and Evaluation*, 2022, **50**(3), 1278–1285, doi: 10.1520/JTE20210377.
13. MOHANTY, D., MOHAPATRA, S., MISRA, S., SAHU, P. Milk derived bioactive peptides

- and their impact on human health – a review. *Saudi Journal of Biological Sciences*, 2015, **23**(5), 577–583, doi: 10.1016/j.sjbs.2015.06.005.
14. HOFFMAN J.R., FALVO M.J. Protein – Which is best? *Journal of Sports and Science and Medicine*, 2004, **3**(3), 118–130.
  15. SARAVANAN, M., BHAARATHI, D., PRISCILLA, S. Development of a safe antibacterial finish for kitchen fabric. *Asian Dyer*, 2016, **13**(1), 47–54.
  16. BHASKARA-AMRIT, U.R., AGRAWAL, P.B., WARMOESKERKEN, M.M.C.G. Applications of  $\beta$ -cyclodextrins in textiles. *AUTEX Research Journal*, 2011, **11**(4), 94–101.
  17. SUNDRARAJAN, S., RUKMANI, A. Durable antibacterial finishing on organic cotton by inclusion of thymol into cyclodextrin derivative. *Journal of Chemistry*, 2012, **9**(3), 1511–1517, doi: 10.1155/2012/863674.
  18. SARAVANAN, M. A study on the influence of natural agents on the absorption properties of cotton fabrics – part two. *Journal of Testing and Evaluation*, 2022, **50**(4), 1994–2008, doi: 10.1520/JTE20210741.
  19. HASHEM, M., EL-AREF, A.T., REFAIE, R. Cotton fabric bearing cationic and  $\beta$ -cyclodextrin moieties: a study of the reaction parameters. *Research Journal of Textile and Apparel*, 2004, **8**(2), 76–94, doi: 10.1108/RJTA-08-02-2004-B010.
  20. BEDNARZ, S., LUKASIEWICZ, M., MAZELA, W., PAJDA, M., FOKS, S.K.S., GARLICKA, A., KABZINSKI, M., KACZMARCZYK, K. Processes of cyclodextrins grafting on cotton. In *11th International Electronic Conference on Synthetic Organic Chemistry (ECSOC-11)*, 2007, 1–30, doi: 10.3390/ecsoc-11-01355.
  21. SARAVANAN, M. Development of *Thespesia populnea* doped PVA electrospun mat for biocompatibility studies. *Journal of Natural Fibres*, 2022, **19**(5), 1951–1961, doi: 10.1080/15440478.2021.2002773.
  22. AATCC 100-2004. Antibacterial finishes on textile materials: assessment of developed from American Association of Textile Chemists and Colorists. AATCC Test Method: AATCC 2004.
  23. AATCC 124-1996. Smoothness appearance of fabrics after home laundering. AATCC Test Method: AATCC 1996.
  24. CHUN, D. T. W., GAMBLE, G. R. Using the reactive dye method to covalently attach antibacterial compounds to cotton. *Journal of Cotton Science*, 2007, **11**(3), 154–158.
  25. ASTM D1777-1996. Standard test method for thickness of textile materials. ASTM test method: ASTM 1996.
  26. ASTM D5035-1995. Standard test method for breaking force and elongation of textile fabrics (Strip method). ASTM test method: ASTM 1995.
  27. ASTM D737-1996. Standard test method for air permeability of textile fabrics. ASTM test method: ASTM 1996.
  28. AATCC 197-2013. Test method for vertical wicking rate of textiles: to specified distances. AATCC Test Method: AATCC 2013.
  29. ASTM D7334-2008. Standard practice for surface wettability of coatings, substrates and pigments by advancing contact angle measurement. ASTM test method: ASTM 2008.
  30. ASTM D1776/D1776 M-2020. Standard practice for conditioning and testing textiles. ASTM test method: ASTM 2020.

Jan Lukas Storck,<sup>1</sup> Bjarte Alexander Feldmann,<sup>1</sup> Johannes Fiedler,<sup>1</sup> Yordan Kyosev<sup>2</sup>

<sup>1</sup> Hochschule Bielefeld – University of Applied Sciences and Arts, Bielefeld, Faculty of Engineering and Mathematics, Germany

<sup>2</sup> Technische Universität Dresden, Faculty of Mechanical Science and Engineering, Institute of Textile Machinery and High Performance Material Technology, Dresden, Germany

---

# Numerical Optimization of Polygon Tessellation for Generating Machine-producible Crochet Patterns

*Numerična optimizacija teselacije z mnogokotniki za generiranje strojno izdelanih kvačkanih vzorcev*

**Original scientific article/Izvirni znanstveni članek**

Received/Prispelo 8-2023 • Accepted/Sprejeto 9-2023

Corresponding author/Korespondenčni avtor:

**Jan Lukas Storck**

E-mail: jan\_lukas.storck@hsbi.de

ORCID: 0000-0002-6841-8791

---

## Abstract

The automation of current crocheting technology offers many possibilities. To fully exploit this potential, it is necessary to develop not only hardware, but also methods that enable the design of novel machine-crocheted fabrics. In the case of manual crocheting, approaches for an automated generation of crochet patterns according to 3D shapes have already been presented in the literature. However, the most technically advanced crocheting machine prototype currently proposed automates the crocheting of flat fabrics starting from a chain row. Given the limitations and operation of this so-called CroMat crocheting machine, a tool for shaping flat machine-crocheted fabrics according to 2D convex polygons is presented here. With this, surfaces can be divided into crochet stitches using a tessellation process and numerical optimization. The rules of the automated crocheting process were thus followed to ensure the machine manufacturability of generated patterns. Computer models of the fabrics were used as previews. In addition, the shaping possibilities of the CroMat crocheting machine, in particular with respect to increase and decrease stitches, are presented and discussed by means of the tessellation optimization of exemplary polygon shapes. Generally speaking, the algorithm extends the toolbox for designing machine-crocheted fabrics through the automated generation of valid crochet patterns corresponding to input shapes and according to the possibilities of the CroMat crocheting machine prototype.

Keywords: crochet, design, tessellation, crocheting machine, numerical optimization

## Izvleček

Trenutni razvoj avtomatizacije tehnologije kvačkanja ponuja veliko možnosti. Da bi v celoti izkoristili njen potencial, ni potreben le razvoj strojne opreme, temveč tudi metod, ki omogočajo oblikovanje novih strojno kvačkanih tekstilij. Pri ročnem kvačkanju je mogoče oblikovanje tekstilij po tridimenzionalni obliki predmetov. Tehnično najnaprednejši prototip kvačkalnika, ki je trenutno znan iz literature, omogoča le avtomatizirano izdelavo ploskih

kvačkanih tekstilij z verižno začetno vrsto. Glede na omejitve in delovanje kvačkalnika CroMat je bilo razvito orodje za oblikovanje plosko izdelane kvačkane tekstilije z vzorcem dvodimenzionalnih konveksnih mnogokotnikov. Članek predstavlja pristop k razdelitvi površin na kvačkane zanke s postopkom teseliranja in numerično optimizacijo. Pri tem se upoštevajo pravila avtomatiziranega kvačkanja, ki zagotavljajo strojno izdelavo generiranih vzorcev. Za predogled se uporabljajo računalniški modeli kvačkanih tekstilij. Poleg tega so predstavljene in obravnavane možnosti oblikovanja pletiv na kvačkalniku CroMat, zlasti za operacije širjenja in oženja s pomočjo optimizacije teselacije vzorčnih mnogokotnih oblik. Na splošno algoritem razširja nabor orodij za oblikovanje strojno kvačkanih tekstilij z avtomatskim generiranjem izvedljivih kvačkanih vzorcev, ki ustrezajo vnesenim oblikam in izdelavnim možnostim prototipa kvačkalnika CroMat.

*Ključne besede:* kvačkanje, oblikovanje, kvačkalnik, geometrijsko sosledje, raport

## 1 Introduction

The first developments for the automation of the textile technology of crocheting have recently started. A prototype for the flat crocheting of rectangular fabrics [1–3] and a prototype for the circular crocheting of seamless tubes [4] have been presented, while digital methods for designing crocheted textiles have been developed [3, 5–11]. Some already established industrial textile machines are mistakably referred to as crocheting machines, although they are warp knitting machines that can only produce structures similar to crocheting [3, 5, 6]. The machine production of crocheted textiles offers great potential in the replacement of commercial crocheted products, which have thus far been produced exclusively by hand under poor working conditions [3, 4]. Moreover, automation will enable the use of crocheted fabrics as a novel technology in the field of technical textiles. In this regard, promising applications have already been proposed, such as tissue engineering scaffolds [12], fibrous sound absorbers [13] and textile sensors [14].

Crocheting is similar to knitting but is more difficult to perform by machine because the loops of a new stitch are drawn both vertically and laterally through old stitches (in knitting, they are only drawn vertically) [15, 16]. Additionally, the formation of one stitch must be completed before the next one can be created [5, 6]. Due to crocheting's potential for creating diverse stitches and complex structures,

such as hyperbolic planes, [17, 18] the automation of this technology should give particular attention to shaping possibilities. Increase (INC) and decrease (DEC) are the fundamental shaping methods used in crocheting to change the number of stitches in one course (fabric row) in flat crocheting or in one round in circular crocheting [4–6].

Perry et al. [4] were the first to present an approach for the creation of crocheted INC and DEC using a circular crocheting machine (called Croche-Matic) based on a magic ring and crocheting in spirals, which is a crocheting technology with similarities to circular knitting. On account of its mechatronic design, chain stitches (CH) and single crochet stitches (SC) can be automatically created. However, the Croche-Matic prototype has encountered major reproducibility problems due to its 50.7% success rate in terms of stitch completion [4].

The first prototype for automating the crocheting of flat rectangular fabrics, through crocheting slip stitches (SL) in courses with alternating directions based on a chain row, was presented back in 2019 [2]. This likewise mechatronic prototype was further developed independently of Croche-Matic and can now produce half double crochet stitches (HDCs) for the first time, in addition to previously automated CHs, SL and SCs [3]. On account of the suitable suspension of crocheted stitches, no serious limitations of reproducibility occur, such those reported by Perry et al. Together with this approach, referred to as CroMat, the first tool specific to the machine

for designing machine crocheted fabrics, including a modelling preview and a generation of the machine code for manufacturing, was recently proposed [3].

Introduced in this paper is the supplementation of the CroMat with the capability of INC and DEC, and with alternative operations for changing the width of courses. Also presented is an alternative approach for the automated designing of flat-crocheted textiles according to the given shapes of 2D polygons. Producibility by the CroMat of the generated crochet pattern and machine instructions are ensured. This method can thus be used in the future in an industrial context for the rapid design of crocheted textiles, without requiring knowledge of crocheting. In this regard, extended topology-based modelling is beneficial as a preview option.

In terms of control of versatile V-bed knitting machines, there is a trend in research towards high-level programming with shape primitives or 3D objects and automated transfer to knitting patterns, [19, 20] as well as translation to machine commands for production [21–24]. For manually crocheted textiles, similar tools have been presented for the automated generation of textual crocheting instructions based on 2D sketches, which are transferred into 3D shape primitives [7], or based on 3D objects [8, 9]. These breakdowns of geometries into individual stitches in a crochetable sequence relates to the technology of circular crocheting based on a magic ring, which can be used to create 3D structures. In addition, there are some programs for the design of hand-crocheted textiles. These are based on the graphical arrangement of crochet symbols in charts to store patterns and provide no automatic generation of instructions for production [5, 6].

In contrast to these fabric design approaches and in the context of high-level programming, the shapes of 2D geometries are transferred to flat-crocheted patterns based on a chain row. Machine instructions for the crocheting of fabric can be automatically generated from output crochet patterns. The focus on the producibility of the CroMat crocheting machine distinguishes the design approach presented

herein from related manual crocheting approaches. Moreover, the structure of flat-crocheted textiles is different than circular-crocheted textiles, especially in terms of stitch sequence, so that it is necessary to develop a new logic for dividing geometry into stitches. An algorithm for subdividing the 2D polygon according to the rules and restrictions of machine-crocheting with the CroMat is thus proposed, and the possibilities of shaping the fabric are discussed by considering automatically generated crochet models.

### 1.1 Representation of crocheted fabrics

Crocheted fabrics are commonly described by text-based instructions on how to crochet them [5, 6]. Pattern information is given by the sequence of stitches, which are represented by short strings. Standardizations and guidelines are introduced by the Craft Yarn Council [25].

Such a representation is used for the programming of the crocheting machine, and information regarding the structure of the crocheted fabric is stored as short strings for stitches in a two-dimensional array. In such an array, as shown in Figure 1, the arrangement of elements corresponds to the topology of the technical face of an automated crocheted fabric. A stitch position is defined by the course and wale (or row and column) numbers. The bottom row represents the first CH course that was initially manually crocheted to the left, while the second course is crocheted by the machine to the right. INC and DEC each comprise two elements, depending on the stitch type (for example `sl_inc_a` and `sl_inc_b` for INC with SL, or `sc_dec_a` and `sc_dec_b` for DEC with SC). T1 denotes a turn with one CH as the first element of a new course. The first turn after the CH course, with which machine production starts, is called the first lay over (FLO). Such a pattern array with the information about the structure of the crocheted fabric is the output of the developed crochet polygon subdividing algorithm, and input of the topology-based modelling and of the G-code generation.

	['sc_dec_b',	'sc_dec_a',	'sl',	'hdc',	'sc',	't1',	'void'],	5
	['t1',	'sl_inc_a',	'sl_inc_b',	'sl',	'sl',	'sl_dec_a',	'sl_dec_b'],	4
	['void',	'sc',	'sc',	'sc',	'sc_inc_b',	'sc_inc_a',	't1'],	3
	['void',	'flo',	'hdc',	'hdc',	'hdc',	'hdc',	'void'],	2
	['void',	'void',	'ch',	'ch',	'ch',	'ch',	'void']]	1
Wale number	1	2	3	4	5	6	7	Course number

Figure 1: Computer representation in a 2D array with strings for stitches arranged topologically and corresponding to the technical face of an exemplary crocheted fabric

It is also common to represent and visualize crochet patterns graphically with crochet chart symbols, which describe the stitches used and how they are connected [5, 6, 26]. Some of the stitch symbols are explained in Figure 2 b). The slanted orientations of the slightly modified symbols for INC and DEC illustrate the stitch connections [5, 6]. These are additionally explained in Figure 2 a) by the small red arrows, while the normal stitch connections

are indicated by blue arrows. A crochet stitch is connected to the element in the course beneath, and to the previous element from the same course, which is the result of drawing loops during the stitch formation through two previously existing stitches. Conveniently, the arrangement of the symbols in rows and columns corresponds to the arrangement of the strings in the two-dimensional array.

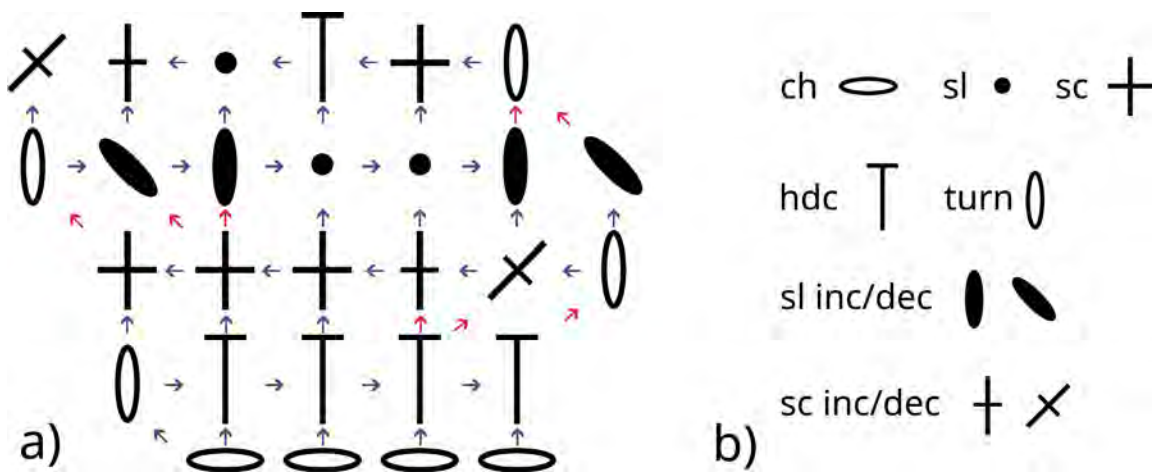


Figure 2: Symbolical representation of the crochet pattern shown in Figure 1: a) graphic representation of the crochet pattern with symbols; b) description of stitch symbols based on international standardization but modified slightly for INC and DEC

The modelling as an additional fabric representation, which was presented in reference 3, was extended here by INC and DEC. In short, the models are based on parameterized key points that are defined for each stitch type as a unit cell and are virtually shifted in space to meet the arrangement of the stitches in the crochet pattern array. A Python script, which is described in more detail regarding the modelling of manually crocheted fabrics in reference 27, was devel-

oped for this purpose. The freeware TexMind Viewer tool [28] was used for the spline interpolation of the key point curves, volume-sweeping along the centre yarn path and the visualization of the freeware tool.

Figure 3 depicts such a topology-based key point model of the yarn path generated as a visualization from the crochet pattern array representation. The construction of the stitches as well as their inter-looping are obtained from the idealized illustration

of a fabric crocheted by the machine. As indicated, different stitches have different heights, while the highest stitches set the height of a course. It is also remarkable that courses are positioned staggered to each other, which is due to the fashion of the wale-wise connections of crocheted fabrics. This renders the structure of crocheted textiles different from the regular wales of knitted fabrics.

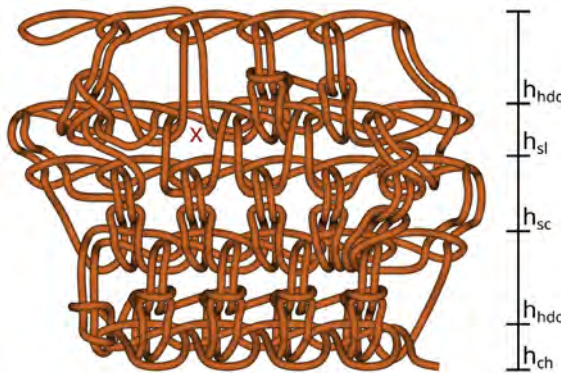


Figure 3: Representation of an exemplary crocheted fabric (cf. Figures 1 and 2) as a topology-based key point model of the yarn path. The red “x” marks one of the points of needle insertion to draw yarn through the working stitch.

With regard to INC with SC at the beginning of the third course, Figure 3 illustrates how two SCs in a course emerge from one stitch in the course beneath. In comparison, the structure of INC with SL (at the beginning of the fourth course) is slightly less obvious, although INC follows the same principle, as can be seen from the symbolic representation in Figure 2. Regarding DEC, however, both stitch types illustrate the drawing of the loops of one stitch through two stitches in the course beneath. Due to machine limitations, only one stitch can be added with INC at the start of a course, while DEC removes only one stitch at the course’s end. If it is necessary to add or remove more than one stitch in a course, further operations described in the supplementary materials are used for these additional stitches. Additional details regarding INC and DEC as well as the CroMat crocheting machine are also presented in those materials.

Similar to the text-based instructions of crochet patterns, the G-code for machine production can be seen as a further representation of automatically crocheted fabrics. Such a G-code program can be generated by traversing the crochet pattern array according to the crocheting sequence and mapping the elements to G-code macros, which are programmed for each stitch in relative coordinates. This has the advantage of easy interchangeability, so that modifications in the stitch formation procedure can be implemented flexibly. More details can be found in reference 3.

## 2 Subdivision of shaping polygons by crochet stitches

### 2.1 Principle of subdividing by stitches

Fundamentally, the breakdown of a polygon into a crochet pattern is a tessellation problem, since the polygon can be seen as a space that is to be partitioned into smaller stitch cells and uncovered areas [29]. To ensure machine manufacturability, pattern generation must follow the constraints of the automated crocheting process. Due to the various rules to be considered, no well-known area tessellation algorithms, for example centroidal Voronoi tessellation [30], can be applied. Moreover, good algorithms excel by being problem-specific, especially regarding real-life applications [31]. A new algorithm was therefore developed which traverses a 2D polygon according to the crocheting process, and decides stitch by stitch whether it may be set according to the rules.

For the purpose of simplification, stitches are represented by rectangles with the width as stitch length ( $l$ ) and the height corresponding to the stitch height ( $h$ ). The stitch dimensions relate to the values used for modelling. The rectangles for modelled SL and SC stitches are shown in Figure 4. It should be noted that the stitches largely overlap with the surrounding stitches, while the stitch rectangles are defined without these overlaps for reasons of simplicity.

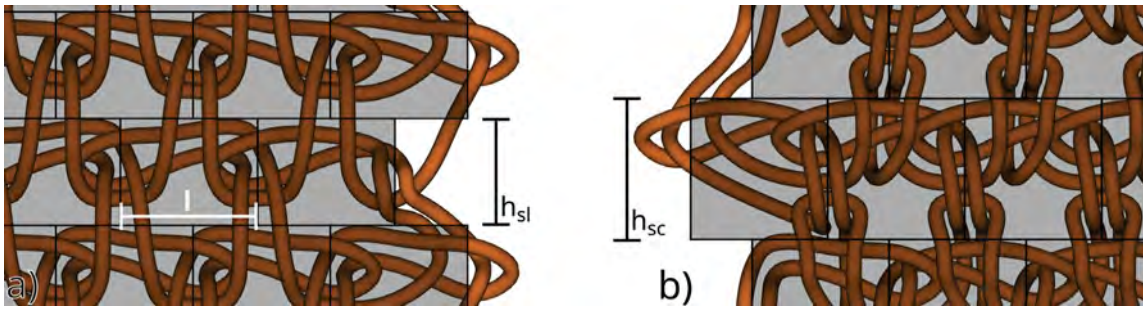


Figure 4: Examples of the arrangement of the stitch polygons with indicated stitch length ( $l$ ) and height ( $h$ ): a) Part of rectangular fabric consisting of SLs; b) Respective SC fabric

According to the taxonomy of Lee et al., [29] such partitioning by polygons representing stitches relates to vector or feature-primary tessellation, where the boundaries of features are described as polylines. In this regard, the shaping polygon is first divided into a course as a feature. This sub-polygon is then further partitioned by the stitch rectangles. Afterwards, the next course is partitioned. Stitches are placed in the polygon according to the sequence of crocheting, gradually filling the two-dimensional array with information regarding the resulting

crochet pattern.

The main steps of the basic structure of the developed tessellation algorithm are shown in Figure 5. If no further course fits into the polygon, or no element can be inserted at the beginning of the course or only one element was inserted in a course (which is then removed), the algorithm terminates and outputs the results. Note that a course with only one element, namely a turn, is not a valid course because the turn aligns next to the last stitch of the previous course.

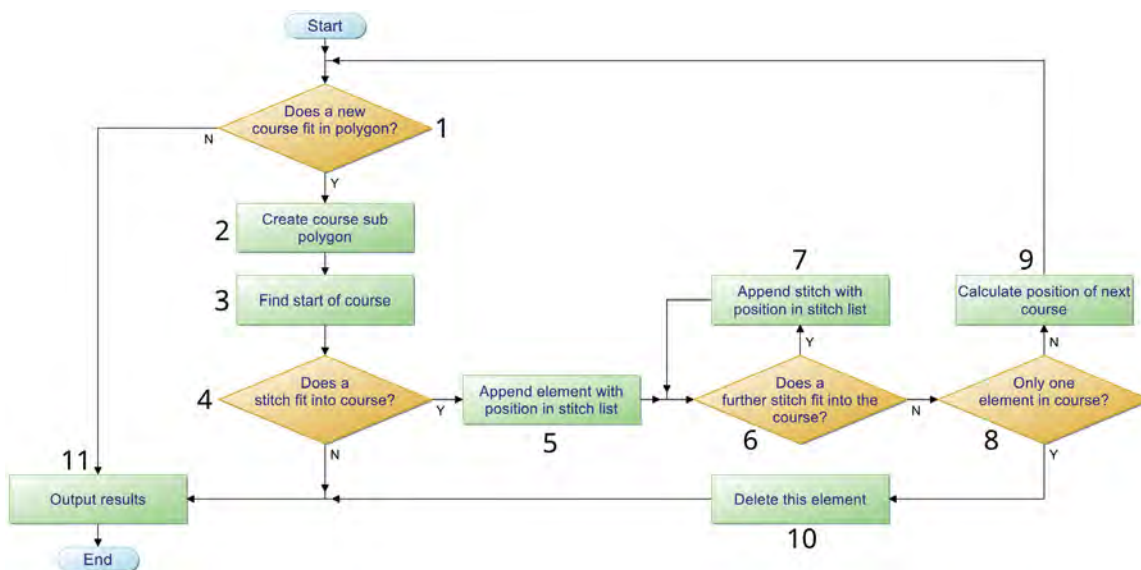


Figure 5: Flow chart of the crochet tessellation algorithm based on a convex input polygon. Y and N are abbreviations for yes and no. Created using the PapDesigner freeware from Friedrich Folkmann [32].

The stitch type and its width, which is set by default to 5 mm according to the needle gauge of the machine, as well as a convex polygon with an arbitrary

size and degree must be defined by the user. One polygon edge must be in line with the x-axis of a Cartesian coordinate system. It can also be decided

whether the stitch rectangles are allowed to exceed the polygon within certain limits, i.e. 30% of the stitch area by default, or without this tolerance, i.e. the polygon limits may not be exceeded.

### 2.2 Exemplary crochet tessellation of a triangle

In Figure 6, the principle of the crochet tessellation is illustrated without (a to c) and with a tolerance (d to f) for exceeding the polygon's boundaries. A stitch is indicated by two green vertical segments, each consisting of two points, which are taken into account for deciding on stitch placement.

According to the first step of the flow chart (cf. Figure 5), it is checked whether the corresponding sub-polygon with the CH height fits into the shaping polygon. The sub-polygon is then calculated (step 2), as well as the start of the course (step 3), which is the position of the outermost segment of the first stitch. This starting point, which can be shifted later to achieve better results, is at the right end of the sub-polygon (the first course goes to the left). In the sub-polygon, stitches are then inserted according to

steps 6 and 7 (cf. Figure 5) until their segments exceed the polygon boundaries or no longer meet the tolerance condition.

An exception occurs at the end of the CH course due to the specificity of the machine, and the CH before the following special turn is removed. This is because the last CH is used as the FLO with which machine production starts (cf. Figure 1). The removed segment is indicated in Figure 6 b) by the dashed line in the area marked  $u_2$ .

Following steps 8 and 9 of the flow chart (Figure 5), the next course is calculated taking into account the stitch height, and steps 1 to 4 are computed. As can be seen in Figure 6 b), the first element of the second course (5), i.e. the FLO, is placed according to the alternating crochet direction and staggered stitch pattern. With the overlapping tolerance, four elements can be fitted in the second course as shown in Figure 6 f) instead of the two elements depicted in Figure 6 c).

In the third course of partitioning without taking into account a tolerance (Figure 6 c), no element is placed. This is because the pattern and the polygon

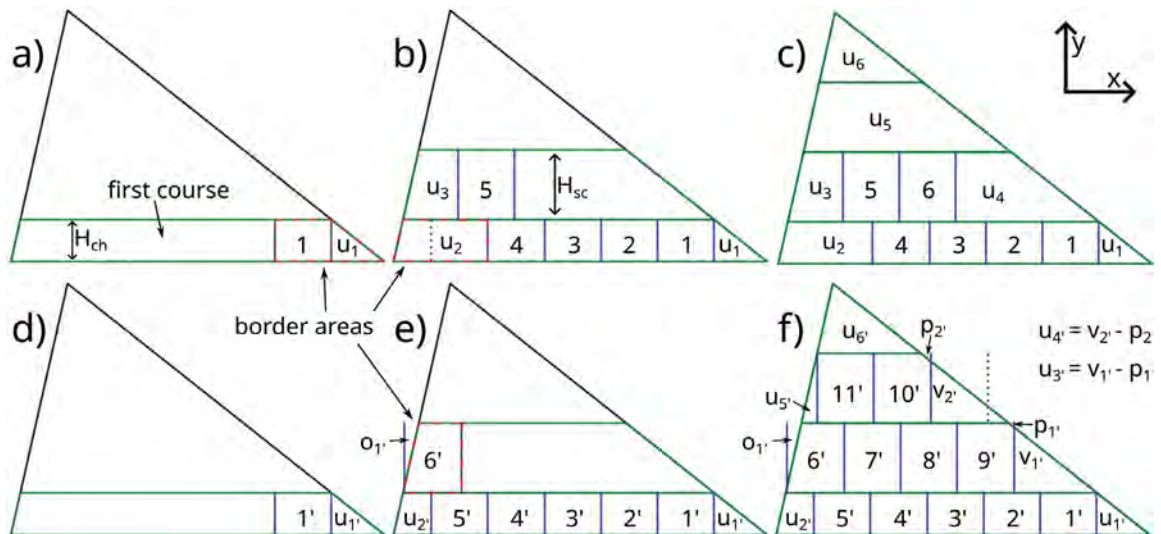


Figure 6: Crochet subdivision of a triangle without allowing the stitches to exceed the shaping polygon (a to c) and with exceeding allowed as long as 70% of a stitch area is inside the polygon: a) placement of the first CH stitch in the first course; b) start of second course; c) result of the crochet subdivision without tolerance; d) initial situation of the subdivision with permitted exceeding of the borders by the stitches; e) start of the second course; f) result of the respective crochet subdivision

shape only allow the placement of one stitch, which is then removed due to the check in step 8 and step 10 of the flow chart (Figure 5).

In partitioning taking into account a tolerance, the program's termination is also the result of the deletion of a single element, but here in the fourth course. Previously, the third course was filled with the turn 10' and the stitch 11'. To illustrate the logic of determining the x-position of the turn's first segment, an alternative position is indicated by the dashed line (near area  $v_2$ ).

Generally, only discrete stitch positions corresponding to the offset of the stitches from different courses are possible. For example, the dashed segment (near area  $v_2$ ) is an option but was deemed unsuitable because the respective stitch would exceed the polygon boundaries by more than 30%. For each turn, the algorithm checks first whether it is possible to add a stitch before it checks the possibilities to not change the number of stitches or to remove a stitch in the beginning of the course (RB; see supplementary materials). If RB is not sufficient to fit the shape, a stitch is dropped at the end of the previous course to allow suitable turn placing.

### 2.3 Assessment of the quality of crochet tessellation

Only uncovered areas ( $u_i$ ) are present in the case of subdivision without exceeding polygon borders

(cf. Figure 6 a to c). When the polygon boundaries may be exceeded, equation 1 is used to calculate the uncovered ( $u_i$ ) and overlapping ( $o_j$ ) areas based on the difference between the border area ( $ba$ ) and the stitch area ( $sa$ ). A  $ba$  refers to the area at the beginning or end of a course, including the first or last stitch (cf. the red dashed lines in Figure 6). In this regard,  $p_i$  is the area of a stitch exceeding the polygon while  $v_i$  is the part of the stitch inside the polygon (cf. Figure 6 f).

$$\begin{aligned} u_i &= v_i - p_i \text{ and } o_j = 0 & \text{if } ba - sa > 0 \\ u_i &= 0 \text{ and } o_j = p_j - v_j & \text{if } ba - sa < 0 \end{aligned} \quad (1)$$

If no stitches are set in a course, the resulting areas are also counted as uncovered areas  $u_i$  (cf. Figure 6 c and f). The absolute values of areas  $u_i$  and  $o_j$  are added to a total area-error value ( $Z$ ; see equation 2). The lower this value is, the better the shaping polygon is filled with crochet stitches, and the better mimicking of the shape.

With the strict condition not to exceed the polygon's boundaries (cf. Figure 6 c), the uncovered area totals 173.61 mm<sup>2</sup>. With regard to the area of the shaping polygon, the subdivision error is 58.45%, which means that most of the area was not covered. In contrast, the error of the second approach, taking into account a tolerance (cf. Figure 6 f), is only 30.00%, with 74.72 mm<sup>2</sup> of non-covered area and

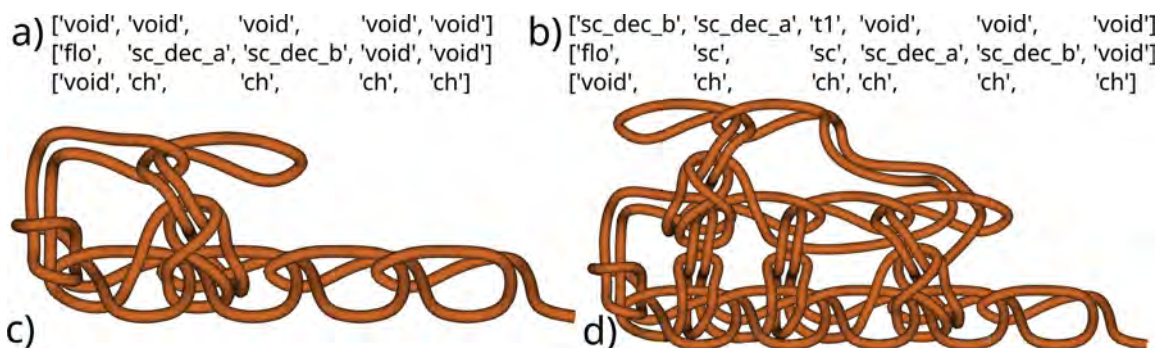


Figure 7: Crochet pattern arrays and models of the results of the exemplary subdivisions of Figure 6: a) output stitch array for the first partitioning approach without a tolerance for stitches exceeding the shaping polygon's border; b) array of the second partitioning approach with a tolerance taken into account; c) computer-generated model of the first approach; d) model of the second approach

14.38 mm<sup>2</sup> overlapping the shaping polygon. Evidence that this approach yielded a better result can also be seen in Figure 7 by comparing the models generated from the output stitch arrays.

Regarding the crochet pattern in Figure 7 b), it is noteworthy that two stitch positions are removed in the second course by combining DEC and removing a stitch at the end (RE). The latter is an additional shaping method described in the supplementary materials. DEC is always used for removing the first stitch at the end of a course, while potential additional stitches are then removed with RE. At the beginning of the third course, the number of stitches is further reduced by one using the RB operation. Below, in order to present better results, only the subdivision with a tolerance for exceeding the polygon boundaries with stitches will be considered.

In general, the stitch pattern and the respective

area-error are determined from the starting point, as the first point on the right segment of the first stitch set in the polygon. This first stitch is placed, by default, as far as possible to the right side of the first course without exceeding the polygon borders. To improve the coverage of all possible polygon shapes, the tessellation can be optimized, depending on the first stitch position.

#### 2.4 Optimization of the tessellation by shifting the starting point

The changing of uncovered and overlapping areas, as well as crochet patterns, depending on a starting point shift in x-direction, is illustrated in Figure 8. Here, a section of the triangle from Figure 6 is considered. Moreover, the specific calculation of  $u_i$  (uncovered) and  $o_j$  (overlapping), depending on the border area according to equation (1), is demonstrated.

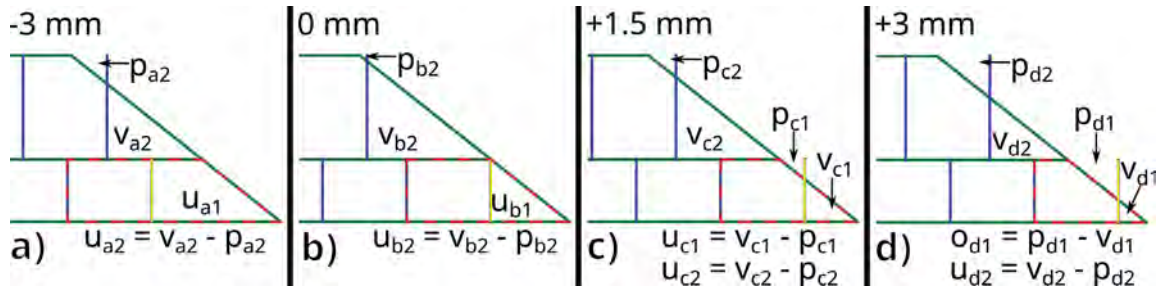


Figure 8: Effect of shifting the starting point in x-direction on the areas  $u_i$  and  $o_j$ , and on the crochet pattern. The border area (ba) is marked with the red dashed line and the shifted right segment of the first stitch is displayed as a yellow line: a) first stitch shifted by -3 mm; b) initial starting point; c) starting point shift of 1.5 mm; d) x-shift of 3 mm

Generally, the problem of finding an optimal subdivision of a 2D polygon by stitch rectangles is similar to the common initial situation of a bi-dimensional cutting stock problem or packing problem, where a set of smaller objects is placed on a set of larger objects under certain conditions [31, 33]. Usually, the partitioning of the objects is then optimized so that the waste is minimized. Optimizing the area coverage with crochet stitches similarly minimizes the uncovered areas seen as waste.

The function  $Z$  is introduced to describe the total

area-error depending on the shifts in x- and y-direction of the starting point of the first stitch placed in the shaping polygon (equation 2). Regarding equations 3 and 4, the boundaries of the x-shift and y-shift, as design variables, are defined with  $s$  as the stitch length and  $h$  as the stitch height, respectively. A farther shift than one stitch width or height in a positive or negative direction does not make sense because the stitch pattern would be repeated with a greater chance of error (cf. Figure 9).

$$Z = f(x_{\text{shift}}, y_{\text{shift}}) = \sum_{i=1}^m u_i + \sum_{j=1}^n o_j \quad (2)$$

$$-l \leq x_{\text{shift}} \leq l \quad (3)$$

$$-h \leq y_{\text{shift}} \leq h \quad (4)$$

Due to the complexity of subdividing countless possible shaping polygons while respecting the various rules of crocheting and the specifics of a machine, the analytical description of the functional relationship between the displacement of the starting point and the resulting area-error is unknown. A corresponding analysis would exceed the scope of this paper. For this reason, commonly known optimization algorithms from cutting stock problems [34] cannot be applied here. Instead, a numerical approach is followed, where many data points are sampled and the best one selected. This is less computationally costly and error prone than approximating function  $Z$  for computing its minimum to find the optimal starting point.

The sampled data points consist of the starting point shifts in the  $x$ - and  $y$ -direction with the associated area-error values. For the respective subdivisions, the step size (depending on the stitch size) and the number of steps for a shift are set by the user. The default value of the step size in  $x$ -direction is divided by the number of steps, while it is divided by the number of steps for the  $y$ -direction.

The algorithms are implemented in Python 3, while the SymPy library [35] is used for the geometric calculations. Also, the NumPy library [36] is utilized for the handling of data. Additionally, the open source Python library pytexlib [37] is applied for describing and saving the modelled textiles. The TexMind viewer [28] is used to visualise the models. Results are plotted using the Matplotlib library [38]. The parallel computing of the tessellation runs is implemented to speed up the algorithm via multiprocessing. All the software developed for surface decomposition, machine code generation and modelling are based on open-source frameworks.

## 3 Results and discussion

Below, the chosen digital representation of crocheted fabrics is discussed and the possibilities of shaping 2D flat crocheted fabrics producible by the CroMat crocheting machine are presented. The respective crochet subdivision algorithm of shaping polygons is also discussed.

### 3.1 Computer representation of crocheted fabrics

The representation of the crochet patterns in python lists is well suited in the context of the extension of the crochet design software from reference 3, and supports the modular approach. This data structure represents the textile in the fabric space. In terms of knitted textiles, this is a known approach, with the advantage that validation is easy to perform [39]. The disadvantage that manufacturability is more difficult to achieve at this level of representation [39] does not arise here, since producibility is already taken into account when populating the data structure. Due to the programming of the crocheting machine at the stitch level by grouping machine instructions to stitches, [3] machine instructions or models of the fabrics can be generated directly from the data structure.

The domain-specific language developed by Seitz et al. [5, 6] for designing manually crocheted textiles also ensures manufacturability and a structure's validity during the creation of a fabric. Beyond 2D, 3D textiles can be represented and visualized via crochet charts. An interesting difference lies in the modelling of SLs. According to Seitz et al., SLs do not add height to the textile and are the only stitch type that provides no insertion points for subsequent stitches. This corresponds to the conditions of manual crocheting, where it is difficult to insert the crochet hook into SLs and where these are mainly used for the seam. In contrast, machine production facilitates the efficient formation of new stitches based on SL working stitches and the construction of entire fabrics from this stitch type. Therefore, unlike Seitz et al., SLs are interpreted here as a normal crochet

stitch and modelled by adding height as well (cf. Figure 10).

Furthermore, Seitz et al. [5, 6] consider generating machine instructions in the future. In terms of the CroMat, this would be possible with the development of the suitable mapping of the representation of Seitz et al. to the machine's G-codes. To meet the limitations of the machine and automated flat crocheting in rows, their validation would have to be revised. Moreover, SLs should be represented differently so that the manufacturing capabilities of the machine are not restricted.

### 3.2 Numerical optimization of the triangle crochet tessellation

In terms of the optimization of the start position, how the quality of the surface tessellation and thus the shaping of the crocheted fabric depends on the position of the first stitch as the starting point is studied. Thus, it can be estimated whether and to what extent such an optimization is necessary for the future application of the tool.

In this regard, the starting point of the triangle subdivision shown in Figure 6 was shifted negatively

and positively in the x-direction by 10 steps, each with a step size of one tenth of the stitch width. According to the default values, the step size in the y-direction was set to one tenth of the height of the subdividing stitches. To avoid repetition of the crochet pattern and to save computation time, only y-shifts smaller than the height of the CHs of the first course were performed. Thus, fewer subdivision runs are calculated with respect to the y-direction. A crochet pattern repetition due to y-shifts would inevitably have a larger area-error, due to the missing coverage or overlap of the entire CH course.

In terms of displacement in the x-direction, a repetition of the crochet pattern can be observed with a deviation of the starting point of one stitch width (5 mm). As shown in Figure 9, the repetitions (see -2.5 mm and 2.5 mm or 0 mm and 5 mm) differ only in the first stitch and thus have deviating area-error values. In terms of the y-shift of -1 mm, the entire first course extends beyond the polygon increasing the  $\sigma_j$  part of the area-error. However, such a shift can lead to another course being filled in the upper part of the polygon, which can be advantageous, depending on the shape of the polygon.

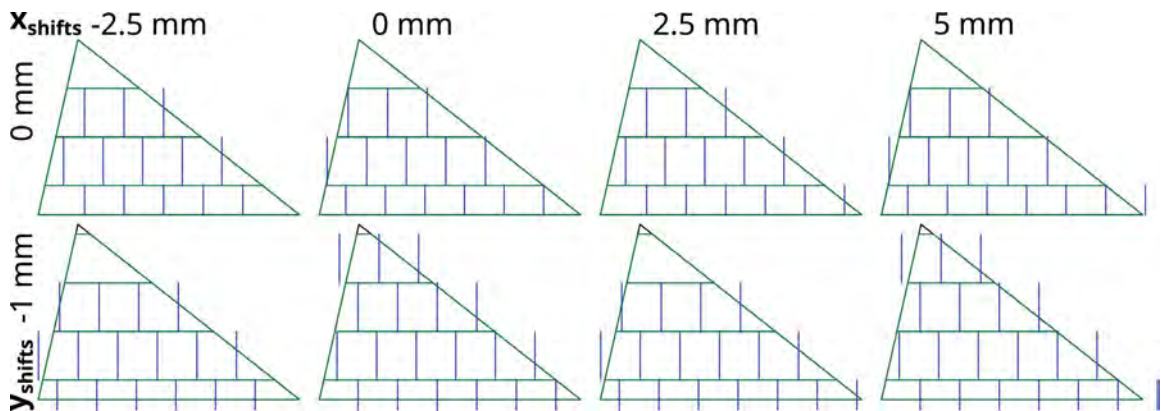


Figure 9: Crochet patterns resulting from exemplary starting point shifts, which were calculated during the numerical optimization of the triangle's crochet subdivision with SCs

In order to visualise the results of all crochet subdivisions of the triangle from Figure 6 and 9, the total area-errors  $Z$  (see equation 2), which depend on the starting point shifts, are colour coded and plotted in Figure 10. It is evident that a positive or negative shift in the y-direction has a greater impact

on the error values than a shift in the x-direction. This is because shifting in the y-direction affects an error area below the first course (cf. Figure 9) and above the last one, while an x-shift only changes the area coverage of the courses' first and last stitches.

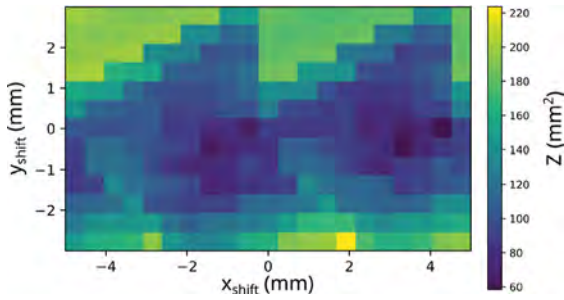


Figure 10: Area-error values depending on shifts of the start position with respect to the polygon in Figures 6 and 9 with colour scale

According to the distribution of small error values in the case of no displacement in the y-direction, a sufficiently optimal crochet subdivision with an area-error value of 19.65% was found with a displacement of the starting point by 4.5 mm in the x-direction. This is shown with the resulting model

in Figure 11. Due to optimization, a better tessellation solution and crochet pattern was found.

Next, the stitch types of SL and SC are compared with respect to a crochet subdivision of a scaled variant of the shaping triangle. The same starting point shifts were performed. More stitches can be placed in a larger polygon, which generally facilitates a better replication of the shape with the crocheted fabric. Accordingly, it is evident from Figure 12 that the area-error values of the initial and optimized starting points are lower and that the shape is better reproduced compared to Figure 11. Figure 12 also shows that the lower stitch height of the SLs facilitates a subdivision with more stitches. Interestingly, the best SC subdivision resulted in a smaller area-error than the best SL subdivision. However, the replication of the shape is similar.

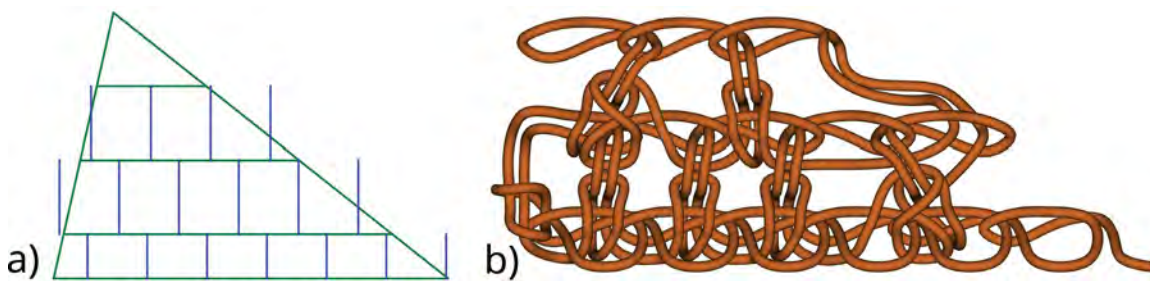


Figure 11: Result of the optimized crochet tessellation: a) Corresponding crochet subdivision and b) respective model

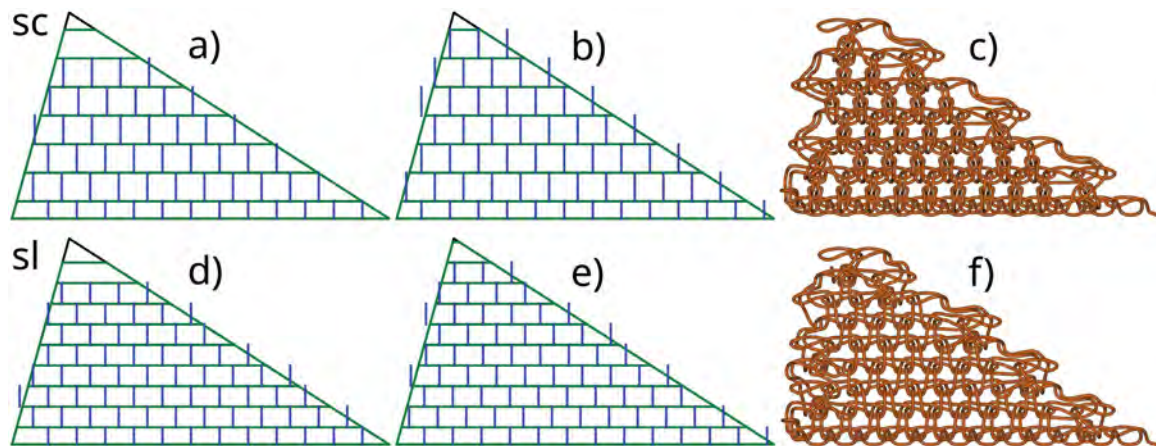


Figure 12: Comparison of crochet subdivision with SC and with SL: a) initial subdivision with SCs and no shifting (area-error value of 18.88%); b) SC subdivision result with minimal area-error value of 5.64% and starting point shifted by 3 mm in the x-direction; c) model corresponding to b); d) initial subdivision with SL and no shifting (area-error value of 13.85%); e) SL subdivision with minimal area-error value of 9.12% and starting point shifted by 3.5 mm in x-direction; f) model corresponding to e)

For both SL and SC, the optimal tessellations show only a shift of the starting point in the x-direction. Accordingly, the area-error values shown in Figure 13 are similar to those in Figure 10 and again

indicate a greater impact of the error values by shifting in the y-direction. The more common SC stitch type is used for subsequent subdivisions.

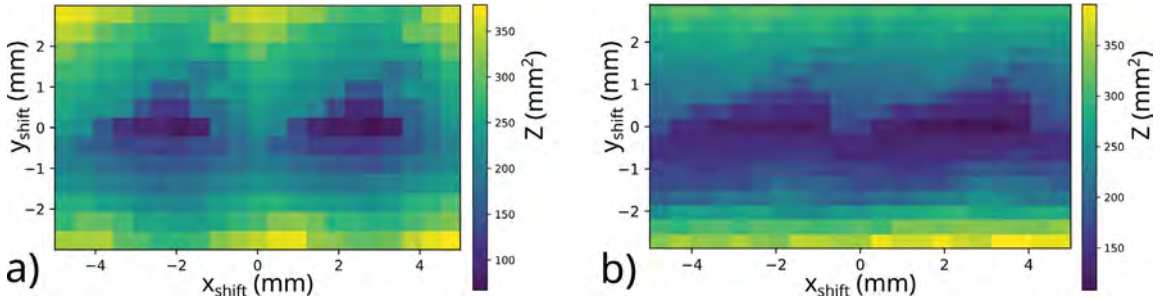


Figure 13: Area-error values of crochet subdivisions with starting point shifts of a scaled triangle: a) SC as stitch type; b) subdivision with SL

To investigate the crochet subdivision results in more detail, in particular with regard to the visible repetitions of the minima regions visible in Figure 13, the resolution is increased. Accordingly, the starting point of the division of the scaled triangle is shifted with a step size of  $l/20$  mm or  $h/20$  mm, respectively. The higher resolution of Figure 14 confirms the presence of two local minima repeating on the x-axis.

computing resources, the shifts with step sizes of one tenth of the stitch size might probably be sufficient. Nevertheless, to further explore the possibilities of the developed shaping tool and the correlation between the starting point and the quality of the subdivision, a finer optimization with a step size of  $l/20$  mm or  $h/20$  mm is applied.

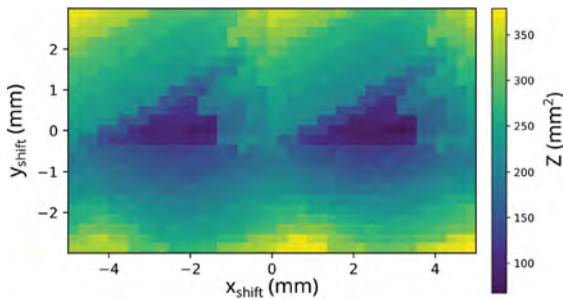


Figure 14: Area-error values with colour scale as crochet subdivision results with a higher resolution by using a step size of stitch length ( $l$ ) / 20 mm or stitch height ( $h$ ) / 20 mm for shifting the starting point

### 3.3 Crochet tessellations of additional shapes

To further investigate the shaping possibilities given by the extended capabilities of the crocheting machine to change fabrics widths, polygons with higher orders are also tested. In this regard, Figure 15 shows the optimization results of the crochet subdivision of a quadrilateral. The illustrated area-error values are similar to the previous polygons in that strong y-displacements affect the area-error more than strong x-displacements. However, for shifts on the x-axis, less distinct local minima of the area-error are seen. Here, with a relatively high computational effort, the area-error of the subdivision could only be improved slightly, from 6.44% to 5.23%, by shifting the first stitch by 0.25 mm in the x-direction.

Despite the significantly higher number of data points (1,024 compared with 272), the same shift of the starting point was again chosen as the best one (cf. Figure 12). However, this may be a coincidence. Depending on the application and the available

in terms of the initial and best subdivisions of the quadrilateral shown in Figure 16 a) and b), it is evident that the first stitch of the last course protrudes significantly more than the allowed 30% beyond the polygon boundaries. This is due to the difficulty of

representing the slight slope of the upper edge (see also Figure 16 c). In general, with a combination of DEC at the end of the previous course and RB (see supplementary materials) at the beginning of the current course, the position of the first stitch of the corresponding course can be shifted by only two stitch positions. If more is required, the last stitch in the previous course is also removed and the beginning of the current course is set accordingly. Here it becomes apparent that the tool will have to be expanded in the future to allow the removing of more stitches in the previous course to better fit the shape.

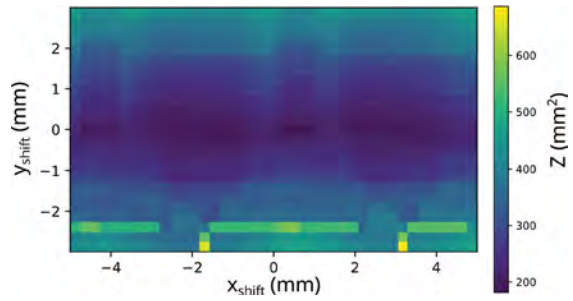


Figure 15: Area-error values with colour scale in terms of the crochet subdivisions of the quadrilateral polygon with starting point shifts

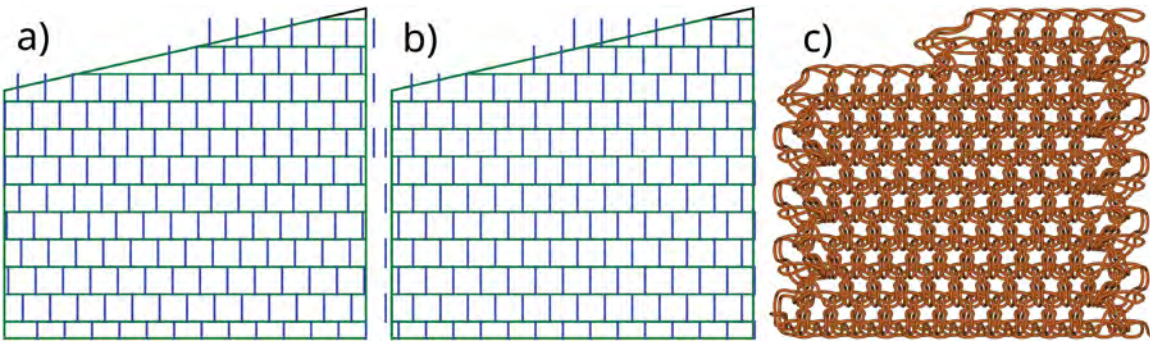


Figure 16: Crochet patterns resulting from the subdivision optimization of the quadrilateral: a) generated crochet pattern with initial starting point; b) optimized crochet subdivision; c) modelled pattern of the best run

The generated crochet patterns according to the shape of an irregular pentagon are presented in Figure 17. Similar to the previous examples, the shape can be fundamentally recreated by the crocheted fabric, while the slopes of the edges and sharp peaks cannot be reproduced efficiently due to the limitations of the

machine’s shaping operations. As shown in Figure 18, the pattern of the area-error values exhibits, similar to the scaled triangle, some kind of repetition along the x-axis with two local minima. Another similarity is that an additional course could be filled with stitches due to the starting point shift (cf. Figure 17).

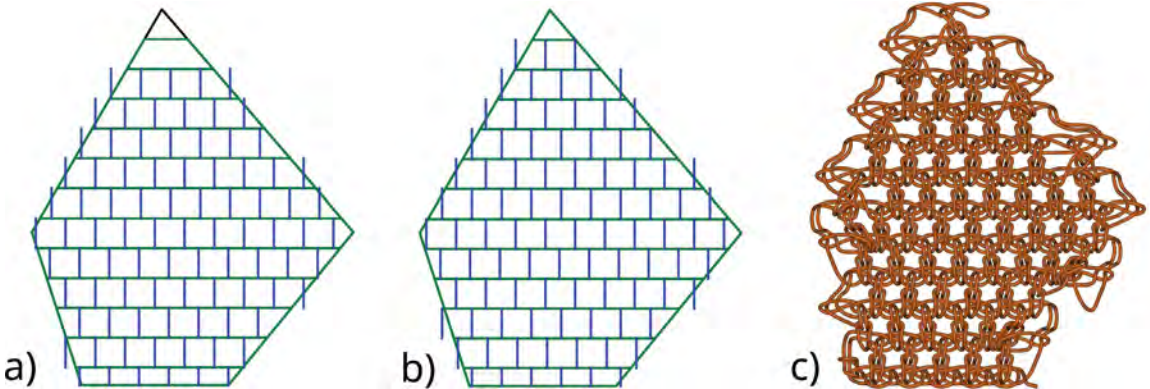


Figure 17: Irregular pentagon as shaping polygon for crochet pattern generation: a) First crochet subdivision pattern with initial starting point and area-error of 10.10%; b) Crochet pattern of the optimization with start position shifted by 0.75 mm in the x-direction and with an area-error of 7.47%; c) Respective model of the best run

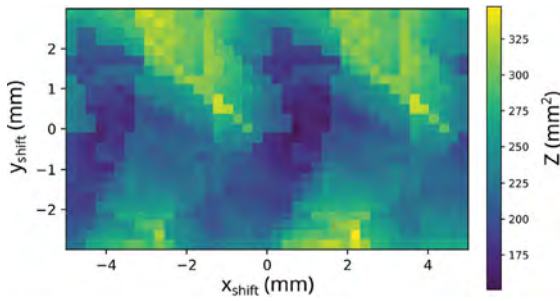


Figure 18: Area-error values with colour scale in terms of the optimization of the irregular pentagon

Lastly, an exemplary crocheted fabric is shaped as a regular hexagon using the developed algorithm. In Figure 19, the corresponding model shows that

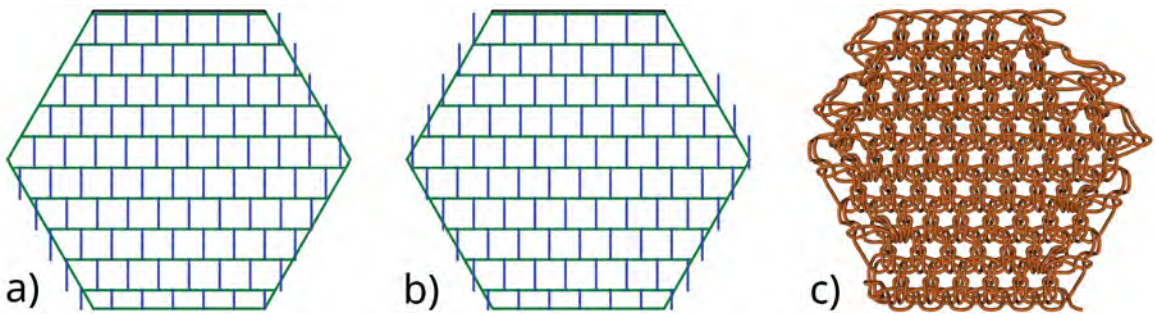


Figure 19: Crochet patterns corresponding to a regular hexagon as shaping polygon: a) Initial crochet subdivision; b) Crochet pattern resulting from the optimization; c) Model of the optimal subdivision

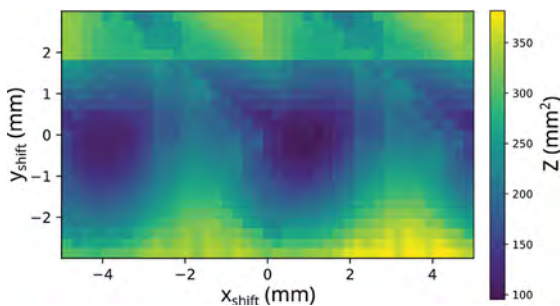


Figure 20: Results of the starting point optimization of the regular hexagon with area-error values in colour scale

### 3.4 Discussion of crochet tessellation results

The observed repetitions of the area-error patterns with local minima along the x-axis emerge because the crochet pattern repeats itself, with the first stitch

the shape is fundamentally reproduced, but the symmetry of the structure is not achieved. The crochet pattern could be improved from an area-error of 6.70% to an error of 4.68% by moving the starting point 1.25 mm in the x-direction.

The visualization of the area-error, depending on the shifts shown in Figure 20, again illustrates two distinct local minima with a close to zero y-shift. At the right side, a further repetition of the error pattern emerges with another potentially local minimum. With a 1.25 mm x-direction shift, the ideal position of the starting point was placed in one local minimum. Large y-shifts result once again in large area-error values.

as the exception, when the starting point is shifted by one stitch width (5 mm) on the x-axis (cf. Figure 9). The local minima further away from the initial starting point are associated with larger error values. In a negative x-shift, the first stitch position of the initial starting point is not covered, while large positive x-shifts cause the first stitch to extend far beyond the shaping polygon.

Overall, the presented crochet subdivisions show that the developed algorithm indeed facilitate the shaping of machine-producible crocheted fabrics according to diverse convex geometries. The quality of shape matching, represented by the error of uncovered and excessively covered areas, can be improved by increasing the computational effort and calculating multiple subdivisions with shifted starting points. This simple numerical optimization

yielded better results in all cases in which the starting points were shifted a few millimetres in the positive x-direction to a minimum of the error values. A step size of one tenth or one twentieth of the stitch width is suitable for this purpose. Depending on the requirements for the quality of the tessellation and shaping, the step size can be adjusted. In addition to the trend of the location of the minima, the tendency was observed that large y-shifts usually result in large area-error values. Based on these findings, computing time can be saved in future applications by scanning a smaller range in the y-direction with perhaps a coarser resolution.

The shaping possibilities of the developed Cro-Mat prototype of a real crocheting machine are much more limited compared to the almost unlimited possibilities of manual crocheting, and compared to technically advanced V-bed knitting machines. This is mainly due to missing loop transfer capabilities, so that INC and DEC can only be performed at the beginning and end of a course, respectively. Nevertheless, the development and demonstration of shaping possibilities are important for technical progress in the automation of crocheting. To expand the shaping possibilities of crocheting machines in the future, loop transfer should be integrated, for example, by means of fashioning points, as known in straight bar frames [40].

### 3.5 Comparison of the crochet tessellation approach with literature

Researchers have already studied the division of surfaces into crochet patterns. Çapunaman et al. [9] followed a similar procedure of inserting the courses or curves before populating them with stitches, while transferring the shape of a 3D geometry applying a non-uniform rational basis spline (NURBS) UV division to crochet patterns. The difference is that the stitches from different curves/rows are not constrained with respect to a stitch offset as it was done in this study. Thus, in contrast to the idealized offset of the stitches modelled here, Çapunaman et al. assumed that the stitches will deform appropriately

according to the desired shape. As a restraint regarding manufacturability, the continuity of the stitch sequence is considered, while the rules of INC and DEC are taken into account. In the approach presented in this paper, additional rules for machine manufacturing, but only 2D geometries, are considered.

Guo et al.'s [8] algorithm for the automated generation of crochet patterns based on a manifold 3D mesh builds on a previous approach for machine-knitted textiles [21, 23]. The stitches are basically represented by squares containing information about topology, connections to others, and instructions for fabrication, but triangles or pentagons for INC or DEC are also used. The data structure in this paper is similar to their approach in that the stitch-representing rectangles are mapped to information about topology or fabrication. The difference is that here the stitch structure is assumed to be slightly offset from course to course, while Guo et al. modelled them without such offsets. This leads to a warped picture compared to the representation chosen here. However, the relaxed state of crocheted textiles remains unexplored. It is thus not possible to judge which representation is more realistic. In general, crocheted textiles are underresearched [27].

Overall, it is quite common in literature to mesh a surface with rectangles representing stitches on a surface [8, 9, 19–21, 23]. The approach presented herein differs because not the whole surface is meshed by rectangles. Instead, the rectangles are placed only at permitted positions in a fixed orientation one after the other, taking into account rules for valid textiles and manufacturability. In this context, the consideration of the manufacturability of a crocheting machine constitutes a new approach. Corresponding to machine manufacturability, crochet pattern generation is here limited to 2D shapes. To date, the manufacturability of a real crocheting machine has only been addressed in reference 3. Thus, an important contribution is made regarding the research of the possibilities of machine-made crocheted textiles and the development of technologies for future, industrial use.

## 4 Conclusion

In this paper, a novel algorithm for automatically generating and shaping crochet patterns manufacturable by a real crochet machine according to 2D polygons is presented and discussed. Machine-productibility is ensured by successively filling a shaping polygon with crochet stitches represented by rectangles according to the rules and limitations in connection with automatically manufacturing the respective fabrics with the CroMat crochet machine prototype. As a result, only valid patterns are generated, which, given the limited capabilities of the crochet machine, can sufficiently replicate shapes of convex polygons. In this regard, the missing capability of stitch transfer is especially limiting, and stitches can only be added or removed in the beginning or end of a course. This is achieved, in particular, by INC and DEC operations, which were presented here for the first time with regard to automated flat crocheting based on a chain row. In the future, the machine will be expanded to facilitate the production of more diverse shapes.

The quality of the subdivision of a polygon by crochet stitches is determined by the area-error, which is calculated by adding the areas not covered by the rectangles and the areas exceeding the polygon boundaries. To increase the quality, the first stitch, on which the crochet pattern depends, can be shifted by fractions of the stitch size to the left, right, top and bottom for a numerical optimization of the replication of the polygon's shape by the crocheted fabric. The tessellation optimizations of exemplary polygons from triangle to hexagon were investigated. In all cases, a vertical shift of the starting point results in larger error values, while better solutions were found using horizontal shifts. Due to repetitions of the crochet pattern in a horizontal shift of one stitch width, the local minima of the error values repeat, with a trend to lower error values near the initial starting point. Based on these findings, the search range of the optimization can be narrowed in the future to reduce the computational effort.

With the developed algorithm, the previously limited possibilities for the design of machine-crocheted textiles are significantly expanded. Specifically, it is an expansion of the design tool presented in reference 3. Accordingly, the 2D shaping and automated creation of producible crochet patterns lends itself to future application in an industrial context. The tool is especially useful since it does not require any knowledge of crocheting for the design of diverse crocheted structures. The presented work constitutes an important step in the development of the thus far unexplored crocheting technology with respect to novel products and the replacement of manually produced commercial crocheted products.

## References

1. GRIMMELSMANN, Nils, FIEDLER, Johannes, EHRMANN, Andrea. *Häkemaschine. DE patent, no. 102016015204A1. 2018-06-21.*
2. GRIMMELSMANN Nils, DÖPKE Christoph, WEHLAGE, Svea, EHRMANN Andrea. The largest crocheting machine in the world. *Melliand International*, 2019, **25**(2), 99–100.
3. STORCK, Jan Lukas, FELDMANN, Bjarte Alexander, KYOSEV, Yordan. Design tool for automated crocheting of fabrics. *Communications in Development and Assembling of Textile Products*, 2023, **4**(2), 254–272, doi: 10.25367/cdatp.2023.4.p254-272.
4. PERRY, Gabriella. *Croche-Matic – building a robot for crocheting 3D spherical form. Master's thesis.* Harvard Graduate School of Design, 2022, <https://nrs.harvard.edu/URN-3:HUL.INSTREPOS:37372333>.
5. SEITZ, Klara, LINCKE, Jens, REIN, Patrick, HIRSCHFELD, Robert. *Language and Tool Support for 3D Crochet Patterns.* Potsdam : Universitätsverlag Potsdam, 2021.
6. SEITZ, Klara, REIN, Patrick, LINCKE, Jens, HIRSCHFELD, Robert. Digital crochet: toward a visual language for pattern description. In *Proceedings of the 2022 ACM SIGPLAN Interna-*

- tional Symposium on New Ideas, New Paradigms, and Reflections on Programming and Software, 2022, 48–62, doi: 10.1145/3563835.3567657.
7. NAKJAN, Pikanate, RATANOTAYANON, Sukanya, PORWONGSAWANG, Natchayar. Automatic crochet pattern generation from 2D sketching. In *10th International Conference on Knowledge and Smart Technology (KST)*. IEEE, 2018, 170–175, doi: 10.1109/KST.2018.8426123.
  8. GUO, Runbo, LIN, Jenny, NARAYANAN, Vidya and MCCANN, James. Representing crochet with stitch meshes. In *SCF '20: Proceedings of the 5th Annual ACM Symposium on Computational Fabrication*. Edited by E. Whiting, J. Hart, C. Sung, N. Peek, M. Akbarzadeh, D. Aukes, A. Schulz, H. Taylor and J. Kim. New York : ACM, 2020, 1–8, doi: 10.1145/3424630.3425409.
  9. ÇAPUNAMAN, Özgüç B., BINGÖL, Cemal K., GÜRSOY, Benay. Computing stitches and crocheting geometry. In *Computer-Aided Architectural Design. Future Trajectories. 17th International Conference, CAAD Futures 2017, Istanbul, Turkey, July 12-14, 2017, Selected Papers. Communications in Computer and Information Science, vol 724*. Edited by G. Çağdaş, M. Özkar and L. F. Gül. Singapore : Springer, 2017, 289–305, doi: 10.1007/978-981-10-5197-5\_16.
  10. ZAHARIEVA-STOYANOVA, Elena, BOZOV, Stefan. Application of XML-based language for digital representation of crochet symbols. *Digital Presentation and Preservation of Cultural and Scientific Heritage*, 2017, 7, 181–190, doi: 10.55630/dipp.2017.7.16.
  11. ZAHARIEVA-STOYANOVA, Elena, BE-SHEVLIEV, Damyan. Digital representation of crochet symbols sets. *Digital Presentation and Preservation of Cultural and Scientific Heritage*, 2018, 8, 159–164, doi: 10.55630/dipp.2018.8.14.
  12. JIANG, Chen, WANG, Kan, LIU, Yi, ZHANG, Chuck and WANG, Ben. Textile-based sandwich scaffold using wet electrospun yarns for skin tissue engineering. *Journal of the Mechanical Behavior of Biomedical Materials*, 2021, 119, 1–9, doi: 10.1016/j.jmbbm.2021.104499.
  13. SHI, Linyan, WANG, Sihan, LIANG, Nanyue, ZHANG, Xinyu, NIU, Lizhong, CHENG, Deshan and TANG, Xiaoning. Sound absorption of crochet fabrics with multi-ply yarns. *Applied Acoustics*, 2022, 199, 1–7, doi: 10.1016/j.apacoust.2022.109017.
  14. BOBIN, Maxence, AMROUN, Hamdi, CO-QUILLART, Sabine, BIMBARD, Franck, AMMI, Mehdi. SVM based approach for the assessment of elbow flexion with smart textile sensor. In *2017 IEEE International Conference on Systems, Man, and Cybernetics (SMC)*, 2017, 2129–2134, doi: 10.1109/SMC.2017.8122934.
  15. EMERY, Irene. *The primary structures of fabrics: an illustrated classification*. New York : Watson-Guptill Publications, 1995.
  16. KARP, Cary. Defining crochet. *Textile History*, 2018, 49(2), 208–223, doi: 10.1080/00404969.2018.1491689.
  17. HENDERSON, David W., TAIMINA, Daina. Crocheting the hyperbolic plane. *Mathematical Intelligencer*, 2001, 23(2), 17–28, doi: 10.1007/BF03026623.
  18. OSINGA, Hinke M., KRAUSKOPF, Bernd. Crocheting the Lorenz manifold. *Mathematical Intelligencer*, 2004, 26(4), 25–37, doi 10.1007/BF02985416.
  19. POPESCU, Mariana, RIPPAN, Matthias, VAN MELE, Tom, BLOCK, Philippe. Automated generation of knit patterns for non-developable surfaces. In *Humanizing Digital Reality: Design Modelling Symposium Paris 2017*. Singapore : Springer, 2018, 271–284, doi: 10.1007/978-981-10-6611-5\_24.
  20. WU, Kui, SWAN, Hannah and YUKSEL, Cem. Knittable stitch meshes. *ACM Transactions on Graphics*, 2019, 38(1), 1–13, doi: 10.1145/3292481.
  21. NARAYANAN, Vidya, WU, Kai and YUKSEL, Cem, MCCANN, James. Visual knitting machine programming. *ACM Transactions on Graphics*, 2019, 38(4), 1–13, doi: 10.1145/3306346.3322995.
  22. MCCANN, James, ALBAUGH, Lea,

- NARAYANAN, Vidya, GROW, April, MATUSIK, Wojciech, MANKOFF, Jennifer, HODGINS, Jessica. A compiler for 3D machine knitting. *ACM Transactions on Graphics*, 2016, **35**(4), 1–11, doi: 10.1145/2897824.2925940.
23. NARAYANAN, Vidya, ALBAUGH, Lea, HODGINS, Jessica, COROS, Stelian, McCANN, James. Automatic machine knitting of 3D meshes. *ACM Transactions on Graphics*, 2018, **37**(3), 1–15, doi: 10.1145/3186265.
  24. KASPAR, Alexandre, MAKATURA, Liane, MATUSIK, Wojciech. Knitting skeletons: A computer-aided design tool for shaping and patterning of knitted garments. In *UIST '19: Proceedings of the 32nd Annual ACM Symposium on User Interface Software and Technology*. New York : Association for Computing Machinery, 2019, 53–65, doi: 10.1145/3332165.3347879.
  25. Standards and guidelines for crochet and knitting [online]. Craft Yarn Council [accessed 30.07.2023]. Available on World Wide Web: <<https://www.craftyarncouncil.com/standards>>.
  26. Crochet chart symbols [online]. Craft Yarn Council [accessed 30.07.2023]. Available on World Wide Web: <<https://www.craftyarncouncil.com/standards/crochet-chart-symbols>>.
  27. STORCK, Jan L., GERBER, Dennis, STEENBOCK, Liska, KYOSEV, Yordan. Topology based modelling of crochet structures. *Journal of Industrial Textiles*, 2022, **52**, doi: 10.1177/15280837221139250.
  28. TexMind textile viewer (free) [online]. TexMind [accessed 30.07.2023]. Available on World Wide Web: <<http://texmind.com/wp/products/neues-produkt/>>.
  29. LEE, Y.C., LI, Zhi-lin, LI, Y.L. Taxonomy of space tessellation. *ISPRS Journal of Photogrammetry and Remote Sensing*, 2000, **55**(3), 139–149, doi: 10.1016/S0924-2716(00)00015-0.
  30. DU, Qiang, FABER, Vance, GUNZBURGER, Max. Centroidal Voronoi tessellations: applications and algorithms. *SIAM Review*, 1999, **41**(4), 637–676, doi: 10.1137/S0036144599352836.
  31. CHU, C., ANTONIO, J. Approximation algorithms to solve real-life multicriteria cutting stock problems. *Operations Research*, 1999, **47**(4), 495–508, doi: 10.1287/opre.47.4.495.
  32. PapDesigner [online]. Friedrich Folkmann [accessed 30.07.2023]. Available on World Wide Web: <<http://friedrich-folkmann.de/papdesigner/Hauptseite.html>>.
  33. HOPPER, E., TURTON, B.C. A review of the application of meta-heuristic algorithms to 2D strip packing problems. *Artificial Intelligence Review*, 2001, **16**, 257–300, doi: 10.1023/A:1012590107280.
  34. ISRANI, Sharat, SANDERS, Jerry. Two-dimensional cutting stock problem research: a review and a new rectangular layout algorithm. *Journal of Manufacturing Systems*, 1982, **1**(2), 169–182, doi: 10.1016/S0278-6125(82)80027-7.
  35. About SymPy [online]. SymPy [accessed 30.07.2023]. Available on World Wide Web: <<https://www.sympy.org/en/index.html>>.
  36. NumPy – main page [online]. NumPy [accessed 30.07.2023]. Available on World Wide Web: <<https://numpy.org>>.
  37. Pytextlib library [online]. GitHub [accessed 30.07.2023]. Available on World Wide Web: <<https://github.com/virtualtextiles/pytextlib/>>.
  38. Matplotlib documentation [online]. Matplotlib [accessed on 30.07.2023]. Available on World Wide Web: <<https://matplotlib.org/stable/index.html>>.
  39. KAPLLANI, Levi, AMANATIDES, Chelsea, DION, Genevieve, SHAPIRO, Vadim, BREEN, David E. TopoKnit: a process-oriented representation for modeling the topology of yarns in weft-knitted textiles. *Graphical Models*, 2021, **118**, 1–19 doi: 10.1016/j.gmod.2021.101114.
  40. SPENCER, David J. The straight bar frame and full-fashioning. In *Knitting Technology: a Comprehensive Handbook and Practical Guide*. Woodhead Publishing, 2001, 194–206, doi: 10.1533/9781855737556.194.

# Supplementary materials

## 1 Crocheting machine prototype and limitations

According to the process of manual flat crocheting, the stitches are formed by the CroMat crocheting machine prototype successively in the direction of the current course. At the end of the course, a turn stitch is made, which comprises one or few chain stitches (CHs) and is the first element of the next course with an alternated crochet direction. Stitches, which also include turns, are the elements produced by the machine to create a whole fabric. In contrast to manual flat crocheting, the fabric in this process is not rotated and thus all stitches are drawn through the fabric from one side. This creates a fabric with a technical front and technical back [1].

The machine features a mechatronic design, unlike conventional textile machines that are operated rather mechanically [2]. The machine elements are moved by electric motors, which are centrally controlled by a microcontroller that receives G-code commands as input. For each stitch type, depending on the crochet direction, G-code macros are defined and must be arranged in the correct order according to the sequence of the crocheting process before they can be sent to the machine. Further details on the design and control of the machine can be taken from reference 1.

Implementation of the machine results in limitations compared to manual crocheting. As such, only slip stitches (SLs), single crochet stitches (SCs), half double crochet stitches (HDCs) and turns with CHs can be created. The insertion point of the special needle, which functions as a crochet hook, into the working stitch is restricted to the common case of insertion under the top loop of the working stitch, as marked in Figure 3 of the paper. The stitches of the last course can be used solely as working stitches for the creation of new stitches, while in manual

crocheting the crochet hook can form a new stitch anywhere in the fabric. As another characteristic of the machine, there is never a CH below the first turn, which is the first operation formed by the machine and is called first lay over (FLO). Moreover, the first CH course, namely the chain row with which each crocheted fabric starts, is always directed to the left and must be manually crocheted on the needles of the needle bed.

Due to the single needle bed and no additional machine elements such as fashioning points known in straight bar frames, [3] the loop transfer of previously produced stitches to other needles is not possible. Thus, the number of stitches in a course can only be changed at the beginning or end of a course by adding or removing needles. Adding one stitch with INC is only possible at the course's beginning, since needles can be added there without the need of a loop transfer, while removing one stitch with DEC is only possible at the end of a course. In manual crocheting, no restrictions exist regarding the position or numbers of stitches manipulated with INC or DEC. As a rule, with INC, multiple stitches are worked into one stitch of the previous course to widen the fabric. With DEC, the fabric is tapered by working one stitch in multiple stitches of the previous course.

## 2 Machine operation to alter a fabric's width

The crocheting machine is capable of adding one stitch at the start of a course by performing an INC operation. For this, the leading loop (LL) of the turn's CH is suspended at one needle position further out. Thus, the first stitch built in the working stitch can be placed in the usual position of the turn's LL, and the second stitch based on the same working stitch is suspended at the former needle position of this working stitch. The resulting INC structure is depicted in Figure 3. A special rule is that no INC can be executed at the beginning of the second course due to the special operation of the FLO. However, if

the polygon shape requires this, a CH is added in the first course as a workaround.

Forming an additional stitch based on the same working stitch used for INC is not possible because the turn's LL would be stretched too far, resulting in severe forces on the machine elements due to yarn friction. Performing multiple INCs in one course is also not possible because this would require stitch transfer. For the same reasons, only one stitch can be dropped at the end of the course by DEC. The structure of INC and DEC is shown in Figure 3 of the paper. For DEC, one stitch is built on two working stitches (in crochet abbreviated as sc2tog) by drawing a loop through each working stitch and then drawing the new LL through these loops and through the old LL.

Besides these automated methods, which are commonly used in manual crocheting for altering the number of stitches in a course, additional options are provided by the machine. Again, these methods are based on adding or removing stitches in the end or at the beginning of a course. In general, removing stitches from needle positions is easier than adding

additional stitches to needle positions.

As can be seen in Figure S1 a) and b), a stitch can be added at the beginning of a course (AB) by placing the CH of the turn at one needle position further outward and building a CH at the usual turn position. This is similar to INC, which is preferred here because it is more like manual crocheting, and thus only one stitch can be added in this way.

In contrast to AB, up to three stitches can be added at the end of a course (AE) by forming CHs, as illustrated in Figure S1 c) and d). The CHs are suspended on new needles and can be used as working stitches in the next course. The limited number of added CHs with an AE is to prevent them from tightening excessively due to the fabric take-off and causing errors in drawing loops through them in the next course.

Additional methods for reducing the number of stitches in a course are illustrated in Figure S2. By dropping the stitch at one position further inward next to the usual turn position and suspending the LL of the latter at this cleared position, a stitch is removed at the course's beginning (RB). With this method, shown in Figure S2 a) and b), the number of

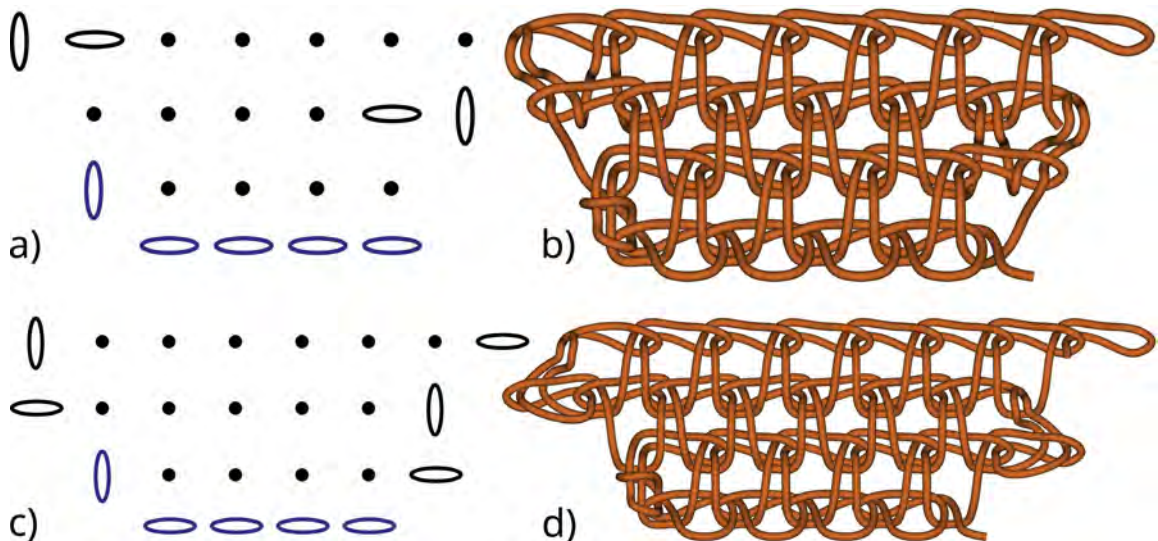


Figure S1: Options to increase the width of machine-crocheted fabrics. **a)** Crochet chart of an exemplary SL fabric by adding a stitch at the beginning of a course (AB); **b)** Topology-based model of the fabric with added stitches at the beginning of the course; **c)** Example crochet chart for adding a stitch at the end of a course (AE); **d)** Model of a respective fabric with added stitches at the ends of the courses. The basic CHs of the first course with crochet direction to the left and the first turn (FLO) are displayed in blue.

discarded stitches is limited to one to avoid stresses on the needle holding the LL, which would occur if the LL of the turn was stretched over more than one stitch position.

Lastly, stitches can be removed by dropping an arbitrary number of remaining working stitches, which were not used as working stitches to form stitches in the current course, at the end of a course (RE). This is illustrated in Figure S3 c) and d). Here, an arbitrary number of discarded stitches is possible, because no stitch transfer and no stretching of the LL over multiple needle positions is required. To make it more similar to hand crocheting, DEC is always performed for the first stitch by which the course is to be reduced at the end. Further stitch positions can then be removed with RE.

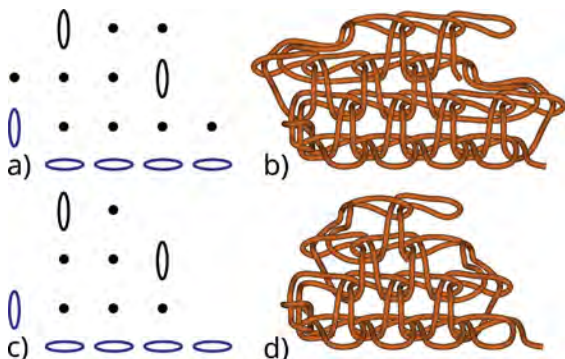


Figure S2: Options to decrease the width of machine-crocheted fabrics. The basic CHs (going to the left) and the FLO are marked in blue similar to Figure S1; **a)** Crochet chart of an exemplary machine-crocheted fabric, where a stitch is discarded at the beginning of the second and third course (RB); **b)** Model of the fabric with discarded stitches at the beginnings of courses; **c)** Crochet chart of a fabric showing the discarding of stitches at the ends of the courses (RE); **d)** Respective model for discarding a stitch at the end of a course.

## References

1. STORCK, Jan Lukas, FELDMANN, Bjarte Alexander, KYOSEV, Yordan. Design tool for automated crocheting of fabrics. *Communications in Development and Assembling of Textile Products*, 2023, 4(2), 254–272, doi: 10.25367/cdatp.2023.4.p254-272.
2. SPENCER, David J. Electronics in knitting. In *Knitting technology: a comprehensive handbook and practical guide*. 3th ed. Cambridge : Woodhead Publishing, 2001, 134–144.
3. SPENCER, David J. The straight bar frame and full-fashioning. In *Knitting technology: a comprehensive handbook and practical guide*. 3th ed. Cambridge : Woodhead Publishing, 2001, 194–206.

Mohammad Ehsan Momeni Heravi,<sup>1</sup> Mohammad Hossein Moattar<sup>2</sup>

<sup>1</sup> Department of Textile and Fashion Design, Mashhad Branch, Islamic Azad University, Mashhad, Iran.

<sup>2</sup> Department of Computer Engineering, Mashhad Branch, Islamic Azad University, Mashhad, Iran

---

# Carpet Back Sizing Quality Assessment by Measuring the Amount of Resin Using Image Processing and Machine Learning Approaches

*Ocenjevanje kakovosti utrjevanja hrbtni strani preproge z določanjem količine zamreževala s pomočjo obdelave slik in strojnega učenja*

**Original scientific article/Izvirni znanstveni članek**

Received/Prispelo 6-2023 • Accepted/Sprejeto 10-2023

Corresponding author/Korespondenčni avtor:

**Mohammad Hossein Moattar, Associate Professor**

Tel.: +989155030540

E-mail: moattar@mshdiau.ac.ir

ORCID: 0000-0002-8968-6744

---

## Abstract

The mechanical properties of the carpet, such as dimensional stability, bending stiffness, handle and creeping on the surface during use, have a direct relationship with the amount of resin applied to the back of the carpet in the sizing process. In today's factories, the optimal amount of resin and the mechanical quality of the carpet are controlled by the operator touching the carpet on the machine carpet finishing line or manually while rolling the carpet. Proposed in this paper is an automatic method based on the evaluation of the bending stiffness of the sized carpet that uses digital image processing and machine learning to measure the optimal amount of size concentration and control this index. For this purpose, during the final stage of carpet production, the carpet is folded in the middle, and two edges of the carpet are placed on top of each other. A side view image is then taken of the carpet. Using edge detection methods, the edges of the carpet are identified, and different features, such as the average, maximum and minimum statistics for the curve and contour angles, are then extracted. Different conventional machine learning approaches, such as KNN, CART and SVM, are applied. To evaluate the proposed method, a dataset containing 220 different images is used in a 10-fold cross-validation scheme. Different performance measures resulting from the evaluations demonstrate the effectiveness and applicability of the method.

Keywords: carpet quality assessment, carpet back sizing, digital image processing, machine learning, edge detection

## Izveček

*Mehanske lastnosti preproge, kot so dimenzijska stabilnost, upogibna togost, otip in drsenje na površini med rabo, so neposredno povezane s količino zamreževala, nanesenega na hrbtno stran preproge pri procesu izdelave. Opti-*

malno količino zamreževala in mehanske lastnosti preproge pri izdelavi danes ocenjuje operater z ročnim otipom preproge v strojni liniji v fazi plemenitenja ali med njenim zvijanjem v svitek. V članku je predlagan samodejni postopek, ki temelji na ocenjevanju upogibne togosti utrjene preproge. Ta zajema obdelavo digitalne slike in strojnega učenja za določitev optimalne koncentracije zamreževala in njenega nadzora. V ta namen je bila preproga v zadnji fazi izdelave na sredini prepognjena, pri čemer sta bila dva robova preproge položena drug na drugega. Nato so bile posnete fotografije preproge s stranskim pogledom. Z metodami zaznavanja robov so bili razpoznavni robovi preproge, za krivulje obrisa in kotov krivulje obrisa pa določeni statistični parametri, kot so srednje, minimalne in maksimalne vrednosti. Uporabljeni so bili različni konvencionalni pristopi strojnega učenja, kot so KNN, CART in SVM. Za ovrednotenje predlagane metode z 10-kratno navzkrižno validacijo so bili uporabljeni podatki 220 različnih fotografij. Različna merila uspešnosti, ki izhajajo iz ocen, so dokazala učinkovitost in uporabnost metode.

*Ključne besede:* ocena kakovosti preproge, utrjevanje hrbtni strani preproge, digitalna obdelava slik, strojno učenje, zaznavanje robov

---

## 1 Introduction

Mechanical and visual properties significantly affect the quality of the carpet. Mechanical properties are used to explain dimensional stability, comfort while walking on the carpet and abrasion properties in use, while visual properties are used to explain the appearance of the carpet. To respond to the demand for measuring the visible properties of carpets, many methods and useful tools have been used in the past, including microscopy, photography, densitometry, reflectometry and image processing. The work done in evaluating the mechanical properties of the carpet often relates to the reversibility of the carpet under static or dynamic load. Another characteristic that has been studied in the evaluation of the mechanical properties of the carpet is the fatigue mechanism of the carpet. Fatigue mechanism refers to the durability of carpet piles against shear forces during use, which may cause the piles to come out of the carpet, and is evaluated by weighing the carpet before and after use or testing [1–3].

Gentry [4] investigated the effect of the type of backing, the density of the tufting machine needle, and the density of the piles per surface unit in a study on carpets that had different primary and secondary backings. One of the important indicators of carpet efficiency is the durability of the carpet's appearance during use. Among the things that can affect these

characteristics is the type, quality and quantity of the latex (resin) on the back of the carpet [5, 6]. In today's factories, the optimal amount of latex is controlled by touching the carpet with fingers on the production line or when rolling the carpet. The method of checking by a human agent usually leads to defects and inherent errors that make this difficult. The need for automatic methods is thus greater than ever. Although machine carpet factories are in the midst of a technological transformation, the benefits of using computer-assisted manufacturing (CAM) methods are becoming established in this industry.

Because the amount of resin transferred to the back of the carpet on the finishing line is influenced by many variables and affects many variables of the mechanical properties of the carpet, the optimal amount of resin that is placed on the back of the carpet must be determined and controlled. Bending stiffness is effective in terms of characteristics such as handle, shrinkage and resistance to wrinkles [7]. In the past, many experimental methods have been developed to measure indicators that can quantitatively express the bending stiffness of textiles. Those methods can be divided into two categories. The first category comprises methods that deal with the measurement of the movement, force or energy required to cause bending deformation. The second category involves the measurement of the deformation of the fabric under the influence of its own weight. The

tests based on the second method are simpler and faster, provide better control of the final product and can even be shared online [8].

One of the methods of expressing bending stiffness using the deformation of the fabric under the influence of its own weight, which was invented by Pierce, is the measurement of bending length. Bending length is the length of fabric that bends under the influence of its own weight at a certain angle. A longer bending length means a fabric is harder. The authors of [9] stated that this height of the loop is proportional to bending length measurement and can be used to calculate bending length. In other words, harder fabrics create a higher loop than limper fabrics. Figure 1 shows the basis of this method. Zhou and Ghosh [9] measured the bending behaviour of fabric in terms of the sensitivity of their sizes to shape change. Four types of loops were used for this purpose. Type 1 loops were created by hanging the fabric vertically between two rollers, and type 2 loops were obtained by turning the fabric on itself while there was a separating plate between them. Type 3 and 4 loops were obtained by holding the fabric between two clamps. Each loop was described by several features.

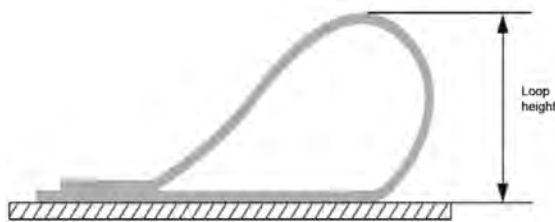


Figure 1: Basis of the fabric folded loop test [9]

There are a few works that have proposed image processing or other automatic artificial intelligence-based approaches for the quality assessment of fabrics and carpet. In [10], Cassidy et al. used a bending box to measure the bending properties of fabrics whose bending length is difficult to calculate using Pierce's method. They stated that the width and length of the fabric that are placed on top of each other have a negligible effect on the height of

the loop. Xu [11] presented an approach based on image processing to measure the appearance of the carpet, in which the image parameters such as shape, direction and spatial patterns that the human agent uses visually when evaluating the carpet were automatically analysed. Quinones et al. [12] presented a solution based on geometric local binary patterns to examine carpet warp and weft images, which measured the carpet quality based on the balance of grey points in the images. Shady et al. [13] presented a method to evaluate fabric structure characteristics using a Wiener filter to detect weave patterns.

In [14], convolutional neural networks (CNNs) were used as a classification tool for the patterns and colours of the carpets. In [15], visual spectral comparator (VSC) and conventional CT scanning were used for the visual examination of the weaving details and present condition of two 17th-century knotted-pile carpets. An interesting work regarding the use of machine learning, in particular deep learning approaches, in the carpet industry is [16], which proposed deep convolutional generative adversarial networks (GANs) for automatic carpet pattern design and creation. In [17], a method for comparing two carpet photos and determining the best placement of several carpet images was proposed.

The present work, is the first study that attempts to propose a machine learning and image processing-based approach for estimating the amount of coated resin on the back of the carpet and find an automatic method to assess the mechanical quality of carpets. In this research, we first attempted to evaluate and measure the characteristics of the arc in the carpet as a reflection of the bending stiffness by hanging a part of the carpet between two rollers. After coming off the sizing line, the carpet was placed on a flat surface and turned over on itself, and an analysis was performed on the arc created in the carpet in this state. A series of transformations and operations were then performed to extract features, which seemed effective in characterizing the bending loop. Using the extracted features from the images, conventional machine learning classifiers were

trained to discriminate and decide on the amount of the coated resin and to classify carpets based on this aspect.

The rest of this paper is organized as follows. Section 2 presents materials and methods. Experimental setup and evaluation results are presented and discussed in Section 3. Finally, Section 4 presents conclusions and the bases for future works.

## 2 Materials and methods

### 2.1 Experimental data

In this research, bending stiffness was used as a feature that is influenced by the amount of resin on the back of the carpet for evaluating the mechanical properties thereof. After the carpet came off the sizing line and was placed on a flat surface, it was fold-

ed in the middle; the two edges of the carpet were placed on top of each other and the created curve was then photographed. The amount of protrusion and arch resulting from the folding of the carpet was measured. To evaluate the optimal amount of resin in carpet back sizing, samples of carpets with a density of 490 piles/cm (reed 700 dents/m, weft density 1400 ends/m) were selected. Other structural parameters were as follows: warp yarn count 29.5/4 tex, 80% polyester/20% cotton; weft yarn count 44.8/2 tex jute; pile yarn count 49.2/2 tex acrylic. The resin used was vinyl acetate homopolymer. The prepared samples were divided into five equal parts with a width of 60 cm and a length of 180 cm. One part was coated with the appropriate and optimal amount of resin, and four other parts were coated with 10% and 20% more and less resin than usual, as shown in Figure 2.

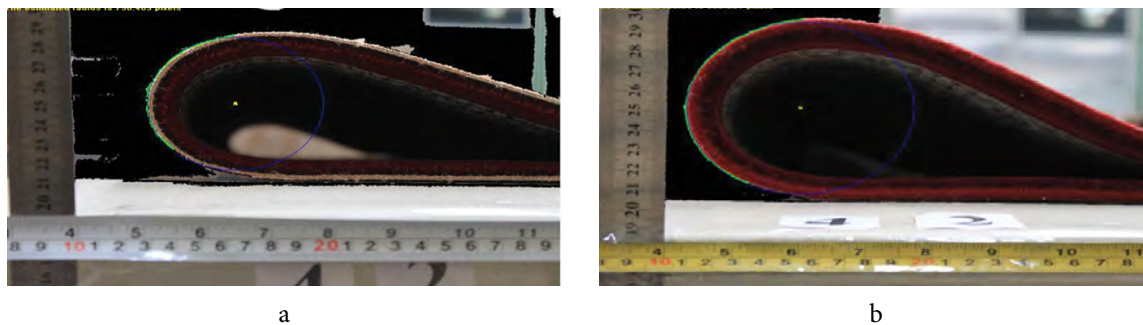


Figure 2: Radius of curvature of the arc formed in the folded carpet a) before back sizing b) after back sizing

The optimal and usual amount of resin to reach the appropriate density in the factory from which the sample was prepared was 135 grams of dry matter per square meter. A 12 Megapixel CCD camera was used for image capturing, where the working distance, or the distance between the objective lens and the folded carpet, was set at 60 cm. The colour temperature for the setting was between 5000 K and 5500 K, and diffuse LED lighting was used as the applied lighting configuration. A total of 220 photos were taken of each of sample, and were used for testing, verifying and comparing edge detection methods. In this way, carpets were classified according to quality in the following six predefined categories:

negative 10 relative sizing, negative 20 relative sizing, normal sizing, positive 10 relative sizing, positive 20 relative sizing and pre-sizing.

### 2.2 Image processing and feature extraction procedure

The proposed image processing and feature extraction process is presented in this section. For this purpose, first the outer contour (outer edge) of the carpet was extracted, followed by the average, maximum and minimum statistics for the curve and angles of the contour. To extract features from folded carpet images, the edges of the carpet had to be detected in the images. Edges are local changes in

image brightness. On the other hand, shadow changes result in brightness changes but are not edges. For this reason, extracting the true working edges was difficult.

A large number of edge detection operators function based on the first derivative of the brightness intensity. Derivatives of an image show changes in brightness in both vertical and horizontal directions. Several operators were presented to calculate local derivatives. Sobel is the best and most general derivative calculation operator. From the convolution of windows and in the image, the derivatives in the x and y directions were calculated, respectively. In equations 1 and 2, represents the derivative in the x direction and represents the derivative in the y direction [18].

$$G_x = \frac{1}{8} \begin{bmatrix} -1 & 0 & 1 \\ -2 & 0 & 2 \\ -3 & 0 & -1 \end{bmatrix}$$

$$I'_x(i,j) = \frac{1}{8}(-I(i-1, j-1) - 2 * I(i,j-1) - I(i+1, j-1) + I(i-1, j+1) + 2 * I(i,j+1) + I(i+1, j+1)) \tag{1}$$

$$G_y = \frac{1}{8} \begin{bmatrix} 1 & 2 & 1 \\ 0 & 0 & 0 \\ -1 & -2 & -1 \end{bmatrix}$$

$$I'_y(i,j) = \frac{1}{8}(I(i-1, j-1) + 2 * I(i-1,j) + I(i-1, j+1) - I(i+1, j-1) - 2 * I(i+1,j) - I(i+1, j+1)) \tag{2}$$

To calculate the magnitude of the gradient, the square root of the derivatives was calculated in two directions, as in equation 3. This relation was calculated for each pixel of the image.

$$G_{Magnitude} = \sqrt{I'_x + I'_y} \tag{3}$$

It should be noted that, as a rule, all the points of an image have some difference relative to their adjacent points. Thus, the magnitude of the gradient will not be zero for most points. On the other hand, there is a considerable difference with their neighbours at edge points. For this reason, thresholding can be used to distinguish edges from non-edges.

### 2.2.1 Fixed threshold limit edge detection

The simplest solution to determine the edge is fixed thresholding on the magnitude of the gradient. In other words, the magnitude of the gradient for all points of the images is compared with a predefined threshold. If the magnitude of the gradient is greater than the threshold, that point is located on the edge. In equation 4, represents the magnitude of the gradient of the pixel, T represents the threshold and E represents the existence of an edge point at

$$E(i,j) = \begin{cases} 1 & \text{if } G_M(i,j) > T \\ 0 & \text{else} \end{cases} \tag{4}$$

Considering the variety of the colour of carpets, as well as the different darkness and brightness of the upper and lower background of the carpet, using a fixed threshold to determine the edge does not provide a favourable result.

### 2.2.2 Canny edge detection

Canny is one of the most common edge detection algorithms. Since the images have noise and small edge changes, a smoothing filter can be applied to the image. A smoothing filter is a filter that removes small changes in the image. In this way, image noises are removed. Most smoothers consider the weighted average of the neighbouring points of each pixel as the new value of the pixel. Many smoothers are proposed according to the size of the neighbourhood and weight matrixes. Canny edge detection uses a Gaussian smoothing filter (equation 5). This relation defines the weight of the neighbouring points, in which x and y are the coordinates of the neighbouring point and σ is the smoothing parameter. From the convolution of the window with the image, the smoothed image is obtained [19].

$$G(x,y) = \frac{1}{2\pi\sigma^2} e^{-\frac{x^2+y^2}{2\sigma^2}} \tag{5}$$

After applying the Gaussian filter, the gradient of the image was calculated using equation 3 to identify

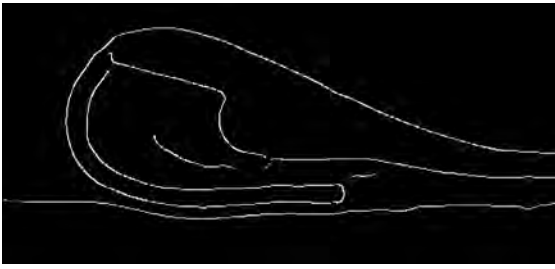


Figure 3: Edges extracted using canny edge detection

the areas with the highest changes. Canny uses two thresholds for the edge determination step. If the magnitude of the gradient is less than the small threshold, its value is set to zero, i.e. it is not considered an edge. If its value is between two threshold limits, its value becomes one if there is a path from this pixel to another pixel with a gradient higher than the second threshold limit (upper limit), and if the pixel value is greater than the upper threshold, we select that pixel as the edge. To increase the accuracy of edge detection, the primary smoothing filter and the gradient window can be changed. Moreover, an edge thinning algorithm was applied at the end of the work.

The use of edge detection methods in determining the edge of the carpet created many unwanted

edges that cannot be easily removed. The edges resulting from canny edge detector are shown in Figure 3.

### 2.2.3 Pixel navigation

It is evident from Figure 3 that edges inside the carpet were also detected in the Canny method. Since the colour of the carpets has many variations, and black and white colours are also used within the carpets, Canny edge detection considers the top black background to be the same as the inside of the carpet. This may result in many false positives in edge point detection. Thus, to make the edge extraction simpler and more accurate, pixel navigation was used.

Since only the top and left edges of each carpet were needed, the pixel traversal method was suitable for obtaining these edges. In the available image, the background colour is very different from the edge of the carpet. Thus, by scrolling vertically from top to bottom, the image of the upper part of the contour was obtained, and by scrolling horizontally from left to right, the side part of the outer contour of the carpet was obtained. Figure 4 shows how to calculate the contour using the pixel navigation method.



a



b

Figure 4: Determining contour using the pixel navigation method: a) Contour obtained after vertical navigation; b) Contour obtained after horizontal navigation

In vertical pixel navigation, navigation starts from the top of the image and each pixel is compared with its bottom pixel. If their difference is greater than a certain threshold, it is an edge pixel. In equation 6, which determines the final edges of the image,  $\text{abs}()$  represents the absolute value function.

When the first edge point is seen in a column, the navigation of that column ends.

$$E(i,j) = \begin{cases} 1 & \text{if } \text{abs}(I(i,j) - I(i,j+1)) > T \\ 0 & \text{else} \end{cases} \quad (6)$$

### 2.2.4 Jump-based pixel navigation

In the pixel navigation method, the distance between the value of two neighbouring pixels,  $p$  and  $q$ , is calculated at each step of the navigation, and if that distance is lower than the threshold, it means that the contour is not yet found. In this situation, the algorithm moves one pixel down in the column. This single pixel navigation method works very slowly in high resolution images. To improve the pixel navigation method, jump-based pixel navigation can be used.

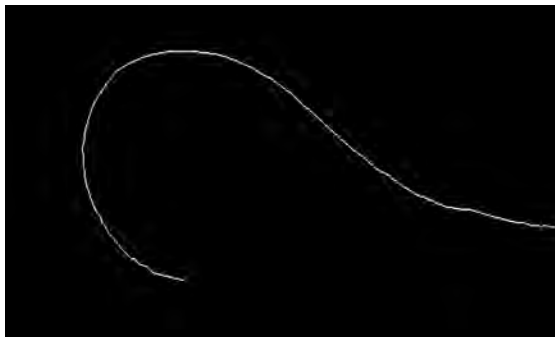
In this approach, navigation is done in multi-pixel steps. A navigation step of  $s$  is used for this purpose, and each pixel is compared with a pixel in the column-wise spatial distance of  $s$ . Moreover, to increase the resistance of the method to noise, the average values of five adjacent pixels are considered instead of comparing the values of two pixels. These two approaches for determining the edge point positions are denoted in equation 7.

Horizontal row-wise scrolling was also performed to calculate the left contour to increase the

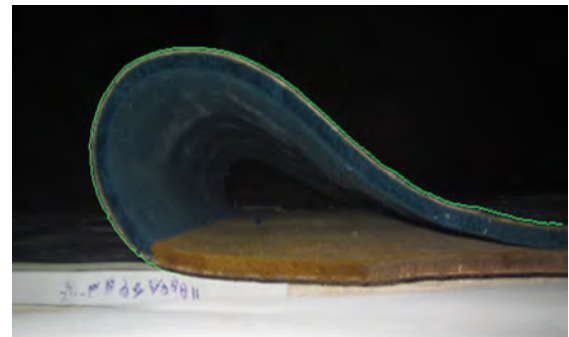
speed and accuracy, and the contour obtained from the previous step was used. Since the contour is continuous, the location of the contour in each row is close to the location of the contour in the upper row. Thus, horizontal scrolling was performed to obtain the exact location of the contour near the contour location of the upper row. Supposing that  $(r, c)$  was the location of the contour in the previous line, horizontal scrolling was performed in the spatial row-wise distance of  $(r, c-k)$  and  $(r, c+k)$ , where  $k$  is an arbitrary number. Again in horizontal scrolling, instead of comparing the value of two adjacent pixels, the average difference, as calculated in equation 7, was used.

After determining the edges, probable noises were removed using a morphological thinning operation, which is a morphological closing followed by a morphological opening to repair possible edge discontinuities. After morphological operations, carpet contour with a thickness of one pixel is obtained. Figure 5 shows the contour calculation steps.

$$E(i, j) = \begin{cases} 1 & \text{if } \text{abs}(\frac{1}{5} \sum_{n=-2}^2 I(i, j+n) - \frac{1}{5} \sum_{n=-2}^2 I(i, j+s+n)) > T \\ 0 & \text{else} \end{cases} \quad (7)$$



a



b

Figure 5: Contour resulting from the jump-based pixel navigation method: (a) final contour after the morphology operation; (b) location of the contour on the carpet

### 2.2.5 Comparing the proposed edge detector

In this section, a comparison is made between the stated methods on real images. The results of applying different edge detection methods are shown in Figure 6. As is evident, the methods of fixed threshold and Canny (b and c) created many unwanted

edges, while the pixel navigation method determined a pure edge contour for the carpet. The results of the application of pixel navigation and jump-based pixel navigation are similar in most cases, while the latter was faster.

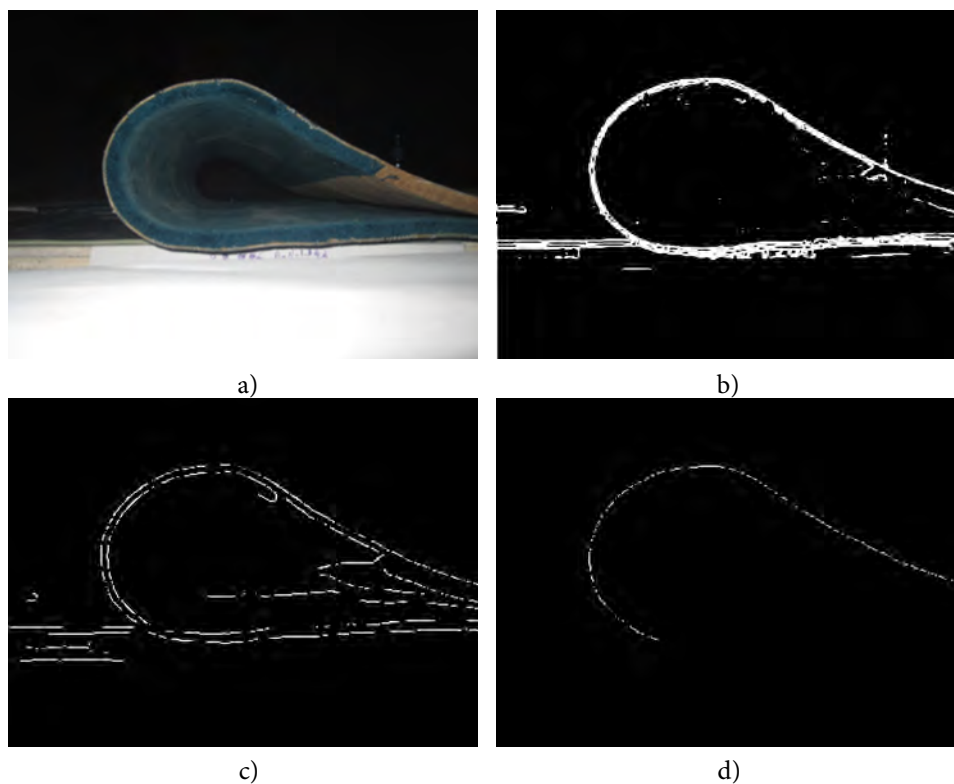


Figure 6: Results of the application of different edge detection methods: (a) original image; (b) fixed threshold method; (c) Canny method; (d) proposed navigation method

As seen in the pictures, the jump-based pixel navigation method demonstrated good accuracy and its execution speed can be increased by adjusting the jumping parameter. The results of the implementation of this method on 220 carpet images show that it can accurately identify the edges of the carpet at a suitable speed. The results of the edge detection were then used for carpet classification based on the contour. Different features, such as carpet curvature, angle, length-to-width ratio and contour radius, were extracted and used for the quality classification of manufactured carpets. It is also evident that the lower edge was omitted, since the lower edge of the carpet does not possess any information regarding fold and curvature.

#### 2.2.6 Feature extraction

For classification purposes, we needed to extract descriptive features from the curvatures resulting

from the edge detection step. These features should express the curvature of the carpet. For this purpose, the features of carpet curvature, including the angle of the oblique line, length-to-width ratio and contour radius, were extracted, as shown in Figure 7.

The features of the length-to-width ratio and the angle of the oblique line that each carpet makes with the horizontal axis were independent of the distance of the camera from the carpet. The maximum and minimum column difference of the contour denotes the width, while the maximum and minimum row difference of the contour denotes the length of the curvature. Using the Hough transform, which is a transformation that finds geometric shapes in an image, the largest interior curvature of the carpet was obtained. To make it independent from the distance between the camera and the carpet, it was then divided by the length-to-width ratio feature.

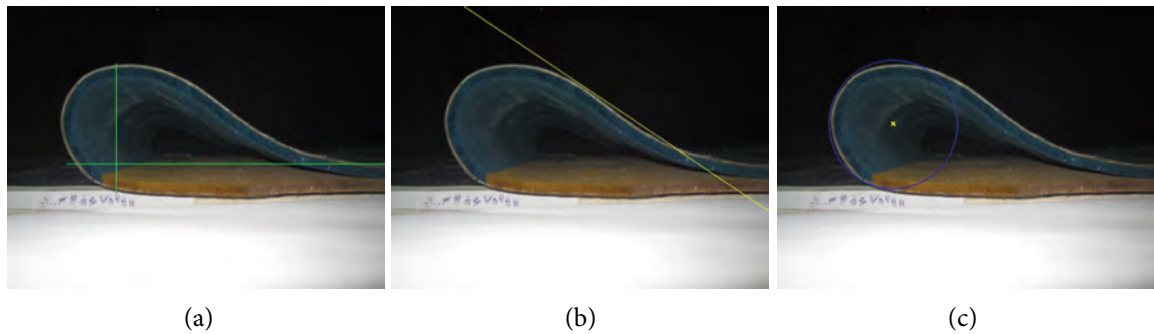


Figure 7: First three primary features of the curvature: a) length-to-width ratio; b) the angle of the oblique line; c) contour radius

On the other hand, the contour of the carpet is a curve, and the main goal was to describe this curve in such a way that it could help the classification process. Hence, the coefficients of this curve were considered features of the contour. For this purpose, equation 8 was used to calculate the curvature or bending of a contour, where  $p$  and  $q$  are the pixel coordinates at the beginning and end of a contour segment, respectively. Moreover, equation 9 denotes the angle of curvature between two edge points  $p$  and  $q$ . In fact, the curvature is the ratio of the Euclidean distance to the Manhattan distance of the first and last pixels of the sequence.

$$\text{Curvature} = \text{Euclidean distance } (p, q) / \text{Manhattan distance } (p, q) \quad (8)$$

$$\text{Angle} = \arctan(q_y - p_y / q_x - p_x) \quad (9)$$

where  $q_x$  and  $q_y$  represent the  $x$  and  $y$  coordinates of point  $q$ . Since calculating a single value does not reflect the total shape of the curve, edge pixels were sorted from the right-most pixel to the left-most pixel. The array was then divided to  $C$  parts and, considering the points at the beginning and end of each segment, the curvature features were calculated for each one. The curvature and angle statistics of these  $C$  segments, including the maximum, minimum and mean values, were then determined as the final describing features. In summary, the extracted features for describing the contour of the folded carpet are as presented in Table 1.

Table 1: Extracted features from the contour of the folded carpet

Feature	No. of coefficients
Length-to-width ratio	1
Angle of the oblique line	1
Folding radius	1
Curvature statistics (i.e. maximum, minimum and mean of the curvature)	3
Angle statistics (i.e. maximum, minimum and mean angle of the angle)	3

The initial size of the images was  $3000 \times 4000$  pixels. However, to reduce the calculations, the size of the images was changed to  $375 \times 500$  pixels. Also, other parameters of the approach were set according to Table 2.

### 3 Experimental results and discussion

After feature extraction, three different methods were used as learners and classifiers. In the following evaluations, three traditional classifiers, i.e. K nearest neighbour (KNN), classification and regression tree (CART) and support vector machine (SVM), are used. Although deep learning approaches are the most recent classification paradigms, they could not be applied because the problem was a low dimensional one and the size of the evaluation database was not large. Since SVM is a binary classifier, it was trained in a one-versus-all scheme.

All the experiments were performed using the Windows 10 Pro operating system with an i5 core (3.20 GHZ) CPU and 16 GB of RAM, while Python version 3.6 was used to implement the proposed method. Traditional 10-fold cross validation was used for evaluations and classification accuracy, which is the number of correct decisions divided by the total number of reported decisions as the evaluation metric.

Table 2: Values of parameters of specific approach

Parameters	Values
S	20
K	10
C	30
T	10

### 3.1 Discussion about features

The first step was to analysis the discriminating power of the extracted features. To do so, the histograms of the features were plotted and compared in Figures 8 and 9. Figure 8 illustrates the distribution of the folding radius feature for different classes, while Figure 9 presents a histogram of the angle of the oblique line

for the five different classes. As seen in both figures, different classes have wide overlapping regions considering the two investigated features, while the features are not discriminative by themselves. For example, as seen in Figure 8, all neighbouring and similar classes have a decision region in common, which is approximately half of the width of the distribution. On the other hand, it can clearly be seen that even two distant classes have common decision regions. This means that the features are not independently good ways for differentiating between the classes. It is the main reason that classification models are trained using a set of nine different features and used for the decision.

Another measure for determining the discriminating power of the features is the Fisher ratio. The Fisher ratio can quantify the discriminativeness of the features and is the ratio of between-class scatter to within-class scatter. Since the problem was a multiclass classification problem, we had to average the value over all possible class combination as denoted in equation 10. The Fisher ratio values are summarized in Table 3 for each feature. As denoted, features such as the angle of the oblique line and folding radius had the highest Fisher ratio, which indicates the greater effectiveness of the features.

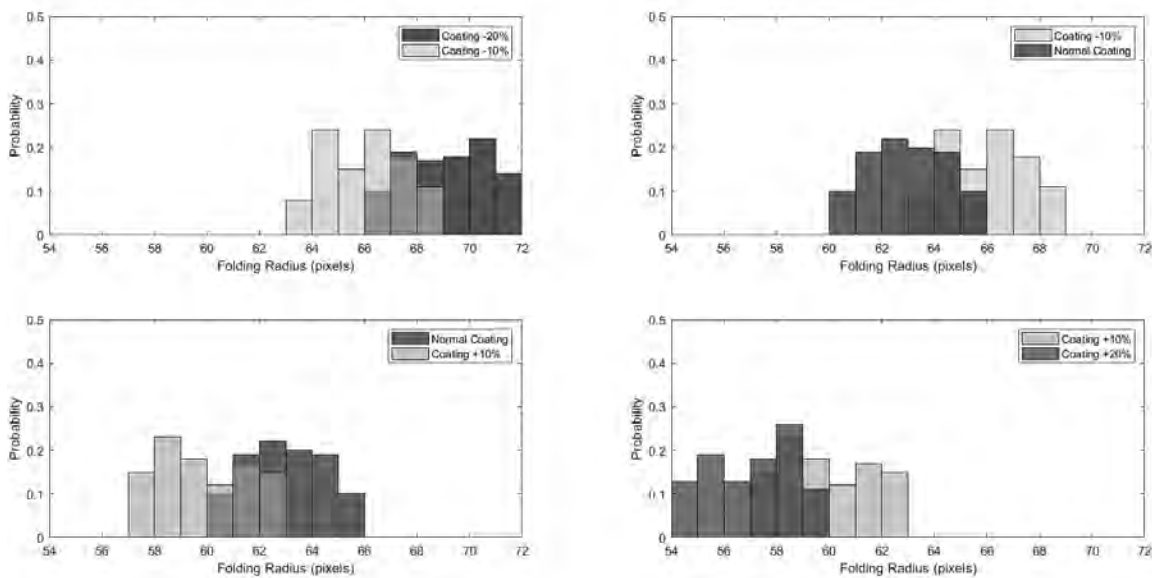


Figure 8: Distribution of folding radius feature for different classes. The overlap between every two classes is shown in a different colour.

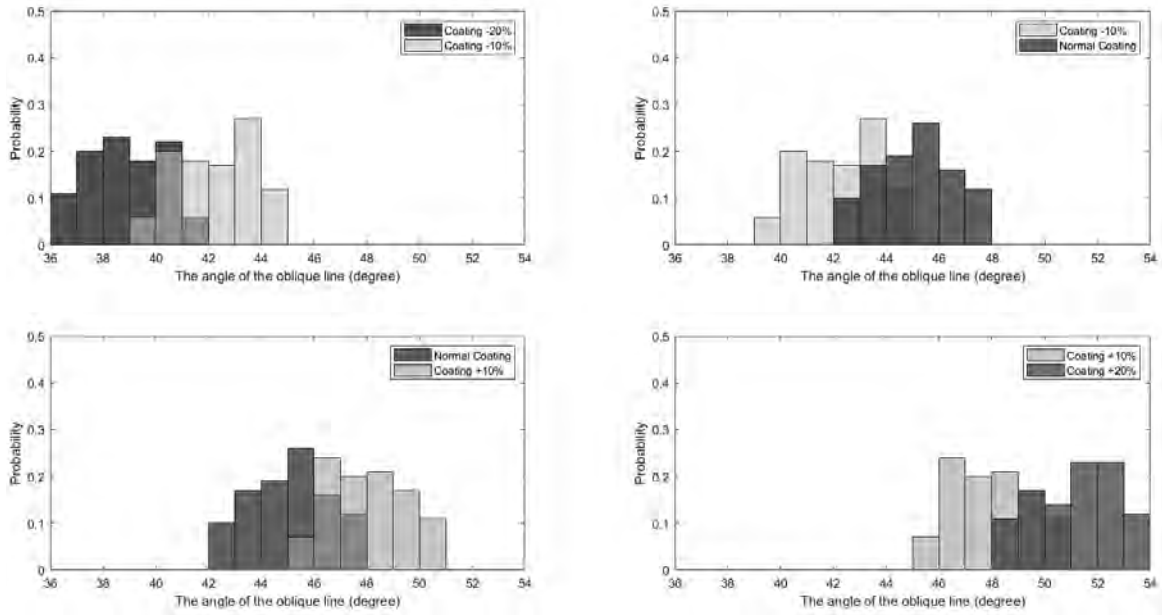


Figure 9: Distribution of the folding angle of the oblique feature for different classes. The overlap between every two classes is shown in a different colour.

$$Average_{Fis} \text{ ratio} = \frac{2}{Nc(Nc - 1)} \sum_{i=1}^{Nc} \sum_{j=i+1}^{Nc} \frac{(m_i - m_j)^2}{v_i + v_j} \tag{10}$$

### 3.2 Discussion about classification results

Since the features were not effective by themselves, a second phase of feature transformation using linear discriminant analysis (LDA) was performed on the initial feature vector of size 9. LDA is usually used as a dimension reduction approach, but here it was used for feature transformation. Table 4 indicates the classification performance of each machine learning model, with and without LDA. Moreover, since the evaluations were performed in a 10-fold cross validation scheme and the results were averaged, performance standard deviations are also included in the table.

The best accuracy on each assessment condition is shown in italics and the best overall accuracy is denoted in bold typeface. Moreover, for the better discussion of the results, the average accuracies of the classifiers are summarized in the last column. The number in parenthesis indicates the rank of each

Table 3. Average Fisher ratio of each extracted feature

Feature category	Feature name	Average Fisher ratio
Length-to-width ratio		4.11
Angle of the oblique line		11.42
Folding radius		10.64
Curvature	Min. curvature	2.3
	Max. curvature	9.21
	Average curvature	7.43
Curvature angle statistics	Min. angle	1.2
	Max. angle	14.5
	Average angle	10.23

classifier based on its average performance. In this table, the classifiers are also evaluated with different parameters and settings. For the SVM classifier, two different traditional kernel functions, referred to as radial basis functions (RBF), and a linear kernel were investigated. KNN classifier is evaluated with different K values (i.e. 3, 5, 7). Since there were not

many samples in the classes, higher values for K are not useful. In addition, as seen in the table, the average performance of the KNN classifier degrades when K increases to 7.

Table 4: Classification accuracy of the different classifiers on the proposed approach

Classifier	Parameters	LDA	Accuracy (%)	Average accuracy (%)
SVM	RBF kernel	No LDA	76.11±2.83	<b>85.19 (1)</b>
		LDA(d = 3)	82.44±3.57	
		LDA(d = 4)	<b>91.69±2.85</b>	
		LDA(d = 5)	90.54±3.01	
	Linear kernel	No LDA	69.13±3.37	79.77 (4)
		LDA(d = 3)	82.13±3.60	
LDA(d = 4)		88.08±3.4		
KNN	K = 3	No LDA	69.60±4.07	80.32 (3)
		LDA(d = 3)	79.78±7.18	
		LDA(d = 4)	86.51±4.37	
		LDA(d = 5)	85.39±6.98	
	K = 5	No LDA	72.29±5.93	81.09 (2)
		LDA(d = 3)	77.15±7.06	
		LDA(d = 4)	88.94±7.53	
		LDA(d = 5)	85.99±4.46	
	K = 7	No LDA	68.28±7.92	78.46 (6)
		LDA(d = 3)	79.66±5.9	
		LDA(d = 4)	87.89±5.96	
		LDA(d = 5)	78.02±5.56	
CART	No LDA	68.04±3.12	78.67 (5)	
	LDA(d = 3)	78.75±6.62		
	LDA(d = 4)	85.99±5.35		
	LDA(d = 5)	81.93±6.9		

The results of Table 4 are also summarized in Figure 10. This figure illustrates both the effectiveness of the SVM classifier and the LDA feature transformation. This figure shows that using LDA can considerably increase the classification accuracy of the approach, with SVM with an RBF kernel being the best choice on this problem from amongst the evaluated classifiers.

A lingering concern is the time complexity of the process, especially the proposed edge detection approach. Table 5 presents the running time of the edge detection process and shows the lower computational time of the proposed edge detector. It should be noted

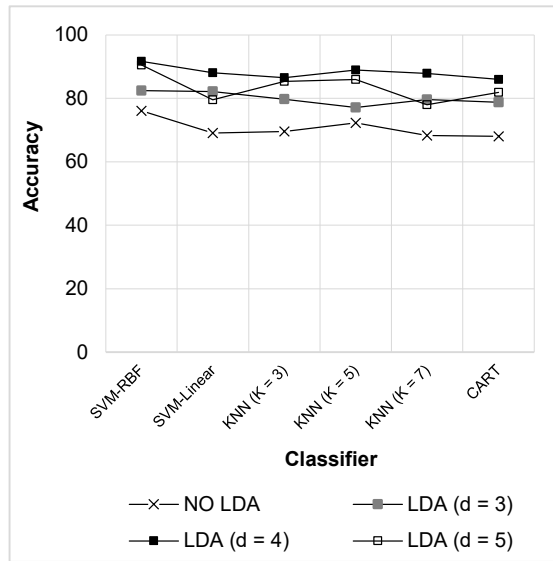


Figure 10: Classification accuracy of the different classifiers on the proposed approach

Table 5: Average processing time of the edge detection approaches per image

Method	Processing time (s)
Fixed threshold	0.0164
Canny edge detection	0.246
Pixel navigation	0.0047
Proposed jump-based pixel navigation	0.0041

that the proposed edge detector is customized for this problem and its efficiency is due to the fact that the edge detection process is designed specifically for this problem.

## 4 Conclusion

This paper represents the first attempt at the mechanical quality assessment of the carpets based on the amount of their back sizing using an automatic image processing and machine learning based approach. The approach proposes a novel edge detection scheme for this purpose, which is followed by the extraction of representative features. A traditional LDA approach was the used for feature determination and was followed by some

traditional simple classifiers, from which SVM with an RBF kernel demonstrated the best results. The evaluations show the effectiveness of the proposed approach in determining the number of coatings and the achievement of a classification accuracy of 91.69 percent. Moreover, the proposed approach was evaluated from a computational time point of view, which proves the real time applicability of the method. For future works, using the back texture of the carpet is suggested for the purpose of quality assessment. More complex learning approaches, such as convolutional neural networks, may be better suited for this purpose.

*Availability of data and materials: The datasets used and/or analysed during this study are available from the corresponding author upon reasonable request.*

*Competing interests: The authors hereby declare that they have no known competing financial interests or personal relationships that could have influenced the work reported in this paper.*

*Funding: The authors hereby declare that no funding was received for this research.*

## References

1. ÖNDER, Emel, BERKALP, Ömer Berk. Effects of different structural parameters on carpet physical properties. *Textile Research Journal*, 2001, **71**(6), 549–555, doi: 10.1177/004051750107100613.
2. DAYIARY, M., SHAIKHZADEH NAJAR, S., SHAMSI, M. A new theoretical approach to cut-pile carpet compression based on elastic-stored bending energy. *The Journal of the Textile Institute*, 2009, **100**(8), 688–694, doi: 10.1080/00405000802170242.
3. DAYIARY, M., SHAIKHZADEH, NAJAR S., SHAMSI, M. An experimental verification of cut-pile carpet compression behavior. *The Journal of the Textile Institute*, 2010, **101**(6), 488–494, doi: 10.1080/00405000802542242.
4. GENTRY, David R. Dimensional stability of carpets in installation: part I: stability to mechanical actions. *Textile Research Journal*, 1977, **47**(7), 459–463, doi: 10.1177/004051757704700703.
5. ERDOĞAN, Ümit Halis. Effect of pile fiber cross section shape on compression properties of polypropylene carpets. *The Journal of the Textile Institute*, 2012, **103**(12), 1369–1375, doi: 10.1080/00405000.2012.685558.
6. TAYLAN, Osman, DARRAB, Ibrahim A. Fuzzy control charts for process quality improvement and product assessment in tip shear carpet industry. *Journal of Manufacturing Technology Management*, 2012, **23**(3), 402–420, doi: 10.1108/17410381211217434.
7. STUART, I.M., BAIRD, K. A new test for bending length. *Textile Research Journal*, 1966, **36**(1), 91–93, doi: 10.1177/004051756603600112.
8. ZHOU, Naiyue, GHOSH, Tushar K. On-line measurement of fabric bending behavior: part I: theoretical study of static fabric loops. *Textile Research Journal*, 1997, **67**(10), 712–719, doi: 10.1177/004051759706701003.
9. ZHOU, Naiyue, GHOSH, Tushar K. On-line measurement of fabric-bending behavior: background, need and potential solutions. *International Journal of Clothing Science and Technology*, 1998, **10**(2), 143–156, doi: 10.1108/09556229810213845.
10. CASSIDY, T., CASSIDY, C., CASSIE, S., ARKISON, M. The stiffness of knitted fabrics: a new approach to the measurement of bending: part 1: development. *International Journal of Clothing Science and Technology*, 1991, **3**(5), 14–19, doi: 10.1108/eb002982.
11. XU, B. Assessing carpet appearance retention by image analysis. *Textile Research Journal*, 1994, **64**(12), 697–709, doi: 10.1177/004051759406401201.
12. QUINONES, Rolando, ORJUELA, Sergio A., ORTIZ-JARAMILLO, Benhur, VAN LANGENHOVE, Lieva, PHILIPS, Wilfried. Quantifying appearance retention in carpets using

- geometrical local binary patterns. In *Advanced Concepts for Intelligent Vision Systems. ACIVS 2011. Lecture Notes in Computer Science, vol 6915*. Edited by Jacques Blanc-Talon, Richard Kleihorst, Wilfried Philips, Dan Popescu and Paul Scheunders. Berlin, Heidelberg : Springer, 2011, doi: 10.1007/978-3-642-23687-7\_30.
13. SHADY, Ebraheem, QASHQARY, Khadijah, HASSAN, Mounir, MILITKY, Jiri. Image processing based method evaluating fabric structure characteristics. *Fibres & Textiles in Eastern Europe*, 2012, 6A(95), 86–90.
  14. HOSSEINI, Sayedeh Marjaneh, MOHAMMAD-DJAFARI, Ali, MOHAMMADPOUR, Adel, MOHAMMADPOUR, Sobhan, NADI, Mohammad. Carpets color and pattern detection based on their images. *Proceedings*, 2019, 33(1), 1–7, doi: 10.3390/proceedings2019033028.
  15. SERRANO, Ana, MEIJER, Suzan, VAN RIJN, Rick R., COBAN, Sophia Bethany, REISLAND, Birgit, HERMENS, Erma, BATENBURG, Kees Joost, VAN BOMMEL, Maarten. A non-invasive imaging approach for improved assessments on the construction and the condition of historical knotted-pile carpets. *Journal of Cultural Heritage*, 2021, 47, 79–88, doi: 10.1016/j.culher.2020.09.012.
  16. GÜRBÜZ, Feyza, EYI, Sabiha Unal. New carpet pattern design with deep learning. *Journal of Engineering Research*, 2023, online first, doi: 10.36909/jer.16781.
  17. LI, Ming, HAM, Chan, WANG, Ying. Similarity inspection and optimal arrangement of carpet images using deep learning and genetic algorithms. In *IEEE 2020 SoutheastCon Proceedings*. Raleigh : IEEE, 2020, 1–2, doi: 10.1109/SoutheastCon44009.2020.9249722.
  18. RUSS, John C. *The image processing handbook*. Boca Raton : CRC Press, Taylor & Francis, 2007.
  19. GOLABI, Sasan, SAADAT, Saiid, HELFROUSH, Mohammad Sadegh, TASHK, Ashkan. A novel thinning algorithm with fingerprint minutiae extraction capability. *International Journal of Computer Theory and Engineering*, 2012, 4(4), 514–517, doi: 10.7763/IJCTE.2012.V4.522.

Volodymyr Dvorzhak,<sup>1</sup> Mykola Rubanka,<sup>1</sup> Alla Rubanka,<sup>1</sup> Oleh Polishchuk<sup>2</sup>

<sup>1</sup> Kyiv National University of Technologies and Design, Mala Shyianovska (Nemyrovycha-Danchenka) Street, 2, 01011 Kyiv, Ukraine

<sup>2</sup> Khmelnytskyi National University, 11, Instytut'ska str., Khmelnytskyi, 29016, Ukraine

---

# Computer Modelling of Yarn Winding on Conical Bobbins

## *Računalniško modeliranje navijanja preje na stožčaste navitke*

*Original scientific article/Izvirni znanstveni članek*

Received/Prispelo 9-2023 • Accepted/Sprejeto 10-2023

Corresponding author/Korespondenčni avtor:

**Assoc. Prof. Volodymyr Dvorzhak, Ph.D.**

E-mail: dvorzhak.vm@knutd.edu.ua

ORCID: 0000-0002-1693-9106

---

### Abstract

The article presents the results of the computer modelling of yarn winding on conical bobbins based on the analytical method of constructing tubular-shaped surfaces as a partial case of channel surfaces using the vector algebra apparatus. It is stated that the guide line takes the shape of a conical spiral line along which the forming moves (in the form of a circle with a diameter equal to the average diameter of the yarn), and is set using the moving Frenet basis. The obtained mathematical models facilitate the building, in MathCAD 3D visualization graphics, of a tubular-shaped surface, which represents the layers of yarn winding on a conical cartridge, and the reinforced yarn, which comprise the core component and the wrapping component, as well as the determination of both the lengths of individual layers of winding and the total length of winding (not including the transition sections). Well-known methods of forming geometric objects and computer modelling were also used in the work. The theoretical studies are based on the basic principles of textile production technology.

Keywords: yarn, rewind, bobbin, tubular-shaped surfaces, Frenet basis, computer modelling

### Izvleček

V članku so predstavljeni rezultati računalniškega modeliranja navijanja preje na stožčaste navitke, kjer so bile kot primer žlebičastih površin z uporabo analitične metode vektorske algebre konstruirane cevaste površine. Vodilna linija ima obliko stožčaste spirale, vzdolž katere poteka oblikovanje (v obliki kroga s premerom, ki je enak povprečnemu premeru preje) in se nastavi s pomočjo gibljive Frenetove baze. Dobljeni matematični modeli omogočajo vizualizacijo cevaste površine s pomočjo grafičnega orodja MathCad 3D, tj. plasti preje, navitih na cevko stožčaste oblike, ojačitvene preje iz jedra in ovojne komponente in določanje dolžine posameznih plasti navitja kot tudi celotne dolžine navitja (brez prehodnih odsekov). Pri tem so bile uporabljene znane metode oblikovanja geometrijskih objektov in računalniškega modeliranja. Teoretične študije temeljijo na osnovnih principih tehnologije za izdelavo tekstilij.

Ključne besede: preja, navijanje preje, stožčasti navitek, Frenetova osnova, računalniško modeliranje

---

## 1 Introduction

One of the main tasks of the textile industry is the development of new textile technologies that meet modern specific production requirements. Such technologies include the technology of winding during the formation of specialized winding packages, for example, winding threads and thread-like materials on cartridges, coils, etc.

Today, winding has turned from a separate technological operation of yarn preparation into an independent technological process of obtaining an original product. The process of forming winding packages, which are original products, requires theoretical research, in particular, using the computer modelling of packaging and the computer modelling of the winding mechanism [1].

The need to use computer modelling is explained by requirements to shorten the time to develop technologies and mechanisms of technological machines, and to increase the accuracy of research results and the efficiency of researchers' work.

Modern information technologies are tools used for creating simulated computer models that ensure automated production control for yarn rewinding [2], which is evidenced by the researchers' interest in the use of modern information technologies, and whose scientific works are devoted to the computer modelling of packaging and winding mechanism using various methods. In particular, the computer model of yarn winding described in research [3] is implemented based on Ls-Dyan software using the finite element modelling of the yarn winding process to analyse the change in yarn tension during and after winding.

To study the change in the tension of cotton yarn during the winding process, a finite-element model of yarn based on three-dimensional beam elements using the Abaqus dynamic explicit software is proposed in the paper [4]. In the work [5], the 3DS MAX 2010 software was chosen to simulate the geometry of yarn. The research [6] describes methods for modelling yarn structures using three-dimensional

computer graphics, and results in a mathematical model that reproduces yarn (computer visualization of yarn). The work [7] describes a computer-integrated environment for the simulation of the yarn winding process that includes design, production and quality control, which resulted in the development of yarn winding machines.

Therefore, the development of computer modelling methods and the use of modern applied computer programs for this purpose are timely tasks.

The results of this research can contribute to the development of modern information technologies for the modelling of textile processes based on its use as a tool for researching the analytical method of constructing tubular-shaped surfaces using the vector algebra apparatus and through its implementation in the MathCAD CAE program.

The tasks of the research were:

- to create mathematical models based on vector algebra that describe yarn packaging;
- to create a software code based on the obtained mathematical models; and
- to make a computer modelling of yarn packaging with the construction of visualization graphs in the MathCAD application program.

## 2 Research methodology

Technology and equipment for yarn rewinding are constantly being improved, as evidenced by recent active research on these issues, in particular, works on the development of winding machines [1, 8–10] and research on winding processes [11–18].

When yarn is prepared for knitting on knitting machines, it is rewound from incoming packages onto a conical cartridges using a cross-winding process, resulting in cross-wound conical bobbins.

Since the size of the yarn in length is much larger than the size of the cross-section, the cross-section of the yarn is assumed to be circular, disregarding the change in cross-sectional area during winding.

For the computer modelling of the turns of yarn

winding, the expression [19] can be used, which determines the location of the points of the surface (described by the radius-vector  $S_1$ ) in MathCAD (Figure 1) that forms the turns of yarn winding

$$S_1(u, v) = P_1(u) + l_2 \cdot \cos(v) \cdot \nu(P_1, u) + l_2 \cdot \sin(v) \cdot \beta(P_1, u) \tag{1}$$

where  $P_1(u)$  represents a radius-vector that depends on the angular parameter  $u$  and determines the coordinates of the points of the conical spiral guide line; the hodograph of the radius-vector  $P_1(u)$  represents the axial line of the tubular-shaped surface;  $u$  represents the rotation angle of the projection of the radius-vector  $P_1(u)$  on the horizontal plane, which is counted from the abscissa axis;  $l_2 = \frac{d_{fil}}{2}$  represents the length of the vector  $P_2(v)$ , which determines the coordinates of the points of forming in the form of

along the conical spiral guide line (described by the radius-vector  $P_1$ ), by which the forming moves (in the form of a circle with a diameter equal to the average diameter of the yarn  $d_{fil}$ ):

a circle with a diameter  $d_{fil}$ ;  $v$  represents a parameter that determines the rotation angle of the radius-vector with a length equal to  $d_{fil}$ ;  $\nu(P_1, u)$  represents the component (orth) of the normal vector of the Frenet basis; and  $\beta(P_1, u)$  represents the component (orth) of the binormal vector of the Frenet basis.

The angle  $v$  is counted from the vector  $\nu$  towards the vector  $\beta$  while rotating around the orth of the tangent vector  $t$  to the hodograph of the radius-vector  $P_1(u)$  counterclockwise.

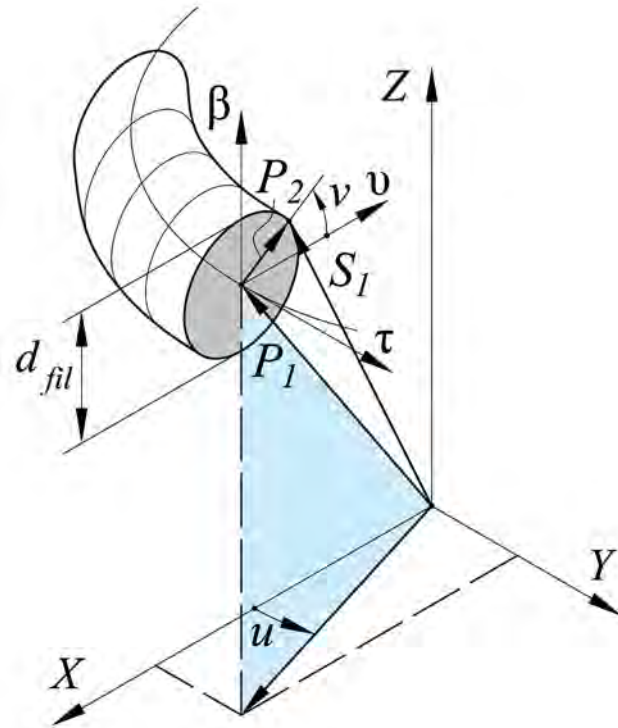


Figure 1: Calculation scheme for determining the location of the points of the surface in MathCAD that forms the turns of yarn winding

The average diameter of the yarn  $d_{fil}$  can be determined by the expression:

$$d_{fil} = \sqrt{\frac{T \cdot 10^{-3}}{\pi \cdot \rho_1}} + \sqrt{\frac{T \cdot 10^{-3}}{\pi \cdot \rho_2}} \tag{2}$$

where  $T$  represents the linear density of yarn in g/km,  $\rho_1$  represents the average density of yarn in g/m<sup>3</sup> and  $\rho_2$  represents the density of fibre in g/m<sup>3</sup>.

To determine the orthos of the Frenet basis  $\tau(PL_1, u)$ ,  $\nu(PL_1, u)$  and  $\beta(PL_1, u)$ , it is possible to use the expressions from differential geometry [20], which will be written in the program code in

$$r'(r, u) = \begin{bmatrix} \frac{d}{du}(r(u)_x) \\ \frac{d}{du}(r(u)_y) \\ \frac{d}{du}(r(u)_z) \end{bmatrix}; \quad r''(r, u) = \begin{bmatrix} \frac{d^2}{du^2}(r(u)_x) \\ \frac{d^2}{du^2}(r(u)_y) \\ \frac{d^2}{du^2}(r(u)_z) \end{bmatrix} \tag{3}$$

$$\tau(r, u) = \frac{r'(r, u)}{|r'(r, u)|}; \quad \beta(r, u) = \frac{r'(r, u) \times r''(r, u)}{|r'(r, u) \times r''(r, u)|}; \quad \nu(r, u) = \beta(r, u) \times \tau(r, u) \tag{4}$$

The body of winding is a conical surface that is formed when the yarn is wound on a conical cartridge. Let's consider the process of winding, during which the conical cartridge carries out only a rotation movement, as a result of which the ends of the bobbin do not have a spherical, but rather a flat surface, as is the case when the conical cartridge carries out a rotational movement and a translational movement simultaneously along the axis of rotation towards the end with a larger diameter. To model the surface of the conical cartridge, the radii  $R_1$  of the larger and  $r_1$  of its smaller ends, located at the distance of the winding height  $h_1$ , need to be entered. The number of turns of winding that fit at the height  $h_1$  is designated as  $n_1$ . Taking a discrete variable  $n$  that specifies the number of the winding layer:

$$n = n_0 - n_{\max} \tag{5}$$

where  $n_0$  and  $n_{\max}$  represent, respectively, the numbers of the initial and final layers with a pitch equal to one.

### 3 Results

To model conical surfaces, tubular-shaped surfaces and conical spiral lines, the matrix of the vector lying in the XY plane that rotates around the Z axis can be used:

$$T_z(u) = \begin{bmatrix} \cos(u) & -\sin(u) & 0 \\ \sin(u) & \cos(u) & 0 \\ 0 & 0 & 1 \end{bmatrix}; \quad M_1(u, v) = \begin{bmatrix} R_1 - v \cdot \frac{R_1 - r_1}{h_1} \\ 0 \\ v \end{bmatrix} \tag{6}$$

where  $M_1(u, v)$  represents the equation of the cone (conical cartridge) in parametric form.

accordance with MathCAD requirements using own functions (user functions) to calculate the derivatives of the radius-vector  $r$ , which is given in a parametric form:

To visualize the conical cartridge on 3D graphics in MathCAD (Figure 2), the following expression can be used:

$$Plot_1 = CreateMesh(M_1, 0, 2\pi, 0, h_1, 36, 10) \tag{7}$$

where the  $u$  parameter is in the interval  $0 \leq u \leq 2\pi$  (the number of grid lines is 36); and the  $v$  parameter is in the interval  $0 \leq v \leq h_1$  (the number of grid lines is 10).

Let's present the equation of the line of yarn winding on a tubular-shaped surface in a parametric form:

$$P_1(u, n) = T_z(u) \cdot \begin{bmatrix} R_1 + \frac{d_{pl}}{2} + (n-1) \cdot d_{pl} - \frac{p_1 \cdot u}{2 \cdot \pi} \cdot \frac{R_1 - r_1}{h_1} \\ 0 \\ \frac{p_1 \cdot u}{2 \cdot \pi} \end{bmatrix} \tag{8}$$

where  $p_1$  represents the pitch of the turn of winding;  $p_1 = h_1/n_1$ .

During the reverse movement of the thread guide (thread unwinder), the argument of the rotation matrix  $Tz$  in the expression (8) will be the angle “ $-u$ ”, i.e.,  $Tz(-u)$ .

In addition to the  $u$  angle, the number of the layer  $n$  is entered as a parameter in the expression (8), which facilitates the modelling of the corresponding layer on the visualization graphics in MathCAD and the determination of both the length of each of the layers and the sum of the lengths of the layers, as well as the total length of winding.

To calculate the length of winding layers, we introduce our own function, which is based on the well-known expression for determining the length of a spatial curve given in a parametric form [20]:

$$Length_1(r, \alpha_1, \alpha_2, n) = \int_{\alpha_1}^{\alpha_2} \sqrt{\left(\frac{d}{du}(r(u, n)_x)\right)^2 + \left(\frac{d}{du}(r(u, n)_y)\right)^2 + \left(\frac{d}{du}(r(u, n)_z)\right)^2} du \quad (9).$$

The expression (9) can be used to determine the length function of a separate layer of winding in MathCAD, depending on the layer number  $n$ :

$$L_1(n) = Length_1(P_1, 0, 2\pi \cdot n_1, n) \quad (10).$$

The total length of winding is determined by the expression:

$$L_{SUM} = \sum_n L_1(n) \quad (11).$$

In the expression (10) the length of  $n$  layer with  $n_1$  turns is calculated in the interval  $0 \leq \alpha \leq 2\pi n_1$ .

To simulate the first layer of winding on a 3D graph of the visualization in MathCAD, the following expression can be used:

$$PL_1(u) = P_1(u, 1) \quad (12).$$

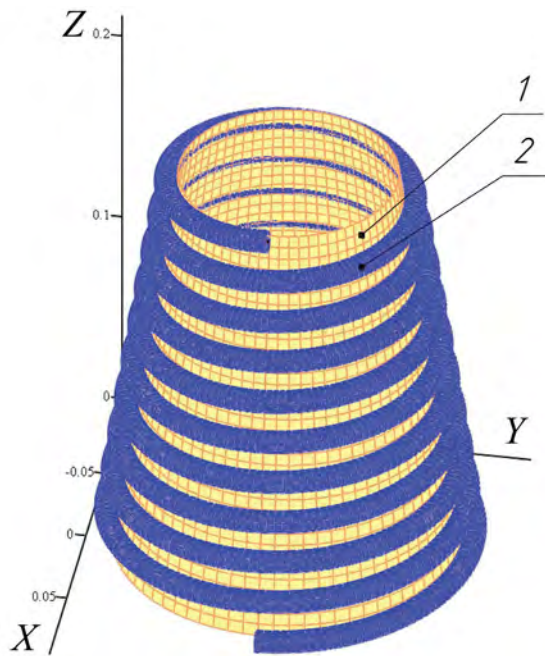
Any layer can be entered according to the expression (12), replacing the index "1" and the value of the parameter "1" in the entry  $PL_1(u, 1)$  with the number of the desired layer.

The graph of visualization of the middle (axial) line of the first layer, as well as the graph of the tubular-shaped surface, which is the yarn, are built using the following expressions in MathCAD:

$$Plot_2 = CreateSpace(PL_1, 0, 2\pi \cdot n_1, 36 \cdot n_1) \quad (13)$$

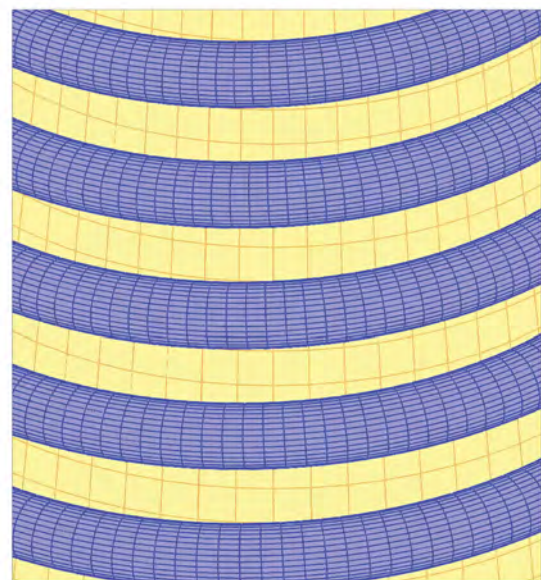
$$Plot_3 = CreateMesh(S_1, 0, 2\pi \cdot n_1, 0, 2\pi, 36 \cdot n_1, 36) \quad (14).$$

Similar to the expressions (13) and (14), it is possible to write expressions for building the graphs of other layers of winding.



Plot<sub>1</sub>, Plot<sub>2</sub>, Plot<sub>3</sub>

a)



Plot<sub>1</sub>, Plot<sub>2</sub>, Plot<sub>3</sub>

b)

Figure: 2. Graphics of visualization of the first layer of winding of yarn on a conical cartridge: a) a conical cartridge with yarn; b) a yarn in the form of tubular-shaped surface

Using the expression (1), it is possible to run the computer modelling of reinforced yarn, which comprises the core component 2 (Figure 3) and the wrapping component 3. It can therefore be rewritten as follows:

$$S_2(u, v) = P_4(u) + l_3 \cdot \cos(v) \cdot v(P_4, u) + l_3 \cdot \sin(v) \cdot \beta(P_4, u) \quad (15)$$

where  $P_4(u)$  represents the radius-vector that determines the coordinates of the points of the spiral guide line (the axial line of the wrapping component in the yarn), which is wound on the surface of the yarn  $S_1(u, v)$  considering the equidistant distance  $l_3$  between the core and the wrapping components, which is equal to half of the diameter  $d_{arm}$  of the wrapping component.

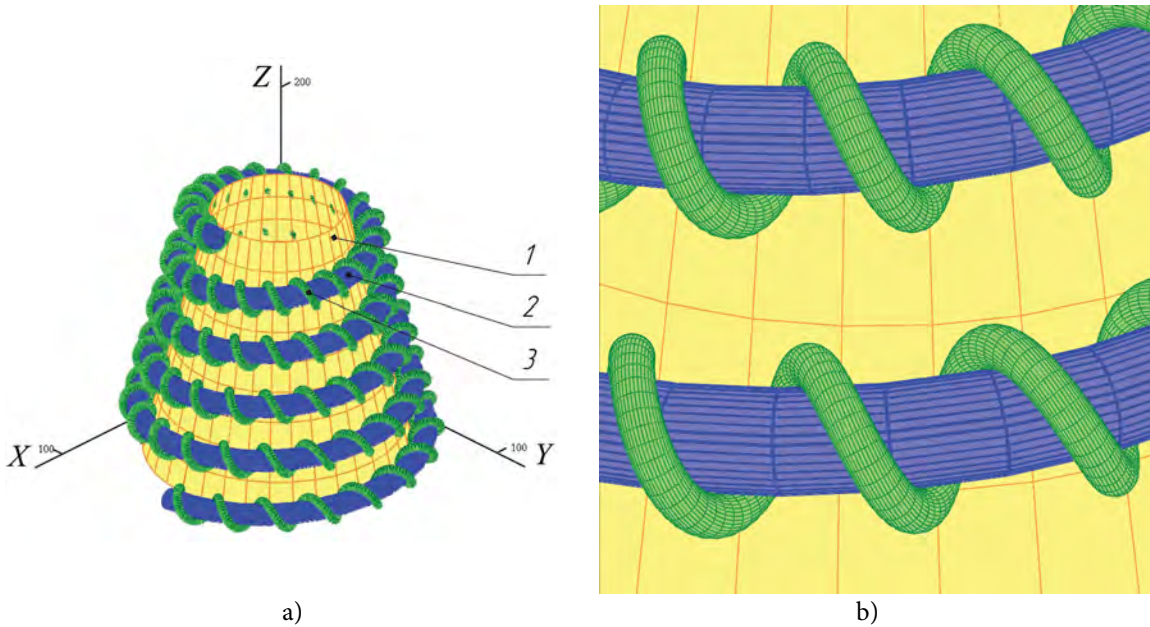


Figure. 3: The graphics of visualization of the first layer of winding of reinforced yarn on a conical cartridge: a) a conical cartridge with reinforced yarn; b) a reinforced yarn in the form of tubular-shaped surface of the core component 2 and the wrapping component 3

The radius-vector  $P_4(u)$  can be determined from the expression (for the first layer of winding):

$$P_4(u) = P_3(u) + (l_2 + l_3) \cdot \cos(u \cdot n_{arm}) \cdot v(P_3, u) + (l_2 + l_3) \cdot \sin(u \cdot n_{arm}) \cdot \beta(P_3, u) \quad (16)$$

where  $P_3(u)$  represents the radius-vector that determines the coordinates of the points of the spiral guide line of the wrapping component:

$$P_3(u) = T_z(u) \cdot \begin{bmatrix} R_1 + \frac{d_{fil}}{2} + \frac{d_{arm}}{2} + (n-1) \cdot (d_{fil} + 2 \cdot d_{arm}) - \frac{P_1 \cdot u}{2 \cdot \pi} \cdot \frac{R_1 - r_1}{h_1} \\ 0 \\ \frac{P_1 \cdot u}{2 \cdot \pi} \end{bmatrix} \quad (17)$$

$n_{arm}$  represents the number of turns of the wrapping component winding, which are placed on the length of one turn of the line of the core component

$P_3(u)$ ; and  $l_3$  represents the radius (the half of the average diameter) of the wrapping component.

## 4 Conclusion

The computer modelling of packaging in the form of a bobbin with a cross winding of yarn is one of the tools used for studying and optimizing processes in the textile industry. The obtained mathematical models and program code in MathCAD can be useful when studying the influence of various factors on the quality of yarn winding. The use of computer modelling allows the user to virtually create a bobbin with a cross winding of yarn, reproducing the position of the turns of yarn winding, and also provides an opportunity to experiment with various parameters that can affect the quality of winding. This enables virtual testing and process optimization without the need for physical experiments, which helps to reduce costs, and improve the quality and efficiency of production in the textile industry. The task of modelling transition sections of winding layers (splice-pieces) remains for the further research.

## References

1. ZAVERTANNYI, B.S. *Structural synthesis of winding mechanisms of rewinding machines: PhD thesis*, 2021, 228 p., <https://er.knutd.edu.ua/handle/123456789/17865>.
2. BRAHMADEEP, THOMASSEY, S. A simulation based comparison: manual and automatic distribution setup in a textile yarn rewinding unit of a yarn dyeing factory. *Simulation Modelling Practice and Theory*, 2014, **45**, 80–90, doi: 10.1016/j.simpat.2014.04.002.
3. LIU, L., CHEN, X., LI, Y., WANG, J. Finite element modeling and simulation of yarn in winding process. *Textile Research Journal*, 2022, **93**(1–2), 70–79, doi: 10.1177/00405175221116665.
4. SHI, Y., LI, Y., CHEN, X., WANG, J. Yarn modeling and winding process simulation based on 3D beam elements. *Textile Research Journal*, 2023, **93**(13–14), 3275–3285. doi: 10.1177/00405175231155834.
5. YAN, Fanlei, YANG, Lianhe. A method of 3D simulation for yarn based on 3DS MAX. In *2010 3rd International conference on computer science and information technology, Chengdu, 2010*, 618–620, doi: 10.1109/ICCSIT.2010.5564115.
6. TANG, W., WAN, T.R. Yarn and fancy yarn design using three-dimensional computer graphics and visualisation techniques. In *Technical textile yarns*. Edited by R. Alagirusamy and A. Das. Woodhead Publishing, 2010, 568–585, doi: 10.1533/9781845699475.2.568.
7. SCHOLLIERS, J., VAN BRUSSEL, H. Computer-integrated filament winding: computer-integrated design, robotic filament winding and robotic quality control. *Composites Manufacturing*, 1994, **5**(1), 15–23, doi: 10.1016/0956-7143(94)90015-9.
8. ZAVERTANNYI, B. S., AKYMOV, O. O., MANOILENKO, O. P., ZENKIN, M. A., KOVALEV, Y. A., PLESHKO, S.A. Research of the influence of the treatment process of three-cone packing on critical speeds of bobbin holder of the winding machine. *Vlákna a Textil*, 2020, **27**(4), 145–149.
9. MANOILENKO, O. P., ZAVERTANNYI, B. S., AKYMOV, O. O. The research of the process of forging a rolling roller through the pack of the final form of rewinding machines. *Vlákna a Textil*, 2020, **27**(2), 69–73.
10. ZAVERTANNYI, B. S., MANOILENKO, O. P., AKYMOV, O. O. Research of the influence of packing displacement along the bobbin holder axis on critical speeds. *Bulletin of the Kyiv National University of Technologies and Design*, 2020, **144**(2), 13–23, doi: 10.30857/1813-6796.2020.2.1.
11. GELAW, B. B., TESFAYE, T., KASAEW, E. Derivation of yarn package radius measuring system for yarn winding machines. *Research Square*, 2022, preprint, 1–12, doi: 10.21203/RS.3.RS-1212570/V1.
12. GANDHI, K.L. Yarn preparation for weaving: winding. In *Woven textiles*. Edited by K. L.

- Gandhi. 1st ed. Soston : Woodhead Publishing, 2012, 35–61, doi: 10.1533/9780857095589.1.35.
13. GANDHI, K.L. Yarn preparation for weaving: winding. In *Woven textiles*. Edited by K. L. Gandhi. 2nd ed. Soston : Woodhead Publishing, 2020, 35–79, doi: 10.1016/B978-0-08-102497-3.00002-7.
  14. CHEN, X. Modelling and simulation of fibrous yarn materials. In *Computer technology for textiles and apparel*. Edited by Jinlian Hu. Soston : Woodhead Publishing, 2011, 93–121, doi: 10.1533/9780857093608.2.93.
  15. ZHAO, H. X., CHANG, D. G. Research of factors affecting the yarn tension of a winding machine. *Applied Mechanics and Materials*, 2014, **496–500**, 1117–1120, doi: 10.4028/WWW.SCIENTIFIC.NET/AMM.496-500.1117.
  16. *Fundamentals of yarn winding*. Edited by M. Koranne. 1st ed. New York : WPI Publishing, 2014, doi: 10.1201/9780367805364.
  17. LAWRENCE C.A. *Fundamentals of spun yarn technology*. 1st ed. Boca Raton : CRC Press, 2003, doi: 10.1201/9780203009581.
  18. PORAT, I., GREENWOOD, K., BANDUK-DA, Z. Computer simulation of cone winding mechanisms with constant rate of yarn delivery systems. *Textile Research Journal*, 1999, **69**(2), 113–120, doi:10.1177/004051759906900206.
  19. ABBENA, E., SALAMON, S., GRAY, S. *Modern differential geometry of curves and surfaces with mathematica*. 3rd ed. New York : Chapman and Hall/CRC, 2017, doi: 10.1201/9781315276038.
  20. Pryshliak, O.O. *Differential geometry*. Kyiv: Publishing and printing center of Kyiv University, 2004, 68 p., <https://www.imath.kiev.ua/~prish/stud/Prish-DG.pdf>.

Marwa A. Ali,<sup>1</sup> Khaled Mohamed Seddik<sup>2</sup>

<sup>1</sup> Spinning and Weaving Engineering Department, Textile Research and Technology Institute, National Research Centre, 33-El Behouth St., Dokki, Giza, Egypt, P.O. 12622

<sup>2</sup> Clothing and Knitting Industrial Research Department, Textile Research and Technology Institute, National Research Centre, 33-El-Behouth St., Dokki, Giza, Egypt, P.O. 12622

---

## Effect of Blending Cotton/Bamboo on UV Protection and Functional Purposes of Trilobal Polyester Microfibers Knitted Fabrics Using Different Structures

*Učinek mešanja preje iz bombaža oziroma bambusove viskoze s filamentno prejo iz poliestrskih mikrovlačen s trilobalnim prečnim prerezom na UV-zaščito in funkcionalne lastnosti pletiv različnih struktur*

*Original scientific article/Izvirni znanstveni članek*

Received/Prispelo 5-2023 • Accepted/Sprejeto 9-2023

Corresponding author/Korespondenčni avtor:

**Dr. Khaled. M. Seddik, Assist. Prof.**

E-mail: dr.khaledseddik@gmail.com

ORCID: 0000-0001-6202-3011

---

### Abstract

Resistance to ultraviolet radiation and electrostatic charge is a basic property that must be considered in the manufacture of fabrics, particularly in light of the climate changes affecting people around the world in various regions, especially in subtropical and tropical regions. It has thus become necessary to focus on the use of different natural fibres to mitigate UV transitions and the formation of electrostatic charges. The aim of this research was to enhance the protection of the ultraviolet effect and reduce electrostatic charge formation by blending cellulose yarns (bamboo and cotton) with trilobal polyester microfiber yarn that has characteristics such as lightweight, low-thickness, high strength, and shine. Knitted samples were produced from two different structures according to their tightness factor (single jersey and fleece structures), the various functional properties of the produced fabrics, such as mass per unit area, thickness, air and water permeability, and bursting strength, were tested. The properties of electrostatic charge and the ultraviolet protection factor (UPF) were also determined. The findings indicate that the samples produced with bamboo resulted in a preferable performance with different structures, especially when considering electrostatic charge and UPF properties. Moreover, the fleece structure had a more significant effect on knitted samples' behaviour than the single jersey (plain) structure.

Keywords: polyester, cellulose fibres, bamboo, knitted structures

## Izvleček

Obstojnost proti ultravijoličnemu sevanju in elektrostatični naboj sta med splošnimi lastnostmi, ki jih je treba upoštevati pri razvoju tekstilij, še posebno v luči podnebnih sprememb, zaradi katerih trpijo ljudje v različnih regijah, zlasti na območjih subtropskega in tropskega podnebja. Za ublažitev vplivov UV-sevanja in elektrostatične napolnitve oblačil se je treba osrediniti na rabo različnih naravnih vlaken. Namen te raziskave je bil povečati zaščito pletiv pred ultravijoličnim sevanjem in zmanjšati nastajanje elektrostatičnega naboja z mešanjem celulozne preje iz bambusove viskoze oziroma bombaža s poliestrsko prejo iz mikrovlaknen s trilobalnim prečnim prerezom, ki se odlikuje po lahкости, tankosti, visoki trdnosti in lesku. Vzorci pletiv so bili izdelani v dveh različnih strukturah glede na faktor kritija (enojni jersey in flis). Preizkušane so bile funkcionalne lastnosti izdelanih pletiv, ploščinska masa, debelina, zračna prepustnost, prepustnost vodne pare in razpočna trdnost; elektrostatični naboj in ultravijolični zaščitni faktor (UZF). Vzorci, ki so vsebovali bambusovo viskozo v različnih strukturah, so se pokazali kot boljši, zlasti z vidika manjše napolnitve z elektrostatičnim nabojem in višjim zaščitnim faktorjem UZF. Poleg tega je bila struktura flisa bistveno učinkovitejša od strukture enojnega (navadnega) jerseyja.

Ključne besede: poliester, celulozna vlakna, bambus, pletene strukture

## 1 Introduction

Ultraviolet radiation is a type of radiant energy from the sun that emits an arrangement of energy known as the electromagnetic spectrum [1]. Ultraviolet irradiation accounts for only about 7% of total solar emissions, with a spectrum ranging from 100 nm to 400 nm, as shown in Figure 1, but has extremely dangerous effects on human skin [2]. In this context, it is important to note that ultraviolet irradiations are classified as UVA (wavelengths of 315–400 nm), UVB (wavelengths of 280–315 nm) and UVC (wavelengths of 100–280 nm) [3]. Generally, UVB irradiation is greatly reduced by a number of factors, such as the sun's height, time of day, amount of cloud cover, geographical latitude and others. It is worth mentioning that UVB radiation is mostly responsible for sunburn and is highly absorbed by DNA, resulting in typical genetic alterations. It has been found that UVB represents a crucial portion of the solar UV spectrum and is the primary factor in human melanoma induction [4]. However, UVA may also be important, as it represents up to 95% of the solar UV energy that reaches the Earth's surface. UVA rays encompass wavelengths that are longer than those in UVB, allowing them to penetrate the

skin more deeply. Although UVA is significantly less potent than UVB in causing erythema, it can elicit various other physiological responses, including immediate and persistent skin pigmentation darkening. This occurrence is particularly noticeable in individuals with darker skin tones [5].

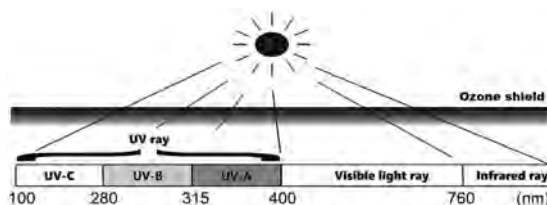


Figure 1: Ultraviolet irradiation classification [6]

Generally, sunscreen applications are the most commonly used for UV protection. The use of textiles as sun protection has been undervalued, despite the fact that proper clothing usually provides simple and effective broadband protection from the sun [7]. Various textile parameters, such as fabric porosity, colour, mass per unit area and thickness, influence the rating system of the ultraviolet radiation blocked by the fabric, namely the ultraviolet protection factor (UPF) for garment products. Additionally, the application of UV absorbers into the yarns significantly improves a garment's UPF property [8].

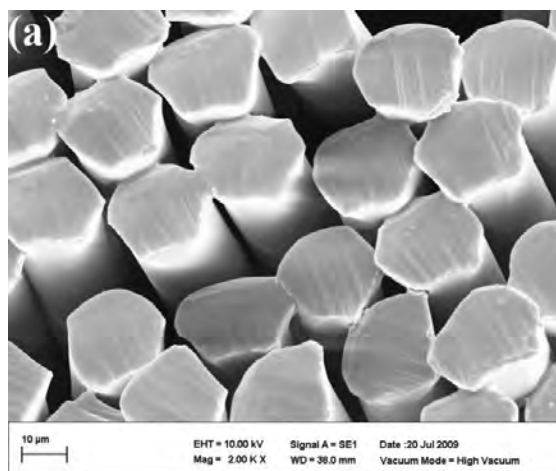
The demand for weft knitted fabrics has increased over the years on domestic and export markets due to their novel characteristics such as breathability, lightness, good stretch-ability and comfortability, which relate to their looped structure and open surface [9]. However, knitted fabrics transmit more UV radiation than woven fabrics due to the composition of the knit structure (loop construction), which offers more gap areas between yarns [10].

Many articles have indicated that polyester has good UV-blocking properties, as it provides relatively low UVB transmission, probably due to a large conjugated system in the polymer chains [8, 11]. Polyester or polyester-blend materials may be the most suitable fabric type for UV-protective garments.

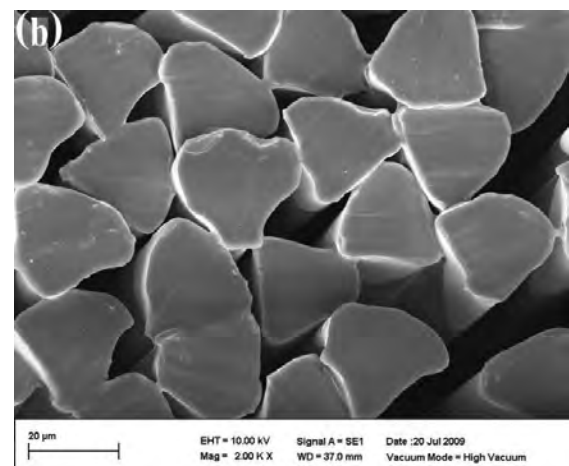
Potentially, any synthetic fibre can be transformed into ultra-fine fibres (microfibers), which typically have diameters smaller than 10 micrometres. Microfibers are increasingly utilised globally for diverse purposes owing to their fineness, top-notch traits and exceptional aptitude to be tailored for particular necessities [12]. Microfibers may be utilised singularly or mixed with customary synthetic fibres and with natural fibres such as cotton, wool, viscose

and silk [11, 13], which enhances the appearance, handling, drape and performance properties of produced fabrics [14, 15]. Microfibers are most frequently manufactured from polyester and nylon [12, 16]. Nylon is purported to offer benefits over polyester in terms of superior coverage, as well as a lower density, increased durability and greater resistance to abrasion. Nevertheless, polyester is simpler to weave and comes in finer filaments than nylon. Therefore, polyester textiles are extensively utilised in manufacturing, giving them an economic edge on the clothing and athletic wear markets [12].

There are various methods that can be employed to produce polyester microfibers, namely melt spinning, wet spinning and dry spinning [16]. Polyester microfiber can be formed into different cross-section shapes. Trilobal polyester microfiber yarn (Y) was invented during the mid-sixties. A triple cross-section is featured with multi-characteristics, such as lightweight, low thickness, high strength and shine, which makes it a good alternative to developing fabrics for different types [17]. Figure 2 presents scanning electron microscopy (SEM) micrographs of the circular and trilobal polyester microfiber cross-sections.



a)



b)

Figure 2: SEM micrographs of polyester microfibers cross-sections; a) circular and b) trilobal taken using a Jeol 840 Model [18]

Daily clothes, such as blouses, T-shirts, sweaters, robes, undergarments and even bed covers, mostly originate from natural cotton fibres. The art of interlacing or looping using cotton fibres results in a flexible and breathable fabric with soft yet sturdy, long-lasting and comfortable characteristics. [19]. Thus, it certainly can be used to create comfortable, wearable and breathable clothes. As it can draw heat away from the skin, it easily absorbs body moisture and evaporates into the air, keeping it cool and refreshing in warm climatic conditions [20, 21]. Furthermore, the possibility of experiencing allergic reactions due to cotton fabric is low, meaning it is commonly recommended for individuals with skin allergies [21]. Thus, mostly medical products, such as bandages and gauze, are made from cotton fibres. Consequently, cotton cloth, with its advantages, has become an ideal preference for individuals to wear in comfort in daily life [22].

The rapid growth and exploration of emerging technology allow different fibres to be generated, designed and manufactured for a broader spectrum of applications; bamboo fibre is one of them and is the most popular fibre today, and has high-yielding sources of cellulose. Bamboo is classified as a regen-

erated fibre and its growing cycle is much shorter, more efficient and more resistant to pests compared with other well-known regenerated fibres, such as Lyocell and Modal [23]. The fabric produced from mechanically extracted bamboo fibres has a rough and stiff feel, whereas viscose fabric based on a bamboo type made using a chemical process has a round cross-section with a small round lumen of fibres and is characterised by many advantages, such as a very soft handle and a good drape like silk. However, it is less expensive and more durable due to the smooth and surface shape of its fibres, biodegradable properties, high moisture absorption capacity, UV protective capability, breathability, and ease of accepting wet processes and colouring. Additionally, its fibres are environmentally friendly and renewable, very fast-growing, and do not occupy cultivated land [24–26]. Bamboo fabric has a natural antimicrobial property, and is also very cool to the touch and non-irritating. It is therefore suitable for people with sensitive skin [27, 28]. Figure 3 shows scanning electron microscopy (SEM) micrographs of the cross-section and longitudinal section of bamboo viscose fibres.

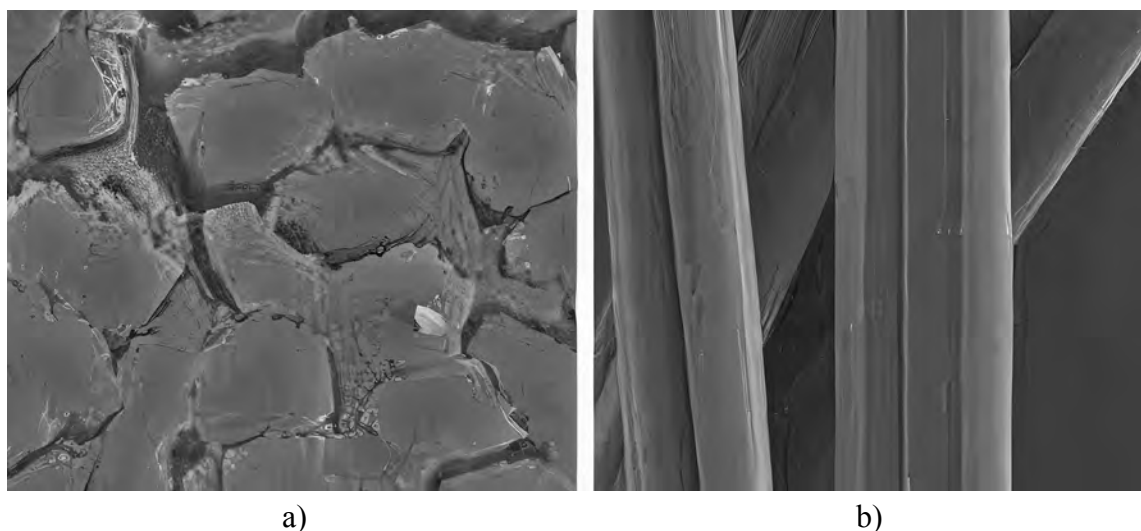


Figure 3: SEM micrographs of bamboo viscose fibres; a) Cross-section view, magnification:  $\times 1500$  and b) Longitudinal view, magnification:  $\times 2000$  [24]

Based on the above, this research aimed to investigate multiple performance characteristics of cotton and bamboo fibres blended with trilobal polyester microfiber (Y), especially for the ultraviolet protection factor and electrostatic behaviour. This is a novel usage of Y polyester in daily garments, such as blouses, T-shirts and even children's clothes, which were produced with different structures of knitted fabrics.

## 2 Materials and methods

### 2.1 Materials

Four knitted samples were manufactured using a circular knitting machine, with the specifications shown in Table 1. Samples were manufactured using two different yarns (cotton and bamboo) of 197 dtex

(30/1 Ne), each blended by a ratio of (50:50)% with trilobal polyester microfiber yarn of 167 dtex / 288 F (150 denier with 288 filaments). Two different knitting structures were used (single jersey and fleece). Table 2 provides the notations and loops formation of produced samples.

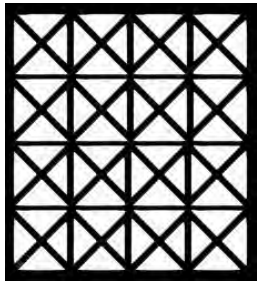
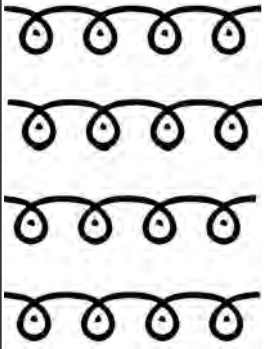
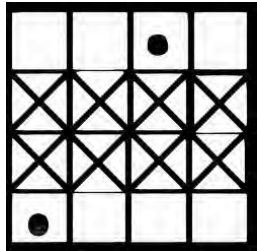
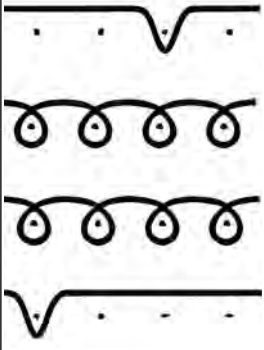
Table 1: Specifications of the circular knitting machine

Manufacturer	Mayer & Cie
Machine model	MV4
Machine gauge	26 E <sup>a)</sup>
Cylinder diameter (inch)	17 <sup>b)</sup>
No. of feeders	42
No. of needles	1632
Efficiency (%)	85
Speed - up to (m <sup>-1</sup> )	20

<sup>a)</sup> Number of needles per inch.

<sup>b)</sup> Approx. 43.2 cm.

Table 2: Notations and loops formation of produced samples

Sample code	Material	Knitting Structure	Notation	Loop formation
KPb	Trilobal/bamboo	Single jersey structure (plain)		
KPc	Trilobal/cotton			
KFb	Trilobal/bamboo	Fleece structure		
KFc	Trilobal/cotton			

## 2.2 Laboratory tests

All samples were conditioned at a temperature of  $20\text{ }^{\circ}\text{C} \pm 2\text{ }^{\circ}\text{C}$  and a relative humidity of  $65\% \pm 2\%$ , and placed in a relaxed state for 24 hours, according to the ISO 139 standard method for fabric testing [29]. Hence, several characteristics were measured as follows:

- Mass per unit area (mass per unit area) was measured using an electronic balance with four digits according to ASTM-D 3776 [30].
- Thickness was measured using a Teclock Corporation instrument according to ASTM-D1777 [31].
- Air permeability was measured using a Toyoseiki (JIKA) instrument according to ASTM-D 737 [32].
- Water permeability was measured using a Toyoseiki (JIKA) instrument according to ASTM-D 461 [33].
- Bursting strength was measured using an M229 auto-burst tester according to ASTM-D3786 [34].
- Electrostatic charge was measured by FTTS-FA-009 utilising an FMX-004 electrostatic field metre according to ASTM-D 4238 [35].
- Ultraviolet transmitting (UPF) was measured using a UV-VIS spectrophotometer according to AATCC-183. This test method was used to examine if UV irradiation was blocked or penetrated through the fabric [36].

Three replicates of each test result were taken for every sample, and the average of the findings was computed for all readings.

## 2.3 Analytical study

All results were collected and tabulated for the manufactured samples. The results were displayed using graphs in the form of a line chart. The significant effect between variables was statistically analysed according to the paired t-test. The significant difference was situated at a p-value  $\leq 0.05$ . Moreover, the radar chart area of all samples was calculated and plotted

at different measured tests in order to illustrate the samples' performance.

## 3 Results and discussion

### 3.1 Functional properties

Tables 3 and 4 show the specifications of knitted samples after manufacturing (in a relaxed state), as well as the average results for the various tests. The results indicate that the tightness factor is influenced by the structures and materials used.

The fleece structure decreased the loop length compared to the single jersey structure with different materials. This can be attributed to the presence of tuck loops within the fleece structure. These tuck loops contribute to the increased shrinkage of the fabrics when in a relaxed state. Furthermore, fabrics made from bamboo yarns (using two different structural compositions) exhibit a higher tightness factor than those made from cotton yarns. This can be explained by the characteristics of bamboo yarns, which tend to undergo more contraction due to the chain arrangement of bamboo viscose, a regenerated material, as opposed to cotton yarns [24].

Table 3: Specifications of knitted samples after manufacturing

Sample code	Wales (cm)	Courses (cm)	Loop length (mm)	Stitch density [ $\text{cm}^{-2}$ ]	Tightness factor <sup>a)</sup>
KPb	12	19	2.6	228	1.70
KPc	12	17	2.8	204	1.58
KFb	11	21.5	2.2	236.5	2.01
KFc	11	20	2.4	220	1.84

<sup>a)</sup>Tightness factor =  $[\sqrt{\text{tex}/\text{mm}}]$ , where yarn count is given in tex and loop length in mm.

In the same context, the results with 95% confidence intervals (CI) relate to the fact that the fabrics produced using bamboo yarns are characterised by increases in mass per unit area and thickness due to the excess specific density of bamboo, which is about  $1.54\text{ g/cm}^3$ , whereas cotton is about  $0.8\text{ g/cm}^3$  and polyester is  $1.38\text{ g/cm}^3$  [37]. On the other hand,

Table 4: Properties of knitted samples

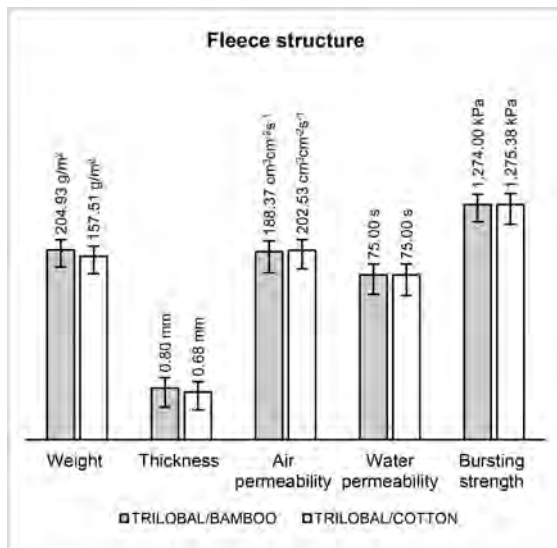
Sample code	Areal mass (g/m <sup>2</sup> )	Thick-ness (mm)	Air permeability (cm <sup>3</sup> cm <sup>-2</sup> s <sup>-1</sup> )	Water permeability (L/s)	Bursting strength (kPa)
KPb	179.96	0.59	276.4	73	882.61
KPc	109.38	0.48	325.07	73	946.36
KFb	204.93	0.80	188.37	75	1274
KFc	157.51	0.68	202.53	75	1275.38

cotton fabrics are characterised by higher air permeability and bursting strength.

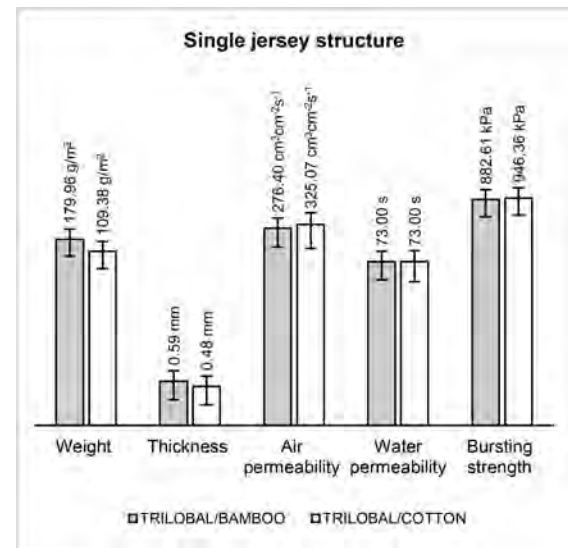
Moreover, the results indicate that the two materials have the same tendency toward water permeability properties, which could be related to the cellulosic base of each of material [23]. Figure 4 illustrates the characteristics of different blended materials with the same knitted structure.

In addition, the results with a 95% CI, as shown in Figure 5, indicate that knitted samples with a fleece structure obtain higher scores in different characterizations except with regarding to air permeability. The reason can be traced to the increase in stitch

density per area affecting fabric porosity and thus airflow (fabric porosity is defined as the creation of pore size among yarn intersections and, in knitted fabrics, it depends on loop length, which is mainly affected by stitch density). Based on wales/cm and courses/cm, as presented in Table 3, the stitch density of fleece fabrics is realised at 236.5 stitches/cm<sup>2</sup> for bamboo and 220 stitches/cm<sup>2</sup> for cotton, respectively. On the other hand, the stitch density for bamboo and cotton knitted samples reach about 228 stitches/cm<sup>2</sup> and 204 stitches/cm<sup>2</sup> respectively, in a single jersey structure (plain).



a)



b)

Figure 4: Characteristic values of different blended materials in the same knitted structure: a) fleece fabrics and b) single jersey fabrics

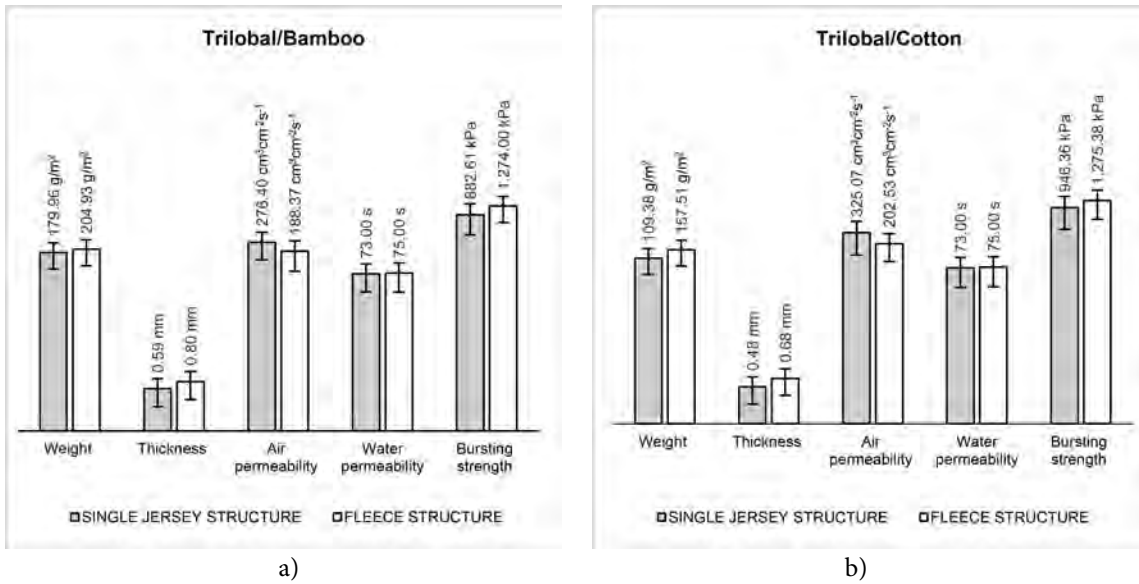


Figure 5: Characteristics of different used structures in the same material; a) trilobal/ bamboo (50:50)% and b) trilobal/cotton (50:50)%

**Significant differences**

According to a paired t-test with a p-value ≤ 0.05, significant differences between variables were identified, as presented in Tables 5 and 6. The results show that the nature of bamboo and cotton yarns act as the main difference in several characteristics

where, based on data analysis, a significant effect was seen, with the exception of air and water permeability. Moreover, the results indicate that the structure composition has a considerable effect on the characteristics of knitted sample, whereby a significant effect was identified among structures with the same material.

Table 5: Significant differences between materials for the same structure

Characteristics	Single jersey structure	Fleece structure
Areal mass (g/m <sup>2</sup> )	1.12E-13 <sup>a)</sup>	7.41E-13 <sup>a)</sup>
Thickness (mm)	0.004785907 <sup>a)</sup>	0.002989 <sup>a)</sup>
Air permeability (cm <sup>3</sup> cm <sup>-2</sup> s <sup>-1</sup> )	0.06253876 <sup>b)</sup>	0.11091 <sup>b)</sup>
Water permeability (s)	0.5 <sup>b)</sup>	0.5 <sup>b)</sup>
Bursting strength (kPa)	0.003845341 <sup>a)</sup>	0.000325 <sup>a)</sup>

a) Significant effect; b) Non-significant effect

Table 6: Significant differences between structures with the same material

Characteristics	Bamboo	Cotton
Mass per unit area (g/m <sup>2</sup> )	1.69E-11 <sup>a)</sup>	6.47E-12 <sup>a)</sup>
Thickness (mm)	0.00124 <sup>a)</sup>	0.00058 <sup>a)</sup>
Air permeability (cm <sup>3</sup> cm <sup>-2</sup> s <sup>-1</sup> )	0.00426 <sup>a)</sup>	0.01053 <sup>a)</sup>
Water permeability (L/s)	0.01048 <sup>a)</sup>	0.03709 <sup>a)</sup>
Bursting strength (kPa)	0.00259 <sup>a)</sup>	0.02181 <sup>a)</sup>

a) Significant effect

### 3.2 Ultraviolet transmitting

Figure 6 shows the UV transmittance and UPF of manufactured fabrics. The reliable results (according to 95% confidence intervals) indicate that the knitted samples with a high tightness factor are more resistance to UV transmittance, and thus increase UV protection. According to the results shown in Table 3, a clear link can be made between the fleece structure, which achieves a high tightness factor in knitted samples, and a reduction in ultraviolet transmittance, which consequently improves UV protection: 5.1 UPF and 5.4 UPF for cotton and bamboo fabric, respectively, compared with those fabrics

made utilising a single jersey structure: 2.4 UPF and 3 UPF for cotton and bamboo fabric, respectively.

Furthermore, the results indicate that, despite there not being substantial differences in the effectiveness of bamboo and cotton yarns on UV protection, bamboo yarns can improve the protection of knitted samples against UV transmittance compared with cotton yarns. This can be attributed to the tendency of bamboo yarn to release more retraction along the loop length in fabrics (in a relaxed state) and thus provide better blocking among loop intermeshing compared to cotton yarns.

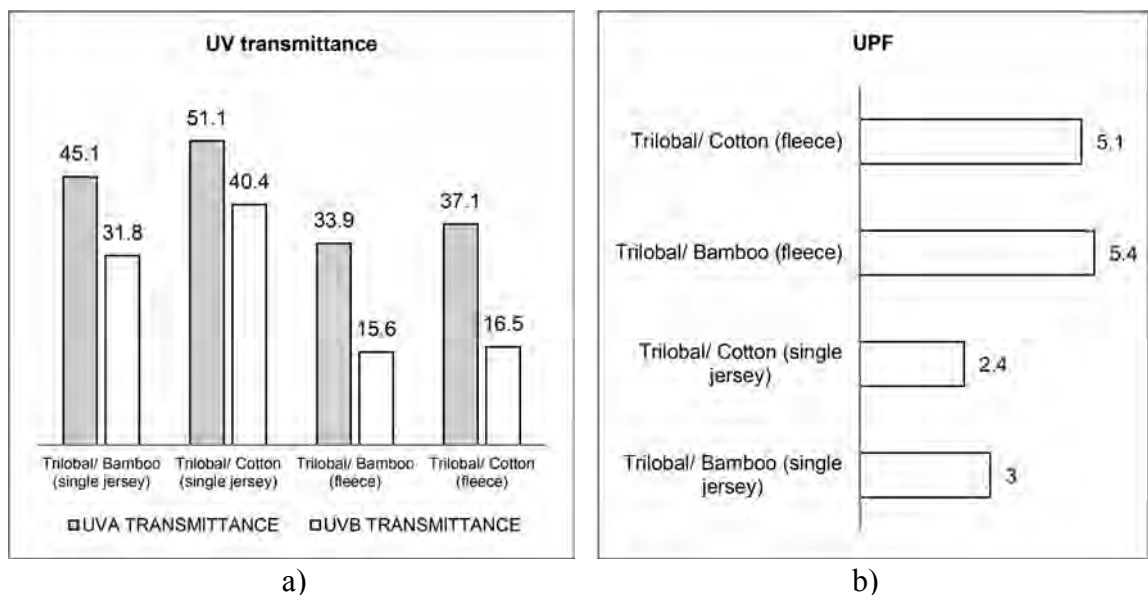


Figure 6: a) Ultraviolet transmittance and b) UPF of manufactured fabrics with 95% confidence intervals

### 3.3 Electrostatic charge

The average results of electrostatic charges were collected and recorded for the produced samples, as shown in Table 7. The results indicated that bamboo and cotton yarns generally produce fabrics that do not generate electrostatic charges, as the obtained scores were close to zero, which could be interpreted as their high capacity to absorb moisture, which supports reducing the formation of electrical charge. Nevertheless, the results showed that bamboo yarns have more electrostatic charge stabilisation than

cotton yarns for different structures, indicating that bamboo yarns can retain moisture longer than cotton yarns. Moreover, the results indicated that the variance of electrostatic charge between bamboo and cotton knitted samples is affected significantly by the tightness factor, where the higher the tightness, the lower the variances, which might be related to reducing air permeability, which promotes moisture absorption within cotton yarn and thus reduces electrostatic charge generation [22, 26, 38].

Table 7: Electrostatic charge of manufactured samples

Sample	Single jersey structure	Fleece structure	Variations
Trilobal/Bamboo	0.01	0.01	<b>0</b>
Trilobal/Cotton	0.03	0.02	<b>0.01</b>
Variations	0.0002	0.00005	

### 3.4 Radar chart area

In order to identify the performance of the produced samples in terms of the different functional properties tested, electrostatic charge and UV protection, the radar area was plotted and calculated as shown in Figure 7. The results indicate that the bamboo-knitted samples had a preferable performance with different structures used, especially when considering

electrostatic charge and UPF. In addition, the results confirmed that the variations of performance among bamboo and cotton samples increased when using unconventional structures, which can be attributed to the enlarged shrinkage occurrence in a relaxed state, where calculated variations reach 403.23 between radar areas in a single jersey structure and 899.99 between radar areas in a fleece structure.

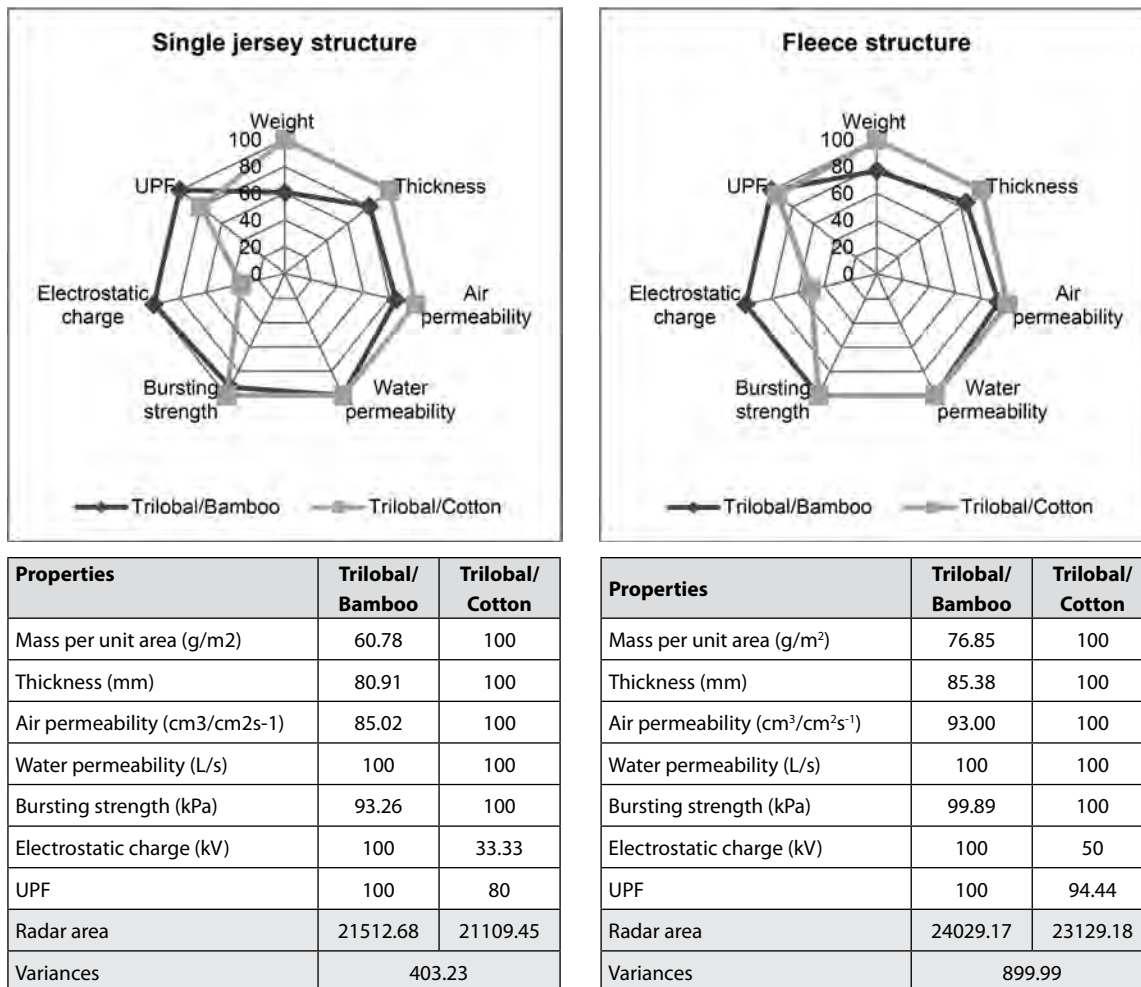
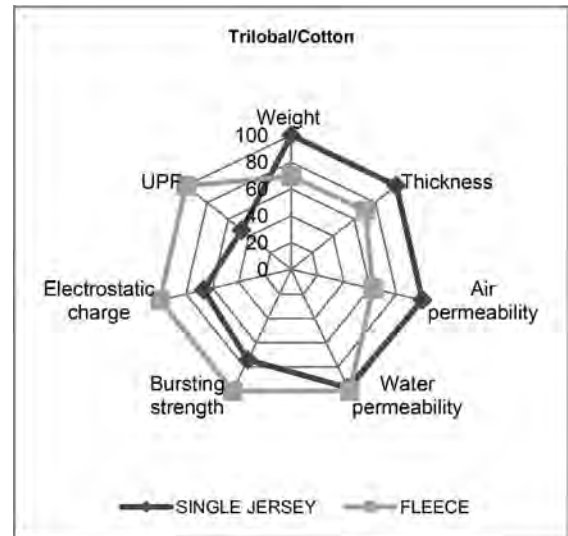
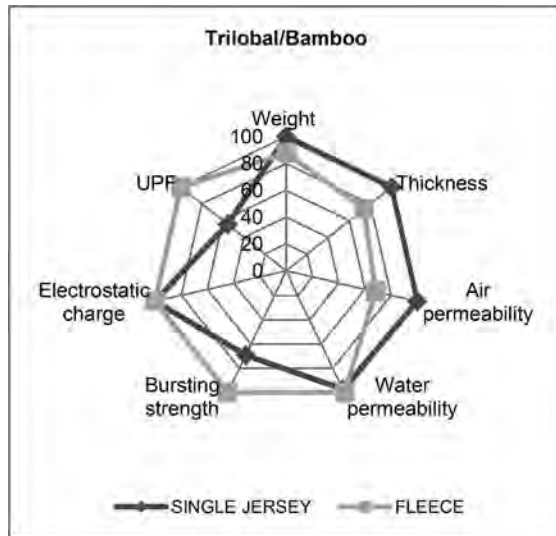


Figure 7: Radar chart area of knitted samples produced with a different structure

In the same vein, the results indicate that the fleece structure has a greater effect on the knitted samples' behaviour than the single jersey structure, whether with bamboo or cotton yarns, as demonstrated in Figure 8. Furthermore, the variance of radar areas among applied structures with trilobal/

bamboo yarns (1,034.34) is less than the variance of radar areas with trilobal/cotton yarns (1,050.29), indicating that the knitted structures are more operative with cotton fabric characteristics than bamboo fabrics.



Properties	Single jersey	Fleece
Mass per unit area (g/m <sup>2</sup> )	100	87.81
Thickness (mm)	100	74.15
Air permeability (cm <sup>3</sup> cm <sup>-2</sup> s <sup>-1</sup> )	100	68.15
Water permeability (L/s)	97.33	100
Bursting strength (kPa)	69.27	100
Electrostatic charge (kV)	100	100
UPF	55.55	100
Radar area	21310.96	22345.31
Variances	1034.345052	

Properties	Single jersey	Fleece
Mass per unit area (g/m <sup>2</sup> )	100	69.44
Thickness (mm)	100	70.26
Air permeability (cm <sup>3</sup> cm <sup>-2</sup> s <sup>-1</sup> )	100	62.30
Water permeability (L/s)	97.33	100
Bursting strength (kPa)	74.20	100
Electrostatic charge (kV)	66.66	100
UPF	47.05	100
Radar area	19446.32	20496.62
Variances	1050.296363	

Figure 8: Radar chart area of knitted samples produced from different materials

#### 4 Conclusion

Considering the examined variables, we can conclude based on our findings that the nature of bamboo and cotton yarns acts as the main difference in several functional properties of the produced knitted samples, with the exception of air and water permeability. Even though blending bamboo or cotton yarns

with trilobal polyester microfiber yarns provides approximately similar protection against UV radiation and generally produces knitted samples that do not generate electrostatic charges, the findings show that bamboo yarns have a better ability to decrease UV transmittance and stabilise an electrostatic charge than cotton yarns in different structures. Depending on the radar area, the findings indicate that trilobal/

bamboo knitted samples achieved a preferable performance, especially in terms of electrostatic charge and UPF properties. On the other hand, the findings indicate that all investigated characteristics are significantly affected by the utilised knitted structures. Moreover, the fleece structure achieves significantly better UV protection than the single jersey structure (plain), and has a considerable effect on knitted samples' behaviour.

#### Acknowledgement

The authors gratefully acknowledge the National Research Centre for testing the samples from this study in their textile laboratories.

#### References

1. ARSHIA, Hussain, SHAHNAZ, Jahan. Textiles protection against ultraviolet radiation. *The Indian Textile Journal*, 2010, **120**(9), 20–35.
2. GORENŠEK, Marija, SLUGA, Franci. Modifying the UV blocking effect of polyester fabric. *Textile Research Journal*, 2004, **74**(6), 469–474, doi: 10.1177/004051750407400601.
3. SARAVANAN, D. UV protection textile materials. *AUTEX Research Journal*, 2007, **7**(1), 53–62.
4. Australian Radiation Protection & Nuclear Safety Agency (ARPANSA). *Resource Guide for UV Products*. Yallambie : ARPANSA, 2003.
5. WANG, S.Q, SETLOW, R., BERWICK, M., POLSKY, D., MARGHOOB A.A, KOPF, A.W, BART, R.S. Ultraviolet A and melanoma: a review. *Journal of the American Academy of Dermatology*, 2001, **44**(5), 837–846, doi: 10.1067/mjd.2001.114594.
6. HUNTER, L. Ultraviolet protection of fabrics and garments. In *Engineering Apparel Fabrics and Garments*. Edited by J. Fan and L. Hunter. Cambridge: Woodhead Publishing, 2009, 309–338.
7. MENTER, Julian M., HATCH, Kathryn L. Clothing as solar radiation protection. In *Textiles and the Skin*. Edited by P. Elsner, K. Hatch and W. Wigger-Alberti. Basel : S. Karger, 2003, 50–63.
8. ABDEL-MEGIED, Z.M., SEDDIK, K.M., ABD ELAZIZ, M.Y. Improve UV protection property of single jersey for summer protective clothes. *Journal of Textile & Apparel Technology & Management (JTATM)*, 2018, **10**(3), 1–9.
9. DEĞIRMENCI, Z., ÇORUH, E. The influences of loop length and raw material on bursting strength air permeability and physical characteristics of single jersey knitted fabrics. *Journal of Engineered Fibers and Fabrics*, 2017, **12**(1), 43–49, doi: 10.1177/155892501701200105.
10. SAKTHIVEL, J.C., ANBUMANI, N. Dimensional properties of single jersey knitted fabrics made from new and regenerated cellulosic fibers. *Journal of Textile and Apparel, Technology and Management*, 2012, **7**(3), 1–10.
11. ELGOHARY, Doaa. H., YAHIA, S., SEDDIK, K.M. Characterization the properties of blended single jersey fabrics using different microfiber yarn cross-sections and gauges machine. *Egyptian Journal of Chemistry*, 2021, **64**(6), 3041–3048, doi: 10.21608/ejchem.2021.58596.3265.
12. ANON. Recent advancements in man-made textiles. *New Cloth Market*, 2000, **14**(4), 13–14.
13. SEDDIK, K., BASSYOUNI, F., ELGORY, Z., EL-GABRY, L. Characterization of new coloured materials on different fabrics and application on wool fabrics to comfort and ultraviolet protective garment. *Egyptian Journal of Chemistry*, 2020, **63**(7), 2751–2761, doi: 10.21608/ejchem.2020.19849.2199.
14. ELGORY, Z. M., SEDDIK, K. M., YAHIA, M., EL-GABRY, L. K. The enhancement of the functional properties of polyester microfiber single jersey using some nano-materials. *Egyptian Journal of Chemistry*, 2020, **63**(1), 145–154, doi: 10.21608/EJCHEM.2019.2868.1804.
15. BASU, A. Microfibers: properties, processing and use. *Asian Textile Journal*, 2001, **10**(4), 43–52.

16. PURANE, S.V., PANIGRAHI, N.R. Microfibers, microfilaments and their applications. *AUTEX Research Journal*, 2007, 7(3), 148–158.
17. KORAL KOC, S., MECIT, D., BOYACI, B., ORNEK, M., HOCKENBERGER, A. Effects of filament cross section on the performance of automotive upholstery fabrics. *Journal of Industrial Textiles*, 2016, 46(3), 756–770, doi: 10.1177/1528083715598652.
18. KARACA, E., KAHRAMAN, N., OMEROGLU, S., BECERIR, B. Effects of fiber cross sectional shape and weave pattern on thermal comfort properties of polyester woven fabrics. *Fibres & Textiles in Eastern Europe*, 2012, 3(92), 67–72.
19. NEELLA, N., GADDAM, V., RAJANNA, K., NAYAK, M.M. Low cost, disposable and wearable body warmer using RGO sheets coated on cloth substrate as heating element. In *2017 IEEE 12th International Conference on Nano/Micro Engineered and Molecular Systems (NEMS)*, Los Angeles, CA, USA, 2017, 177–180, doi: 10.1109/NEMS.2017.8017000.
20. PETERMAN, William. The advantages of cotton clothing [online]. Livestrong [accessed 5. 9. 2023]. Available on World Wide Web: <<https://www.livestrong.com/article/59826-advantages-cotton-clothing/>>.
21. *Cotton Fibres: Characteristics, uses and performance*. Edited by Stuart Gordon and Nouredine Abidi. New York : Nova Science Publisher, 2017.
22. SEDDIK, K.M., ALI, M.A. Characterization the performance of elastic band using different polyester microfiber cross-sections and stitch densities. *Egyptian Journal of Chemistry*, 2022, 65(8), 549–556, doi: 10.21608/EJCHEM.2022.111259.5062.
23. ERDUMLU, N., OZIPEK, B. Investigation of regenerated bamboo fiber and yarn characteristics. *Fibres and Textiles in Eastern Europe*, 2008, 16(4), 43–47.
24. XU, Y., LU, Z., TANG, R. Structure and thermal properties of bamboo viscose, Tencel and conventional viscose fiber. *Journal of Thermal Analysis and Calorimetry*, 2007, 89(1), 197–201, doi: 10.1007/s10973-005-7539-1.
25. MAJUMDAR, A., ARORA, S. Bamboo fibres in textile applications. In *Bamboos in India*. Edited by Shailendra Kaushik, Yash Pal Singh, Dinesh Kumar, Manisha Thapliyal and Santan Barthwal. Dehradun : ENVIS Centre on Forestry, 2015, 285–304.
26. IMADI, S.R., MAHMOOD, I., KAZI, A.G. Bamboo fiber processing, properties, and applications. In *Handbook of Biomass and Bioenergy; Processing and Properties*. Edited by Khalid Rehman Hakeem, Mohammad Jawaid and Umer Rashid. Cham : Springer, 2014, 27–46, doi: 10.1007/978-3-319-07641-6\_2.
27. SEKERDEN, F. Investigation on the unevenness, tenacity and elongation properties of bamboo/cotton blended yarns. *Fibres and Textiles in Eastern Europe*, 2011, 19(3), 26–29.
28. SARAVANAN, K., PRAKASH, C. Bamboo fibers & their application in textiles. *Indian Textile Journal*, 2008, CXVIII, 137–140.
29. ISO 139:2005. Textiles – Standard atmospheres for conditioning and testing. Geneva : International Organization for Standardization, 2005, 6 p.
30. ASTM D3776. Standard test methods for mass per unit area of fabric. West Conshohocken : ASTM International, 2002.
31. ASTM D1777. Standard test methods for thickness of textile materials. West Conshohocken : ASTM International, 2002.
32. ASTM D737. Standard test method for air permeability of textile fabrics. West Conshohocken : ASTM International, 2018.
33. ASTM D461. Standard test methods for felt. West Conshohocken : ASTM International, 2004.
34. ASTM D3787-16. Standard test method for bursting strength of textiles – Constant Rate-of-Travel (CRT) ball burst test. West Conshohocken : ASTM International, 2020.

35. ASTM D4238. Standard test method for electrostatic propensity of textiles. West Conshohocken : ASTM International, 2010.
36. AATCC 183. Test method for transmittance or blocking of erythemally weighted ultraviolet radiation through fabrics. Durham : AATCC, 2010.
37. NASSAR, K., NAHLA, M. ABOU-TALEB, E.M. Improving the thermal comfort properties of bamboo and bamboo blended fabrics for sports head scarves. *International Design Journal*, 2020, **10**(4), 131–137, doi: 10.21608/IDJ.2020.38068.1006.
38. HAKEIM, O. A., EL ZAWAHRY, M. M., ALY, N. M., DIAB, H. A., ALI M.A. Anti-static and functional properties of asminosilsesquioxane oligomer treated and dyed fabrics. *Journal of the Textile Association*, 2015, **76**(2), 90–101.

Brigita Tomšič, Nika Savnik, Elena Shapkova, Laura Cimperman, Lara Šoba, Marija Gorjanc, Barbara Simončič  
University of Ljubljana, Faculty of Natural Sciences and Engineering, Aškerčeva 12, 1000 Ljubljana, Slovenia

# Green In-situ Synthesis of TiO<sub>2</sub> in Combination with *Curcuma longa* for the Tailoring of Multifunctional Cotton Fabric

*Zelena in situ sinteza TiO<sub>2</sub> v prisotnosti ekstrakta kurkume za izdelavo večfunkcionalne bombažne tkanine*

**Original Scientific Paper/Izvirni znanstveni članek**

Received/Prispelo 9-2023 • Accepted/Sprejeto 11-2023

Corresponding author/Korespondenčni avtorica:

**Prof. dr. Barbara Simončič**

E-mail: barbara.simoncic@ntf.uni-lj.si

ORCID: 0000-0002-6071-8829

## Abstract

The introduction of green chemistry has become urgent in the development of innovative, high-performance functional textiles to reduce the environmental footprint of their production. This study aims to develop a new eco-friendly process for the hydrothermal in-situ synthesis of TiO<sub>2</sub> in cotton fabric and dyeing with curcumin natural dye to produce a photocatalytically active coloured textile platform with simultaneous UV protection properties. Two approaches were developed: classical, which included dyeing of the cotton samples with *Curcuma longa* (turmeric) extracts at different concentrations (5 g/L, 10 g/L and 15 g/L) and subsequent hydrothermal in-situ synthesis of TiO<sub>2</sub> in the presence of the dyed cotton samples, and greener, in which simultaneous dyeing with turmeric extracts and hydrothermal in-situ synthesis of TiO<sub>2</sub> were carried out. Since increasing the turmeric concentration hindered the photocatalytic performance of TiO<sub>2</sub> in the chemically modified cotton samples, 5 g/L was selected as the most suitable turmeric concentration. A comparison of the chemical modification processes shows that the simultaneous dyeing of cotton with turmeric extract and hydrothermal in-situ synthesis of TiO<sub>2</sub> was beneficial and resulted in a UV protection factor 50+, which corresponds to excellent protection category. The photocatalytic activity of TiO<sub>2</sub> was maintained in the presence of turmeric, indicating the compatibility of both players in the chemically modified cotton, but not the creation of a turmeric–TiO<sub>2</sub> heterojunction with visible-light-driven photocatalysis. The presence of TiO<sub>2</sub> inhibited the photodegradation of the curcumin dye, further confirming the compatibility of the two players. Keywords: cotton, TiO<sub>2</sub>, turmeric extract, photocatalytic activity, UV protection

## Izveček

Pri razvoju inovativnih, visokozmogljivih funkcionalnih tekstilij je za zmanjšanje okoljskega odtisa pri njihovi proizvodnji postala vpeljava zelene kemije nujna. Zato je bil namen raziskave razviti nov okolju prijazen postopek hidrotermalne in situ sinteze TiO<sub>2</sub> na bombažni tkanini in barvanja z naravnim barvilom kurkume za proizvodnjo fotokatalitsko aktivne obarvane tekstilije s hkratnimi UV-zaščitnimi lastnostmi. Razvita sta bila dva pristopa, in sicer

klasični, ki je vključeval barvanje vzorcev bombaža z izvlečki kurkume različnih koncentracij (5 g/L, 10 g/L in 15 g/L) in naknadno hidrotermalno in situ sintezo  $\text{TiO}_2$  v prisotnosti pobarvanih vzorcev bombaža, in bolj zeleni, kjer sta sočasno potekala barvanje z izvlečki kurkume in hidrotermalna in situ sinteza  $\text{TiO}_2$ . Ker je povečanje koncentracije kurkume oviralo fotokatalitsko delovanje  $\text{TiO}_2$  v kemično modificiranih vzorcih, je bila kot najprimernejša koncentracija kurkume izbrana 5 g/L. Iz primerjave postopkov kemične modifikacije je razvidno, da sta bila sočasno barvanje bombaža z izvlečkom kurkume in hidrotermalna in situ sinteza  $\text{TiO}_2$  zelo učinkovita, s čimer je tkanina dobila UV-zaščitni faktor 50+, kar je kategorizirano kot odlična zaščita. Fotokatalitska aktivnost  $\text{TiO}_2$  se je v prisotnosti kurkume ohranila, kar je kaže na združljivost obeh akterjev v kemično modificiranem bombažu, ni pa se tvoril kompozit kurkuma- $\text{TiO}_2$ , s povečano fotokatalitsko aktivnostjo pri osvetljevanju z vidno svetlobo. Prisotnost  $\text{TiO}_2$  je zavrla fotorazgradnjo kurkume, kar dodatno potrjuje združljivost obeh komponent.

Ključne besede: bombaž,  $\text{TiO}_2$ , ekstrakt kurkume, fotokatalitska aktivnost, UV-zaščita

## 1 Introduction

The chemical modification of textiles is one of the most important textile processes to develop innovative textile materials with desired multifunctional properties. The application of nanomaterials to chemically modify textiles has opened new possibilities for creating new functionalities and improving their properties [1–4]. Among nanomaterials, titanium dioxide ( $\text{TiO}_2$ ) is considered as a versatile inorganic semiconductor material for textile functionalisation with unique electronic structure and functional properties such as photocatalysis, UV protection, antimicrobial activity, thermal stability, biocompatibility, and non-toxicity [5, 6].  $\text{TiO}_2$  is a wide bandgap semiconductor material with photocatalytic self-cleaning properties, i.e., the ability to degrade organic pollutants on its surface under UV light irradiation. Namely, when  $\text{TiO}_2$  is irradiated with UV light in the presence of water and oxygen, it can form reactive oxygen species (ROS) on the surface, which have a strong oxidation potential to degrade organic molecules via intermediates to water and carbon dioxide [7, 8]. The ability to absorb or scatter harmful UV radiation gives  $\text{TiO}_2$  a strong UV-blocking effect, which is crucial for its UV-protection properties.

Growing environmental awareness dictates avoiding the use of conventional chemical modifica-

tion processes as they have a negative impact on the environment due to the consumption of significant amounts of water, energy and chemicals [9, 10]. Therefore, the adoption of eco-friendly approaches is crucial to reducing the environmental footprint. In this context, the application of green chemistry principles, which include the use of safer chemicals, minimising waste and reducing water and energy, plays a crucial role [11]. One of the most important principles of green chemistry is the green synthesis of nanomaterials, which has been extensively studied as an alternative to conventional chemical synthesis processes [12–14]. This also applies to the green synthesis of  $\text{TiO}_2$  [15–22]. It can be carried out in various ways, but plant-mediated biological synthesis, in which plant extracts or phytochemicals can serve as stabilizers, has proven to be one of the most promising and well-implemented. It opens up unlimited resources as different plant parts such as roots, stems, leaves, flowers, fruits and seeds can be used. Since biobased materials are found in nature, they are considered non-toxic and safe, inexpensive, and readily available.

Among plants, *Curcuma longa*, commonly known as turmeric, is a flowering plant of the ginger family. It is known for its rhizomes, which are usually dried and ground into a deep orange-yellow powder called turmeric powder. It is used as a natural yellow dye for textiles and food, as a culinary spice, as a

cosmetic ingredient and as a medicine in traditional herbal medicine [23–25]. According to the literature, turmeric powder has not only established itself for textile dyeing [26–31], but also for the green synthesis of TiO<sub>2</sub> [32–38]. Usually, it is used as an extract prepared in a suitable solvent containing a natural polyphenolic compound called curcumin. When the turmeric extract was combined with the titanium precursor solution under suitable conditions, curcumin acted as a capping agent for the synthesis of TiO<sub>2</sub> and facilitated its formation and stabilisation [39]. Furthermore, when curcumin was in intrinsic contact with TiO<sub>2</sub>, the curcumin molecules could act as a sensitising agent that absorbed visible light, resulting in electron excitation in the curcumin molecule from the highest occupied molecular orbital to the lowest unoccupied molecular orbital, followed by electron transfer from the unoccupied molecular orbital to the conduction band of TiO<sub>2</sub>. This significantly improved the photocatalytic efficiency of TiO<sub>2</sub> upon irradiation with visible light [32–37].

In the present work, a new sustainable approach for the chemical modification of cotton fabric was developed using hydrothermal synthesis of TiO<sub>2</sub> in the presence of curcumin and cotton fabric to create photocatalytic and UV protection properties. Two different application procedures were investigated. The first was a two-step process and involved dyeing of cotton fabric with turmeric extract followed by the in-situ synthesis of TiO<sub>2</sub>. The second was a one-step combination of dyeing with turmeric extract and in-situ synthesis of TiO<sub>2</sub> with the aim of reducing water and energy consumption. In addition, the influence of turmeric extract at different concentrations on the functional properties of TiO<sub>2</sub> was thoroughly investigated. A newly developed innovative chemical modification process for the production of multifunctional textiles represents an important technological shift from conventional to green textile chemistry.

## 2 Experimental

### 2.1 Materials

Alkaline-soured, bleached and mercerized 100% cotton plain-weave fabric (Tekstina d.o.o., Ajdovščina, Slovenia), with a mass per unit area of 120 g/m<sup>2</sup>, was used for chemical modification. Turmeric powder (Maestro, Podravka d.d., Croatia) was bought at a local market. Titanium(IV) isopropoxide (TTIP; ≥ 97.8% concentration), isopropanol (≥ 99% concentration) and acetic acid were procured from Sigma Aldrich (United States), Honeywell Research Chemicals (Seetze, Germany) and CARLO ERBA Reagents S.A.S (Barcelona, Spain), respectively.

### 2.2 Preparation of the turmeric extract

The extract of turmeric powder was prepared in distilled water at three different concentrations: 5 g/L, 10 g/L and 15 g/L. A certain amount of the powder was covered with cold distilled water, heated and boiled for 5 minutes. Then, the boiled solution was cooled and filtered. For each concentration, 2 L of extract was prepared. The *Curcuma longa* rhizomes, their powder, the cooled extract solution (5 g/L) and the chemical structure of the natural dye curcumin are shown in Figure 1.

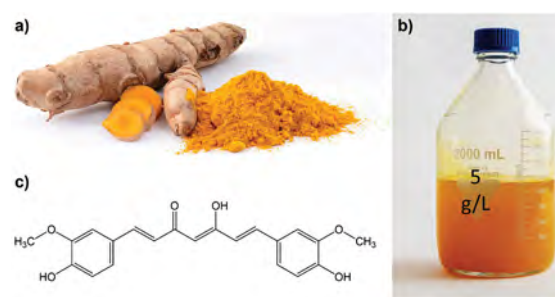


Figure 1: *Curcuma longa* rhizomes and their powder (a), the turmeric extract (b), and the chemical structure of the enol form of the curcumin natural dye in the turmeric extract (c).

### 2.3 Chemical modification of cotton fabric

Chemical modification of cotton fabric was carried out in two different processes. The first classical process involved two steps: the dyeing of cotton samples with turmeric extract followed by the in-situ synthesis of  $\text{TiO}_2$  on the dyed samples. For this purpose, 7 g cotton samples were dyed with 5 g/L, 10 g/L and 15 g/L turmeric extracts (three samples for each extract concentration) by exhaustion with a 1:20 ratio of good to liquor for 40 minutes at 40 °C in the Starlet laboratory dyeing machine (Daelim Starlet, Co., Korea). After dyeing, the samples were squeezed on a two-roll padder (Mathis, Switzerland) with a wet pickup of  $100\% \pm 5\%$  and air-dried. For the in-situ synthesis of  $\text{TiO}_2$ , the TTIP sol (200 g) was previously prepared as a 4% hydrolysed dilution of the TTIP precursor (8 g) in isopropanol (182 g) by adding acetic acid (10 g) and stirred magnetically for about two hours until hydrolysis was completed. The dyed samples were immersed in the TTIP sol and then squeezed out on a two-roll padder with a wet pickup of  $100\% \pm 5\%$  and dried at 100 °C for 1 minute in the laboratory drying apparatus (Mathis, Switzerland). Subsequently, each sample was immersed in 350 g of water and hydrothermally treated for 90 min at 120 °C in the Starlet laboratory dyeing machine. Finally, the samples were squeezed with a wet pickup of  $100\% \pm 5\%$  and air-dried.

The second greener process involved the simultaneous dyeing of cotton samples with turmeric extracts and the in-situ synthesis of  $\text{TiO}_2$ . For this purpose, a hydrolysed TTIP sol was applied to the undyed cotton samples in the same way as in the first procedure (immersion in the TTIP sol, squeezing with a wet pickup of  $100\% \pm 5\%$  and drying for 1 min at 100 °C), followed by the immersion of the samples in 350 g turmeric solutions of different concentrations (three samples for each extract concentration) and hydrothermal treatment for 90 min at 120 °C, squeezing, and drying. For comparison, the dyeing of cotton samples in 5 g/L turmeric extract solution and the in-situ synthesis of  $\text{TiO}_2$  were also performed under the same conditions as the two

processes. The sample codes for the chemical modification processes are summarized in Table 1.

Table 1: Sample codes according to the chemical modification process

Sample code	Chemical modification process
UN	Untreated (no chemical modification)
C5	Dyeing of the cotton sample with 5 g/L turmeric extract
T	Hydrothermal in-situ synthesis of $\text{TiO}_2$ from 4% TTIP in the presence of an undyed cotton sample
C5-T	Dyeing of the cotton sample with 5 g/L turmeric extract followed by the hydrothermal in-situ synthesis of $\text{TiO}_2$ from 4% TTIP in the presence of the dyed cotton sample
C10-T	Dyeing of the cotton sample with 10 g/L turmeric extract followed by the hydrothermal in-situ synthesis of $\text{TiO}_2$ from 4% TTIP in the presence of the dyed cotton sample
C15-T	Dyeing of the cotton sample with 15 g/L turmeric extract followed by the hydrothermal in-situ synthesis of $\text{TiO}_2$ from 4% TTIP in the presence of the dyed cotton sample
C5+T	Simultaneous dyeing of the cotton sample with 5 g/L turmeric extract and hydrothermal in-situ synthesis of $\text{TiO}_2$ from 4% TTIP
C10+T	Simultaneous dyeing of the cotton sample with 10 g/L turmeric extract and hydrothermal in-situ synthesis of $\text{TiO}_2$ from 4% TTIP
C15+T	Simultaneous dyeing of the cotton sample with 15 g/L turmeric extract and hydrothermal in-situ synthesis of $\text{TiO}_2$ from 4% TTIP

### 2.4 Analysis and measurements

#### 2.4.1 Scanning electron microscopy (SEM) and energy-dispersive X-ray spectroscopy (EDS)

The morphological characteristics of samples UN, C5, T, C5-T and C5+T were determined using the scanning electron microscope JSM-6060 LV (JEOL, Japan). Each sample was imaged three times at a different location at 3000- $\times$  magnification. Before imaging, the samples were coated with a thin layer of gold to ensure conductivity.

In addition, the samples were examined using the Thermo Fischer Scientific Quattro S energy dispersive field emission scanning electron microscope (Thermo Fisher Scientific, USA), which works at an accelerating voltage of 1 kV in high vacuum and uses a concentric backscattered electron detector (CBS). An energy dispersive detector (Oxford Instruments Ultim Max 65) was used to verify the chemical composition of the observed particles using AZtec software. EDS spectra and elemental mappings of C, Ti and O were obtained. The samples were coated with a thin carbon layer before analysis.

#### 2.4.2 Add-on

The total quantity of dry solid add-on of the samples UN, C5, T, C5-T and C5+T was determined using an electronic moisture analyser (KERN MLB-C). The samples were preconditioned for 24 h at 65% relative humidity and 20 °C. They were then dried at 105 °C until a constant mass was reached, i.e. until the change in weight within 120 s was less than 1 mg. The add-on value was calculated according to the following equation:

$$\text{Add-on} = \frac{(m_2 - m_1)}{m_1} \cdot 100 (\%) \quad (1)$$

where  $m_2$  is the mass of the finished sample and  $m_1$  is the mass of the untreated sample.

#### 2.4.3 Inductively coupled plasma-mass spectrometry (ICP-MS)

The concentrations of Ti in the samples T, C5-T and C5+T were determined via ICP-MS using a Perkin Elmer SCIED Elan DRC spectrophotometer. A 0.5 g sample was prepared in a Milestone microwave system via acid decomposition with 65% HNO<sub>3</sub> and 30% H<sub>2</sub>O<sub>2</sub>. Ti concentrations were reported as the mean values of two measurements for each sample. Based on the measured Ti values, the TiO<sub>2</sub> concentration was calculated.

#### 2.4.4 X-ray diffraction analysis (XRD)

X-ray diffraction (XRD) patterns of the crystal phase of samples UN, T, C5-T and C5+T were recorded using a Philips PW3830 X-ray diffractometer equipped with Cu-Kα1 1.54060 Å radiation and a secondary graphite monochromator. Data were recorded at 40 kV and a current of 30 mA over a range of 10° to 90° 2θ at a rate of 3° per minute. Diffraction patterns were obtained using X'Pert HighScore Plus software ver. 4.8.

#### 2.4.5 Fourier transform infrared spectroscopy (FTIR)

The chemical composition of the samples UN, C5, T, C5-T and C5+T was analysed using FTIR spectrometer Spectrum 3 (Perkin Elmer, UK). Spectra between 4000 cm<sup>-1</sup> and 600 cm<sup>-1</sup> were recorded with a resolution of 4 cm<sup>-1</sup> and an average of 120 spectra per sample.

#### 2.4.6 Colour measurements

Colour measurements of the samples UN, C5-T, C10-T, C15-T, C5+T, C10+T and C15+T were performed using a Spectrophotometer Spectraflash 600 PLUS CT (Datacolor, Switzerland). The reflectance,  $R$ , of each sample was measured five times at different locations, and the average value was calculated. The colour strength,  $K/S$  value, was calculated from the following equation [40]:

$$\frac{K}{S} = \frac{(1-R)^2}{2R} \quad (2)$$

where  $R$  is the reflectance of the dyed samples at  $\lambda_{max}$ ,  $K$  is the absorption coefficient and  $S$  is the scattering coefficient of the sample.

#### 2.4.7 UV-Vis spectroscopy and determination of the UV protection properties

The transmission and reflection spectra of the samples UN, C5-T, C10-T, C15-T, C5+T, C10+T and C15+T were recorded in the wavelength range 250–750 nm using a Lambda 850+ UV/Vis spectrophotometer

(Perkin Elmer, United Kingdom) equipped with a reflection module—a 150 mm integration sphere—and fully controlled by a computer running WinLab 6 UV software. Three measurements were made for each sample at different angles of warp alignment, and the average value of transmittance,  $T$ , and reflectance,  $R$ , at each wavelength was calculated. Using the UV transmission spectra, the UV protection properties of the samples were determined according to the standard EN 13758-1: 2001. The main values of  $T$  were calculated at wavelengths of 315–400 nm (UVA), 290–315 nm (UVB) and 290–400 nm (UVR). The ultraviolet protection factor, UPF, was calculated as follows [41]:

$$\text{UPF} = \frac{\sum_{290}^{400} E(\lambda) \cdot \varepsilon(\lambda) \cdot \Delta\lambda}{\sum_{290}^{400} E(\lambda) \cdot \varepsilon(\lambda) \cdot T(\lambda) \cdot \Delta\lambda} \quad (3)$$

where  $E(\lambda)$  is the solar spectral irradiance,  $\varepsilon(\lambda)$  is the relative erythral effectiveness,  $\Delta(\lambda)$  is the wavelength interval and  $T(\lambda)$  is the spectral transmittance at the wavelength  $\lambda$ .

UPF rating and protection categories were determined using UPF values, calculated according to the Australian/New Zealand Standard for Sun-Protective Clothing—Evaluation and Classification (AS/NZS 4399, 2020), where UPF values of 15– correspond to the “minimum protection” category, UPF values of 30– correspond to the “good protection” category and UPF values of 50– correspond to the “excellent protection” category.

#### 2.4.8 Photocatalytic activity

The photocatalytic activity of chemically modified cotton samples was investigated using the photocatalytic degradation of Rhodamine B (RhB) dye solution under UV and visible light illumination. For this purpose, the samples UN, C5-T, C10-T, C15-T, C5+T, C10+T and C15+T with a size of 1 cm × 3 cm were immersed in 5 ml of 0.025 mM RhB solution in a Petri dish and exposed to UV light for 60, 120, 180 and 240 minutes in the Color Control Professional chamber (Just Normlicht – Vertriebs GmbH, Germany).

In addition, the samples UN, C5, T, C5-T and C5+T were also placed in a cuvette filled with 3 ml of 0.025 mM RhB solution and illuminated in a Xenotest Alpha instrument (Atlas, USA), equipped with a visible xenon arc lamp (radiation attitude 0.8–2.5 kVA and extended radiation range 300–400 nm). The cuvettes were illuminated for 30, 60, 120, 160 and 240 minutes. After each illumination time, the absorbance of the RhB solution was measured at  $\lambda_{max}$  and the corresponding concentration of RhB dye was determined using a previously prepared calibration curve. Measurements were performed using a Lambda 850+ UV/Vis spectrophotometer (Perkin Elmer, United Kingdom). The RhB dye degradation efficiency was calculated as the percentage of dye degradation,  $D$ , as follows [42]:

$$D = \frac{(c_0 - c_t)}{c_0} \cdot 100 (\%) \quad (4)$$

where  $c_0$  is the concentration of the RhB dye solution before illumination and  $c_t$  is the concentration of the RhB dye solution after a certain time of illumination. For comparison, the photodegradation of the 0.01 mM Methylene blue (MB) dye solution in the presence of the T, C5-T and C5+T samples was also carried out in a Xenotest Alpha instrument under the same conditions as in the case of the RhB dye solution.

#### 2.4.9 Colour fastness to light

The colour fastness of samples C5, C5-T and C5+T to xenon light was tested in accordance with the standard SIST EN ISO 105-B02:2014. The samples were exposed to light in a Xenotest alpha apparatus (Atlas, USA) for a specified time (72 hours). Light fastness was assessed by the colour difference,  $\Delta E_{ab}^*$ . For this purpose, ten measurements of the colour coordinates  $L^*$ ,  $a^*$  and  $b^*$  in the CIELAB colour space were made for each sample examined using a Datacolor Spectro 1050 spectrophotometer (Datacolor, USA). The measurements were performed with a 9 mm aperture under D65 illumination and an observation

angle of 10°. The value of  $\Delta E_{ab}^*$  was calculated using the following equation [40]:

$$\Delta E_{ab}^* = \sqrt{(\Delta L^*)^2 + (\Delta a^*)^2 + (\Delta b^*)^2} \quad (5)$$

where  $\Delta L^*$ ,  $\Delta a^*$  and  $\Delta b^*$  are the differences in the lightness, green–red, and blue–yellow colour coordinates, respectively, calculated between the illuminated and non-illuminated samples.

### 3 Results and discussion

The influence of the concentration of turmeric extract and the process of chemical modification on the colour yield of the cotton samples is shown in Figure 2. From both the photographs (Figure 2a) and the  $K/S$  values (Figure 2b), it can be seen that increasing the concentration of turmeric extract from 5 g/L to 10 g/L significantly increased the colour yield of the samples in both modification processes.

Accordingly, the  $K/S$  values increased from 0.4 for sample C5-T to 0.68 for sample C10-T and from 0.73 for sample C5+T to 1.71 for sample C10+T. In contrast, the additional increase in concentration from 10 g/L to 15 g/L turmeric extract did not contribute to colouration of the samples and even resulted in a slight decrease in colour yield. It is also clearly seen that at the same concentration of turmeric extract, the  $K/S$  values of samples C5+T, C10+T and C15+T are significantly higher compared to samples C5-T, C10-T and C15-T. This indicates that the chemical modification process strongly influenced the intensity of the colouration of the samples. Definitely, the colour strength of curcumin dye was higher in the chemical modification process involving the simultaneous dyeing of the cotton samples with turmeric extract and hydrothermal in-situ synthesis of TiO<sub>2</sub> than in the process where the samples were previously dyed with the turmeric extract followed by the hydrothermal in-situ synthesis of TiO<sub>2</sub> in the presence of the dyed cotton samples.

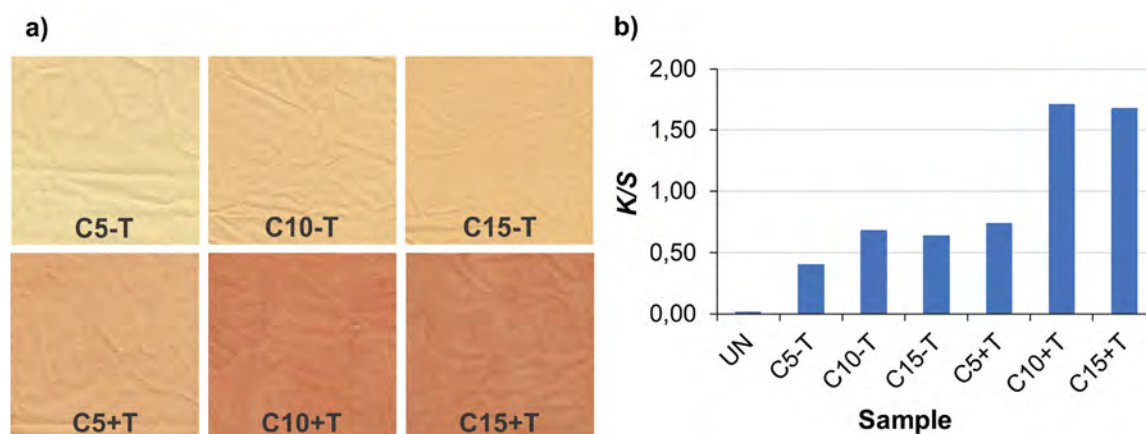


Figure 2: Photos of the chemically modified cotton samples (a);  $K/S$  values of untreated and chemically modified cotton samples (b)

To gain insight into the influence of the curcumin dye and TiO<sub>2</sub> on the functional properties of the chemically modified cotton samples, the UPF values and the efficiency of degradation of the RhB dye were determined (Figure 3). The results in Figure 3a show that the chemical modification of the cotton samples

resulted in a dramatic improvement in UV protection properties, as reflected by an increase in UPF values from 4.1 for sample UN to 42.2, 47.5 and 40.1 for samples C5-T, C10-T and C15-T, respectively, and to 53.2, 58.0 and 77.9 for samples C5+T, C10+T and C15+T. The UPF values of all three samples

C5-T, C10-T and C15-T correspond to the “good protection” category, and the UPF values of all three samples C5+T, C10+T and C15+T correspond to the “excellent protection” category. These results clearly show that simultaneous dyeing with turmeric extract and hydrothermal in-situ synthesis of  $\text{TiO}_2$  is beneficial to achieving maximum protection of cotton fabric against UV radiation. The highest UPF value was obtained for sample C15+T, in which the highest concentration of turmeric extract was used.

The efficiency of the chemically modified cotton samples for the degradation of the RhB dye solution was investigated under UV illumination, which is crucial for the photocatalytic activity of  $\text{TiO}_2$ . The results in Figure 2b clearly show that the photocatalytic degradation of the RhB dye solution was more efficient in the presence of samples C5-T, C10-T and C15-T than in the presence of samples C5+T, C10+T and C15+T, which is contrary to the results obtained for the UV protection properties. In terms of photocatalytic performance, it is reasonable to conclude that the chemically modified cotton samples prepared via the process in which  $\text{TiO}_2$  synthesis was carried out in the presence of the previously dyed

samples provided a more efficient photocatalytic platform for RhB dye degradation than the cotton samples prepared via simultaneous dyeing and  $\text{TiO}_2$  synthesis. Moreover, increasing the concentration of curcumin dye on the cotton samples hindered the photocatalytic efficiency of  $\text{TiO}_2$ , as the cotton samples dyed with 5 g/L turmeric extract exhibited the highest percentage of photodegraded RhB dye at all degradation time intervals. This phenomenon is particularly evident in the C5+T, C10+T and C15+T samples, where the  $\text{TiO}_2$  was synthesised in the turmeric extract. This suggests that the curcumin dye forms the composites with  $\text{TiO}_2$  in which it covers the  $\text{TiO}_2$  particles and hinders the  $\text{TiO}_2$  photocatalytic activity at higher dye concentrations. After considering both results, i.e., UPF and photocatalytic efficiency, samples C5-T and C5+T were selected as representative samples with the optimal multifunctional properties tailored with the combination of curcumin dye and  $\text{TiO}_2$  in both chemical modification processes and were therefore used for further investigations in comparison to the chemically modified samples with solei  $\text{TiO}_2$  or curcumin dye.

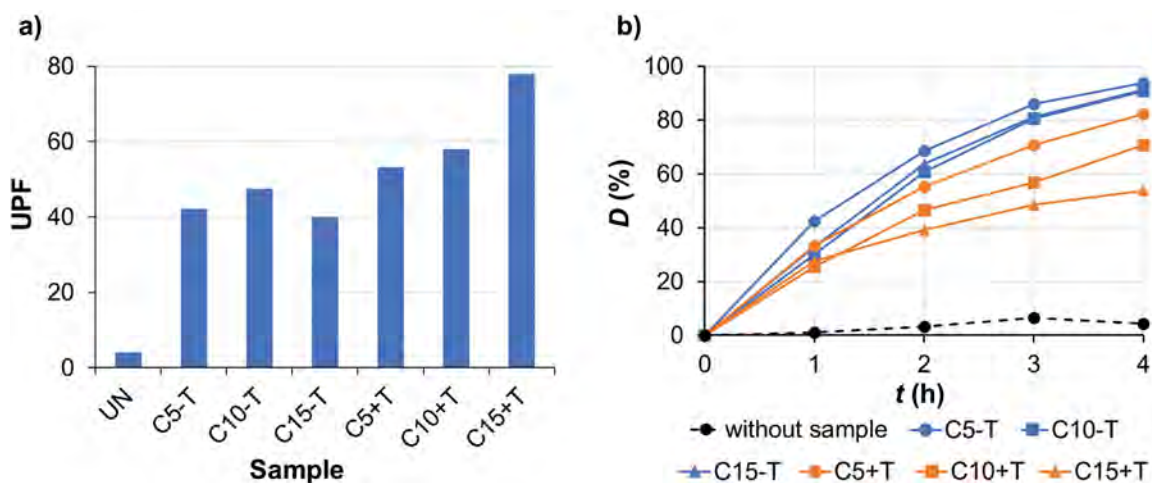


Figure 3: UPF of untreated and chemically modified cotton samples (a), photocatalytic degradation of the RhB dye solution without and in the presence of chemically modified cotton samples after different illumination times under UV light (b)

The SEM images of samples UN, C5, T, C5-T and C5+T are shown in Figure 4. As can be seen in the SEM image of sample UN, the untreated cellulose

fibres have a typical ribbon-like structure with a smooth and even surface, showing some natural impurities. Dyeing of the cotton samples with turmeric

extract did not cause any visible morphological surface changes in the cellulose fibres (sample C5). In contrast, in-situ synthesis of  $\text{TiO}_2$  particles resulted in an increase in the roughness of the cellulose fibres with a clearly visible thin  $\text{TiO}_2$  coating containing many small and larger  $\text{TiO}_2$  agglomerates (samples T, C5-T and C5+T). This phenomenon is most pronounced in sample C5+T.

The successful in-situ synthesis of  $\text{TiO}_2$  on the

cellulose fibres was confirmed by the EDS analysis, which is shown in Figure 5 for the representative sample T. From the EDS spectrum in Figure 5b, obtained from the part of Figure 5a marked with a yellow frame, and from the element mapping images in Figure 5c, it is clear that sample T contains Ti, O and C elements in the structure. The EDS analysis also confirms that the white spots in Figure 5a represent  $\text{TiO}_2$  particles.

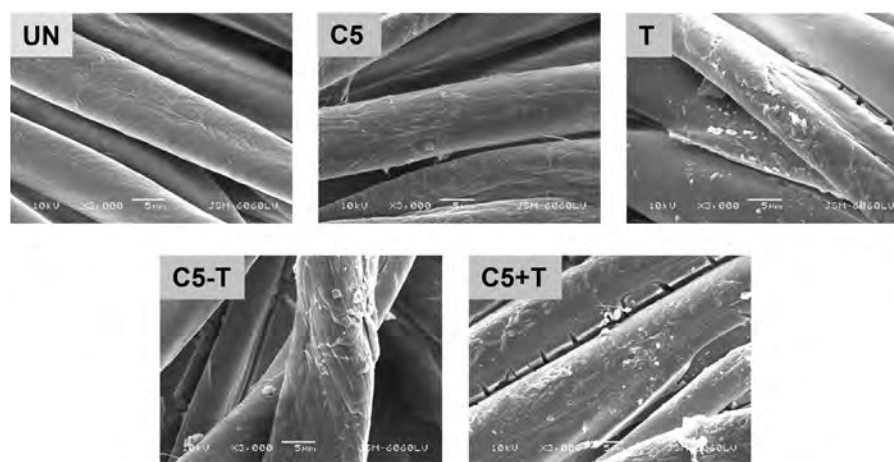


Figure 4: SEM images of the untreated and chemically modified cotton samples at 3000x magnification

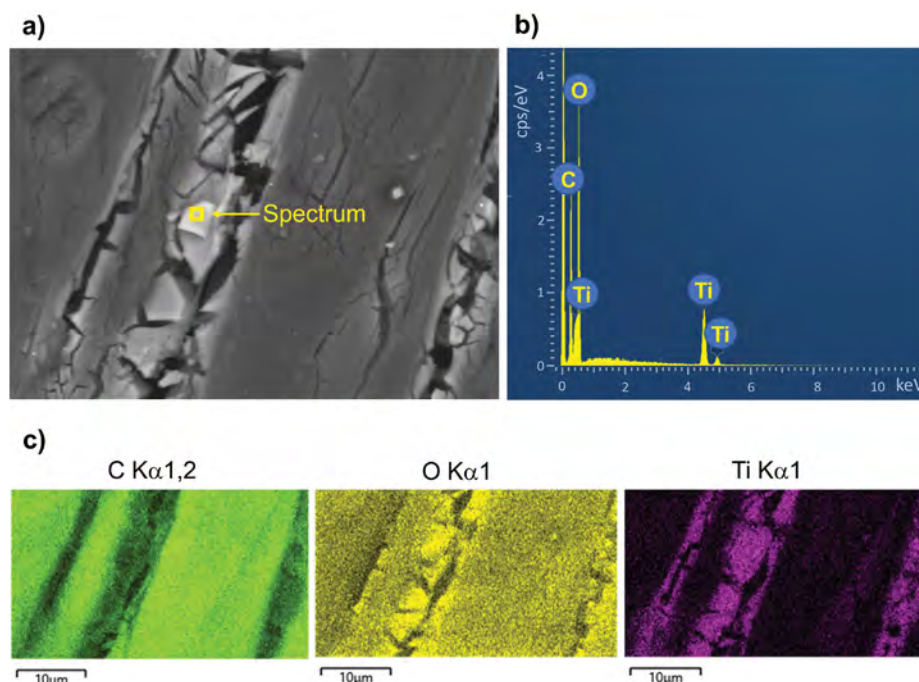


Figure 5: SEM/BSE image of the sample T with the position of the EDS analysis (a), EDS spectrum (b) and element mapping images of C, O, and Ti (c) in the sample T

The total content of  $\text{TiO}_2$  in samples T, C5-T and C5+T was determined by calculating the dry solid add-on and using ICP-MS analysis (Table 2). From Table 2, the amount of  $\text{TiO}_2$  synthesised with the same 4% TTIP sol was highest in sample C5+T, followed by sample T, and the lowest amount was obtained in sample C5-T. This indicates that the hydrothermal in-situ synthesis of  $\text{TiO}_2$  was promoted in turmeric extract (sample C5+T) compared to water (sample T). In contrast, the presence of curcumin dye in the previously dyed cotton samples slightly decreased the amount of  $\text{TiO}_2$  synthesised (sample C5-T). Based on these results, the simultaneous dyeing of cotton samples with turmeric extract and hydrothermal in-situ synthesis of  $\text{TiO}_2$  is favourable for the production of chemically modified cotton fabric.

Table 2: Dry solid add-on and the concentration of  $\text{TiO}_2$  in the chemically modified samples included  $\text{TiO}_2$

Sample	<i>m</i> (g)	Add-on (%)	<i>c</i> $\text{TiO}_2$ (mg/kg)
UN	0.287	/	/
T	0.291	1.39	8600
C5-T	0.289	0.70	8000
C5+T	0.295	2.79	8900

The XRD analysis of the samples UN, T, C5-T and C5+T shown in Figure 6 provided valuable information about the crystal phases of the in-situ synthesised  $\text{TiO}_2$  in the cotton samples. The XRD pattern of sample UN shows well-defined diffraction peaks at  $2\theta = 15.0^\circ$ ,  $16.8^\circ$ ,  $22.7^\circ$  and  $34.5^\circ$ , corresponding to the (110),  $(11\bar{0})$ , (200) and (400) crystallographic planes of the crystalline structure of cellulose, respectively [43]. As expected, these peaks are also clearly visible in samples T, C5-T and C5+T. The prominent diffraction peaks at  $2\theta = 25.3^\circ$ ,  $37.8^\circ$  and  $48^\circ$ , corresponding to the (101), (220) and (022) crystallographic planes of the anatase crystalline phase of  $\text{TiO}_2$  [44], could not be detected in samples T, C5-T and C5+T, suggesting that the in-situ synthesised  $\text{TiO}_2$  has an amorphous structure. This is plausible, since the hydrothermal in-situ synthesis of  $\text{TiO}_2$  was carried out at  $120^\circ\text{C}$ , which is too low for

the calcination of  $\text{TiO}_2$  to produce crystalline phases. The same results have been reported in the literature [44–46].

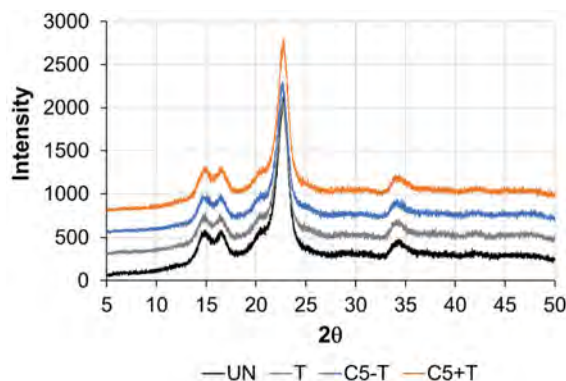


Figure 6: XRD patterns of the samples UN, T, C5-T and C+T

The influence of curcumin dye and  $\text{TiO}_2$  on the chemical properties of the chemically modified cotton samples was determined by FTIR analysis (Figure 7). The IR ATR spectrum of the sample UN showed the absorption bands characteristic of the cellulose fingerprint in the  $1500\text{--}800\text{ cm}^{-1}$  region, corresponding to C–H, C–O, C–C C–O–C and O–H vibrations [47]. A comparison of the IR ATR spectrum of sample C5 with that of sample UN revealed no significant changes. This suggests that the characteristic bands of turmeric occurring at  $1740\text{--}1680\text{ cm}^{-1}$  due to C=O absorption, at  $\sim 1510\text{ cm}^{-1}$  due to aromatic skeletal stretching vibration and at  $\sim 1030\text{ cm}^{-1}$  due to C–OH stretching vibration were blurred by the strong vibrational bands of cellulose [48]. In addition, the characteristic bands of  $\text{TiO}_2$  in samples T, C5-T and C5+T, which appear at  $700\text{--}600\text{ cm}^{-1}$ , could not be detected by FTIR analysis due to the low concentration of  $\text{TiO}_2$  [47]. The  $\text{TiO}_2$  vibrations that appear at wavenumbers below  $600\text{ cm}^{-1}$  could not be analysed.

Transmission and reflection spectra were recorded to determine the influence of the curcumin dye and  $\text{TiO}_2$  on the UV protection properties of the chemically modified cotton samples (Figure 8, Table 3). From Figure 8a, it can be seen that the transmission

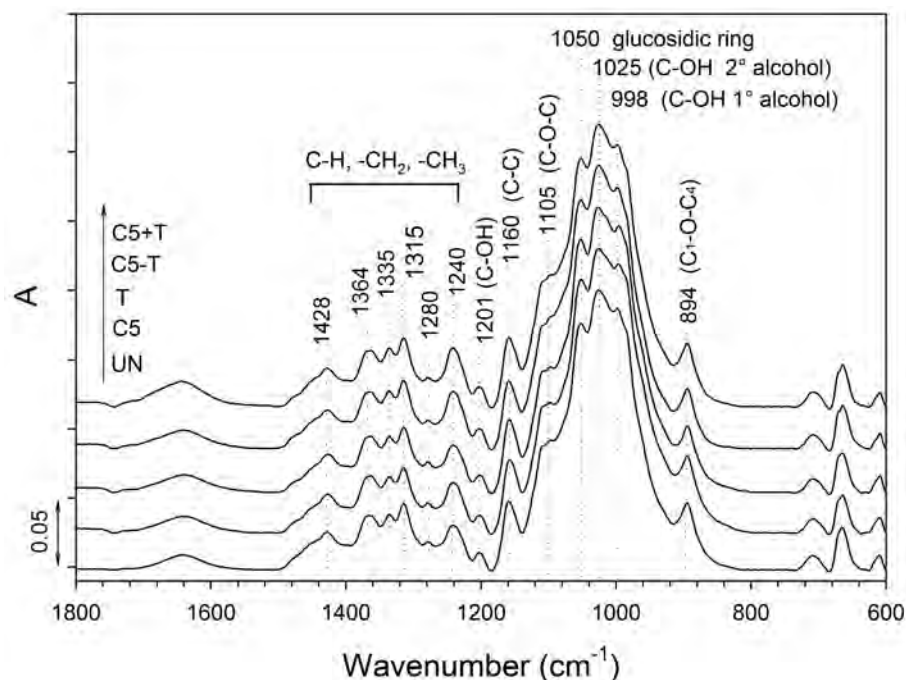


Figure 7: IR ATR spectra of the samples UN, C5, T, C5-T and C5+T

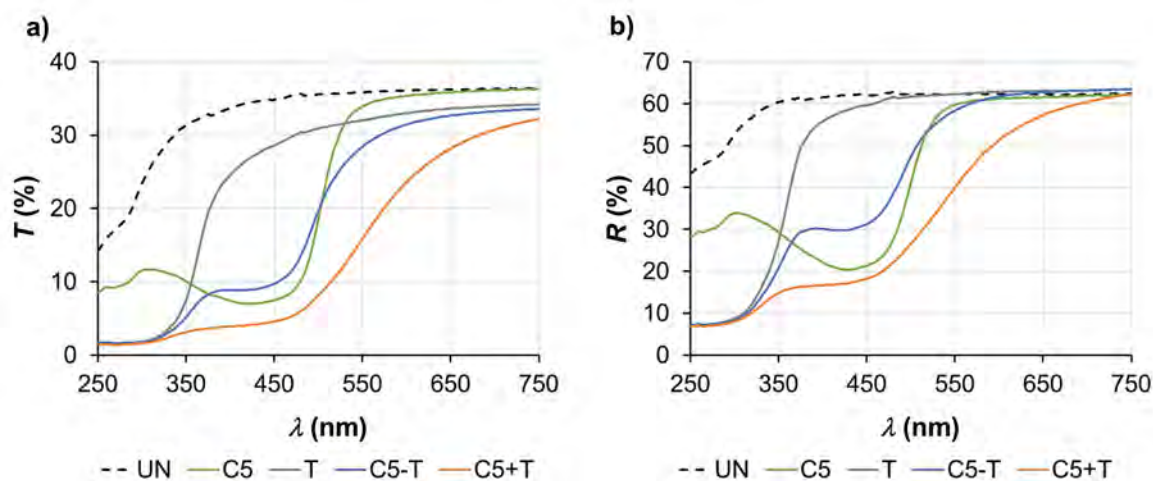


Figure 8: Transmission (a) and reflection (b) spectra of the samples UN, C5, T, C5-T and C5+T.

of UV rays (250–400 nm) through the sample UN was between 15% and 35%, which was too high to provide UV protection properties. Accordingly, the UPF of the sample UN was very low (3.86 in Table 3). The presence of curcumin dye reduced the transmission of UV rays through sample C5 compared to sample UN with  $T$  values of 9.52% for the UVA region and 11.41% for the UVB region (Table 3). However, the  $T$  values of about 10% were too high to provide minimal

UV protection. In contrast to the curcumin dye, the presence of TiO<sub>2</sub> drastically reduced the transmission of UV rays in the UVB (290–315 nm) region, but in the UVA (315–400 nm) region, the transmission increased significantly and even exceeded that of sample C5 (Figure 8a). This resulted in a UPF value of 34.29, which is categorized as good protection. The combination of the curcumin dye with TiO<sub>2</sub> in samples C5-T and C5+T improved their UV

protection properties. In particular, at UVA, the synergism between the curcumin dye and  $\text{TiO}_2$  led to a significant reduction in  $T$  values to 6.04 and 3.15 for samples C5-T and C5+T, respectively. This resulted in a UPF value of 42.17 for sample C5-T and 53.24 for sample C5+T. The latter is in the 50+ category, which corresponds to excellent protection. Since the

reflection spectra of samples C5, T, C5-T and C5+T (Figure 8b) are lower than the spectrum of sample UN, this suggests that the UV blocking mechanism of  $\text{TiO}_2$  is based on the absorption of UV light. As expected, the same phenomenon was observed for the curcumin dye due to the absorption capacity of the conjugated system in its aromatic structure.

Table 3: The arithmetic mean of transmittance,  $T$ , in the UVA, UVB and UVR ranges and the UVR protection categories for the untreated and functionalised cotton samples according to the Australian/New Zealand Standard Sun-Protective Clothing—Evaluation and Classification

Sample	$T$ (UVA) (%)	$T$ (UVB) (%)	$T$ (UVR) (%)	UPF	UVR protection category <sup>a)</sup>
UN	31.28	23.71	29.53	3.86	NR
C5	9.52	11.41	9.96	8.75	NR
T	12.43	1.91	9.98	34.29	G
C5-T	6.04	1.87	5.07	42.17	G
C5+T	3.15	1.64	2.80	53.24	E

<sup>a)</sup> NR – non rateable, G – good protection, E – excellent protection

The photocatalytic activity of  $\text{TiO}_2$  in the cotton samples without and with the presence of the curcumin dye was investigated using the rate of degradation of RhB and MB dyes under visible light illumination (Figure 9). Visible light illumination was chosen to determine whether the presence of the curcumin dye in samples C5-T and C5+T could act as a sensitizer and have a photosensitisation effect on the visible-light-induced photocatalytic performance of  $\text{TiO}_2$ . The results in Figure 9a clearly show that, as expected, samples UN and C5 did not exhibit photocatalytic activity, resulting in insignificant photodegradation of the RhB dye solution, which was still coloured after 4 hours of illumination, very similar to the blank solution without a sample (Figure 9c). In contrast, the photodegradation of the RhB dye solution in the presence of samples T, C5-T and C5+T was very efficient, with the percentage of dye degradation being over 95% in 2 hours of illumination and almost 100% in 4 hours of illumination, resulting in the complete decolourisation of the RhB dye solution (Figure 9c). A close inspection of Figure 9a reveals that the presence of the curcumin dye slightly hindered the photodegradation performance of

$\text{TiO}_2$  at the beginning of the illumination compared to sample T. However, the photodegradation performance of samples C5-T and C5+T was comparable to that of sample T at longer illumination times. In the experiment on the photodegradation of the MB dye (Figure 9b), the C5+T sample showed slightly higher photocatalytic activity than the T and C5-T samples after 1 hour of illumination; however, this phenomenon did not occur at longer illumination times, when the photodegradation efficiency of the T, C5-T and C5+T samples was very similar (Figure 9b). Comparison of the results in Figure 9a and Figure 9b also shows that the photodegradation efficiency of the T, C5-T and C5+T samples is slightly higher for the RhB dye than for the MB dye, resulting in a photodegradation of more than 98% for the RhB dye and about 95% for the MB dye after 4 hours of illumination. This indicates that the chemical structure of the dye influences the photodegradation efficiency of the photocatalyst, which is consistent with literature data [49].

The results in Figure 9 clearly indicate that the photocatalytic activity of  $\text{TiO}_2$  was maintained in the presence of the curcumin dye but was not en-

hanced under visible light. The curcumin dye definitely did not act as a sensitizer for TiO<sub>2</sub> in samples C5-T and C5+T. It can be concluded that the two chemical modification processes investigated do

not provide the conditions for the creation of a curcumin-TiO<sub>2</sub> heterojunction with visible-light-driven photocatalysis.

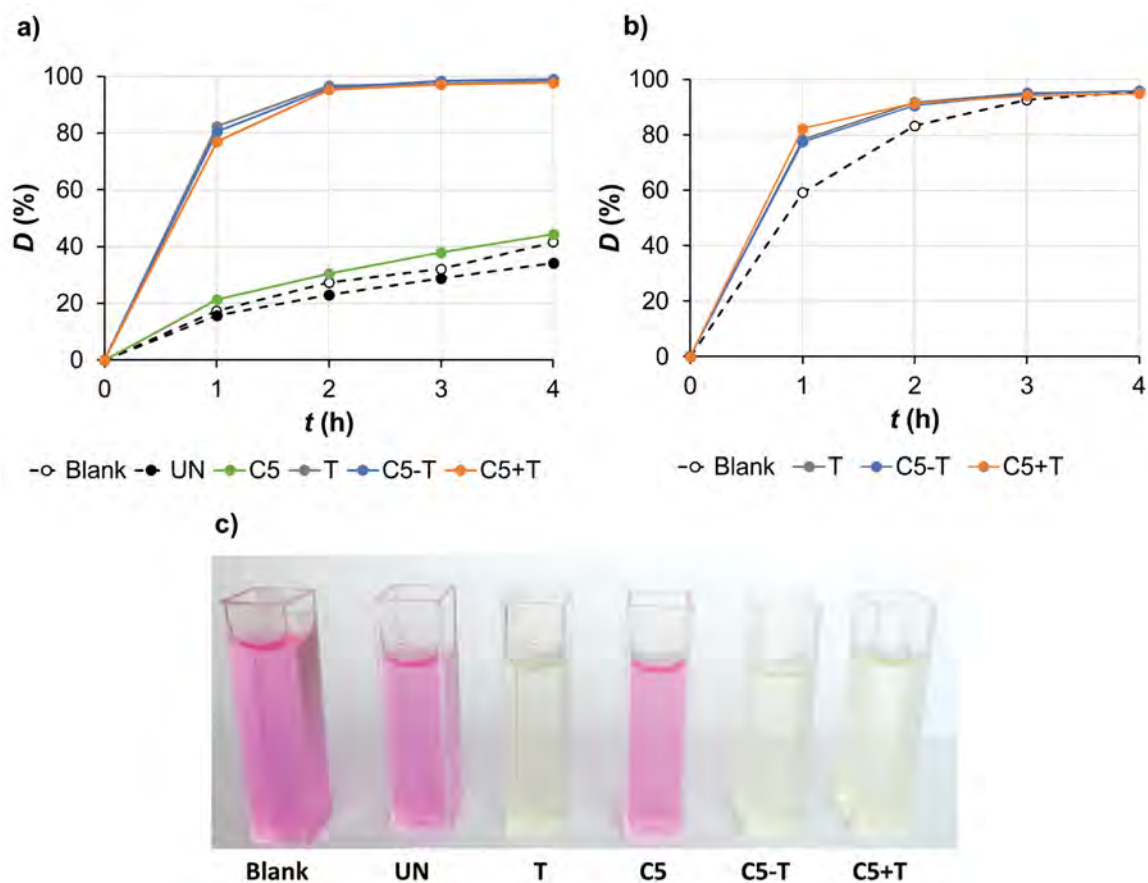


Figure 9: Photocatalytic degradation of RhB (a) and MB (b) dyes solution without sample (blank) and in the presence of samples UN, C5, T, C5-T, and C5+T after different illumination times under visible light; photos of RhB dye solution after 4 hours of radiation without and in the presence of the samples (c)

To verify whether the photocatalytic effect of TiO<sub>2</sub> causes photodegradation of the curcumin dye in samples C5-T and C5+T, the colour fastness of these samples was determined in comparison to sample C5 without TiO<sub>2</sub> and the results are shown in Table 4. It can be seen that the colour of all samples faded during illumination, resulting in high values of  $\Delta E_{ab}^*$ . This phenomenon was expected as it is known that most natural dyes have poor colour fastness to light, which is also true for curcumin [50]. However, the results in Table 4 show that the

highest value of  $\Delta E_{ab}^*$  was obtained for sample C5 and that this value was much higher than the  $\Delta E_{ab}^*$  values of samples C5-T and C5+T, indicating that the presence of TiO<sub>2</sub> did not promote but rather inhibited the photodegradation of the curcumin dye, confirming the compatibility of the curcumin and TiO<sub>2</sub> in the chemically modified cotton samples. This phenomenon may be surprising, as cotton samples loaded with TiO<sub>2</sub> efficiently photodegrade both RhB and MB dyes. However, it should be emphasised that the photodegradation of the RhB and

MB dyes was carried out in the dye solutions, the colour fastness of the curcumin dye was investigated on dry cotton samples. It is evident that for the photocatalytic activity of  $\text{TiO}_2$ , a sufficient amount of water must be absorbed at the surface of the  $\text{TiO}_2$

particles to generate reactive hydroxyl radicals. At the same time,  $\text{TiO}_2$  acted as a UV absorber on the textile surface, which significantly reduced the dose of UV rays reaching the curcumin dye and causing its photodegradation.

Table 4: Colour fastness to light of the chemically modified cotton samples

Sample	Illumination time (h)	$L^*$	$a^*$	$b^*$	$\Delta E^*_{ab}$
C5	0	89.87	-5.73	76.24	74.90
	72	93.54	-0.25	1.63	
C5-T	0	90.16	-5.97	50.75	51.14
	72	94.03	-0.33	0.07	
C5+T	0	73.94	10.11	44.95	47.68
	72	93.24	-0.34	2.62	

## 4 Conclusion

A novel green process for the chemical modification of cotton fabric was developed using the combination of curcumin dye and  $\text{TiO}_2$  to adjust the simultaneous photocatalytic activity and UV protection properties. During development, the influence of concentration of the turmeric extract and the two application processes on the functional properties of the chemically modified cotton fabric was thoroughly investigated. It was found that the optimum functional properties of the cotton fabric were achieved when the lowest concentration (5 g/L) of turmeric extract was applied and that the greener process including the simultaneous dyeing of cotton samples with turmeric extract and in-situ synthesis of  $\text{TiO}_2$  was more beneficial than the classical process in which the cotton sample was first dyed with turmeric extract and then in-situ synthesis of  $\text{TiO}_2$  was performed on the dyed sample.

It was found that the presence of the curcumin dye did not cause any visible morphological changes in the cellulose fibres, while the in-situ synthesis of  $\text{TiO}_2$  particles resulted in an increase in the roughness of the cellulose fibres with a clearly visible thin  $\text{TiO}_2$  coating containing many small and larger  $\text{TiO}_2$  agglomerates. The application of both the curcumin dye and  $\text{TiO}_2$  did not lead to significant changes in

the chemical structure of the cellulose fibres. Hydrothermal in-situ synthesis of  $\text{TiO}_2$  was promoted in turmeric extract compared to water, resulting in a higher total  $\text{TiO}_2$  content in the sample compared to that chemically modified in the absence of turmeric extract. As the hydrothermal in-situ synthesis of  $\text{TiO}_2$  was carried out at 120 °C, an amorphous structure of  $\text{TiO}_2$  was obtained in the chemically modified cotton sample.

The combination of the curcumin dye and  $\text{TiO}_2$  in the chemically modified cotton sample drastically improved the UV protection properties, resulting in a UPF value of 53.24, which corresponds to excellent protection. While  $\text{TiO}_2$  alone provided excellent UV protection in the UVB region, the curcumin dye significantly reduced the transmission of the sample in the UVA region, representing a synergistic effect between the two players. The presence of curcumin did not hinder the photocatalytic activity of  $\text{TiO}_2$  under visible light, but it also did not act as a sensitizer for  $\text{TiO}_2$ . This indicates that the chemical modification process developed did not create a curcumin- $\text{TiO}_2$  heterojunction with visible-light-driven photocatalysis. The inhibition of the photodegradation of the curcumin dye in the presence of  $\text{TiO}_2$  also confirmed the compatibility of the two players in the chemically modified cotton samples.

### Acknowledgments

This research was carried out within the framework of the courses on Advanced Finishing Processes and Chemical Functionalisation of Textiles in the Master Study Programme for Textile and Clothing Planning. The research was co-funded by the Slovenian Research and Innovation Agency (Programme P2-0213 Textiles and Ecology, Infrastructural Centre RIC UL-NTF).

### References

1. RIVERO, P.J., URRUTIA, A., GOICOECHEA, J., ARREGUI, F.J. Nanomaterials for functional textiles and fibers. *Nanoscale Research Letters*, 2015, **10**, 1–22, doi: 10.1186/s11671-015-1195-6.
2. PRINIOTAKIS, G., MARROT, L., STACHEWICZ, U., KRSTIC-FURUNDZIC, A., VENTURINI, E., JONAITIENE, V. Smart textile for building and living. *Autex Research Journal*, 2022, **22**(4), 493–496, doi: 10.2478/aut-2021-0041.
3. SHAH, M.A., PIRZADA, B.M., PRICE, G., SHIBIRU, A.L., QURASHI, A. Applications of nanotechnology in smart textile industry: a critical review. *Journal of Advanced Research*, 2022, **38**, 55–75, doi: 10.1016/j.jare.2022.01.008.
4. POPESCU, M., UNGUREANU, C. Green nanomaterials for smart textiles dedicated to environmental and biomedical applications. *Materials (Basel)*, 2023, **16**(11), 1–27, doi: 10.3390/ma16114075.
5. RADETIĆ, M. Functionalization of textile materials with TiO<sub>2</sub> nanoparticles. *Journal of Photochemistry and Photobiology C: Photochemistry Reviews*, 2013, **16**, 62–76, doi: 10.1016/j.jphotochemrev.2013.04.002.
6. RASHID, M.M., SIMONČIČ, B., TOMŠIČ, B. Recent advances in TiO<sub>2</sub>-functionalized textile surfaces. *Surfaces and Interfaces*, 2021, **22**, 1–33, doi: 10.1016/j.surfin.2020.100890.
7. ETACHERI, V., DI VALENTIN, C., SCHNEIDER, J., BAHNEMANN, D., PILLAI, S.C. Visible-light activation of TiO<sub>2</sub> photocatalysts: advances in theory and experiments. *Journal of Photochemistry and Photobiology C: Photochemistry Reviews*, 2015, **25**, 1–29, doi: 10.1016/j.jphotochemrev.2015.08.003.
8. NAM, Y., LIM, J.H., KO, K.C., LEE, J.Y. Photocatalytic activity of TiO<sub>2</sub> nanoparticles: a theoretical aspect. *Journal of Materials Chemistry A*, 2019, **7**, 13833–13859, doi: 10.1039/c9ta03385h.
9. EID, B.M., IBRAHIM, N.A. Recent developments in sustainable finishing of cellulosic textiles employing biotechnology. *Journal of Cleaner Production*, 2021, **284**, 1–22, doi: 10.1016/j.jclepro.2020.124701.
10. WANG, X., JIANG, J., GAO, W. Reviewing textile wastewater produced by industries: characteristics, environmental impacts, and treatment strategies. *Water Science & Technology*, 2022, **85**(7), 2076–2096, doi: 10.2166/wst.2022.088.
11. RAJ, A., CHOWDHURY, A., ALI, S.W. Green chemistry: its opportunities and challenges in colouration and chemical finishing of textiles. *Sustainable Chemistry and Pharmacy*, 2022, **27**, 1–17, doi: 10.1016/j.scp.2022.100689.
12. HUSTON, M., DEBELLA, M., DIBELLA, M., GUPTA, A. Green synthesis of nanomaterials. *Nanomaterials*, 2021, **11**(8), 1–29, doi: 10.3390/nano11082130.
13. SAMUEL, M.S., RAVIKUMAR, M., JOHN, A., SELVARAJAN, E., PATEL, H., CHANDER, P.S., SOUNDARYA, J., VUPPALA, S., BALAJI, R., CHANDRASEKAR, N. A review on green synthesis of nanoparticles and their diverse biomedical and environmental applications. *Catalysts*, 2022, **12**(5), 1–24, doi: 10.3390/catal12050459.
14. GUPTA, D., BOORA, A., THAKUR, A., GUPTA, T.K. Green and sustainable synthesis of nanomaterials: recent advancements and limitations. *Environmental Research*, 2023, **231**(3), 1–18, doi: 10.1016/j.envres.2023.116316.

15. NABI, G., QURAT-UL-AAIN; KHALID, N.R., TAHIR, M.B., RAFIQUE, M., RIZWAN, M., HUSSAIN, S., IQBAL, T., MAJID, A. A review on novel eco-friendly green approach to synthesis TiO<sub>2</sub> nanoparticles using different extracts. *Journal of Inorganic and Organometallic Polymers and Materials*, 2018, **28**, 1552–1564, doi: 10.1007/s10904-018-0812-0.
16. ILYAS, M., WARIS, A., KHAN, A.U., ZAMEL, D., YAR, L., BASET, A., MUHAYMIN, A., KHAN, S., ALI, A., AHMAD, A. Biological synthesis of titanium dioxide nanoparticles from plants and microorganisms and their potential biomedical applications. *Inorganic Chemistry Communications*, 2021, **133**, 1–9, doi: 10.1016/j.inoche.2021.108968.
17. IRSHAD, M.A., NAWAZ, R., UR REHMAN, M.Z., ADREES, M., RIZWAN, M., ALI, S., AHMAD, S., TASLEEM, S. Synthesis, characterization and advanced sustainable applications of titanium dioxide nanoparticles: a review. *Ecotoxicology and Environmental Safety*, 2021, **212**, 1–14, doi: 10.1016/j.ecoenv.2021.111978.
18. GONÇALVES, R.A., TOLEDO, R.P., JOSHI, N., BERENGUE, O.M. Green synthesis and applications of ZnO and TiO<sub>2</sub> nanostructures. *Molecules*, 2021, **26**(8), 1–39, doi: 10.3390/molecules26082236.
19. SAGADEVAN, S., IMTEYAZ, S., MURUGAN, B., LETT, J.A., SRIDEWI, N., WELDEGEBRIEAL, G.K., FATIMAH, I., OH, W.-C. A comprehensive review on green synthesis of titanium dioxide nanoparticles and their diverse biomedical applications. *Green Processing and Synthesis*, 2022, **11**, 44–63, doi: 10.1515/gps-2022-0005.
20. SHIVA SAMHITHA, S., RAGHAVENDRA, G., QUEZADA, C., HIMA BINDU, P. Green synthesized TiO<sub>2</sub> nanoparticles for anticancer applications: mini review. *Materials Today: Proceedings*, 2022, **54**(3), 765–770, doi: 10.1016/j.matpr.2021.11.073.
21. SINGH JASSAL, P., KAUR, D., PRASAD, R., SINGH, J. Green synthesis of titanium dioxide nanoparticles: development and applications. *Journal of Agriculture and Food Research*, 2022, **10**, 1–14, doi: 10.1016/j.jafr.2022.100361.
22. VERMA, V., AL-DOSSARI, M., SINGH, J., RAWAT, M., KORDY, M.G.M., SHABAN, M. A review on green synthesis of TiO<sub>2</sub> NPs: synthesis and applications in photocatalysis and antimicrobial. *Polymers (Basel)*, 2022, **14**(7), 1–19, doi: 10.3390/polym14071444.
23. DOSOKY, N.S., SETZER, W.N. Chemical composition and biological activities of essential oils of curcuma species. *Nutrients*, 2018, **10**(9), 1–42, doi: 10.3390/nu10091196.
24. STATI, G., SANCILIO, S., BASILE, M., ANGELELLI, A., DI PIETRO, R. *Curcuma longa* aqueous extract: a potential solution for the prevention of corneal scarring as a result of pterygium surgical excision (review). *International Journal of Molecular Medicine*, 2020, **46**(6), 1951–1957, doi: 10.3892/ijmm.2020.4738.
25. FULORIA, S., MEHTA, J., CHANDEL, A., SEKAR, M., RANI, N.N.I.M., BEGUM, M.Y., SUBRAMANIYAN, V., CHIDAMBARAM, K., THANGAVELU, L., NORDIN, R., WU, Y.S., SATHASIVAM, K.V., LUM, P.T., MEENAKSHI, D.U., KUMARASAMY, V., AZAD, A.K., FULORIA, N.K. A comprehensive review on the therapeutic potential of *Curcuma longa* Linn. in relation to its major active constituent curcumin. *Frontiers in Pharmacology*, 2022, **13**, 1–27, doi: 10.3389/fphar.2022.820806.
26. SELVAM, R.M., ATHINARAYANAN, G., NANTHINI, A.U.R., SINGH, A.J.A.R., KALIRAJAN, K., SELVAKUMAR, P.M. Extraction of natural dyes from *Curcuma longa*, *Trigonella foenum graecum* and *Nerium oleander*, plants and their application in antimicrobial fabric. *Industrial Crops and Products*, 2015, **70**, 84–90, doi: 10.1016/j.indcrop.2015.03.008.
27. JOSE, S., GURUMALLESH PRABU, H., AMMAYAPPAN, L. Eco-friendly dyeing of silk and cotton textiles using combination of three natural colorants. *Journal of Natural Fibers*, 2017, **14**(1), 40–49, doi: 10.1080/15440478.2015.1137530.

28. PERKIČ, N., GORJANC, M. Vpliv poobdelav na obarvljivost surovega in beljenega bombaža s kurkuminom in doseganje motivov s tehniko antotipije. *Tekstilec*, 2017, **60**(1), 4–13, doi: 10.14502/Tekstilec2017.60.4-13.
29. GORJANC, M., MOZETIČ, M., VESEL, A., ZAPLOTNIK, R. Natural dyeing and UV protection of plasma treated cotton. *The European Physical Journal D*, 2018, **72**, 1–6, doi: 10.1140/epjd/e2017-80680-9.
30. KABIR, S.M.M., HASAN, M.M., UDDIN, M.Z. Novel approach to dye polyethylene terephthalate (PET) fabric in supercritical carbon dioxide with natural curcuminoid dyes. *Fibres & Textiles in Eastern Europe*, 2019, **27**, 65–70, doi: 10.5604/01.3001.0013.0744.
31. TOPRAK-CAVDUR, T., UYSAL, S., GIBERT-PAYA, J. Dyeing recycled cotton fibers using *Curcuma longa* and *Pterocarpus santalinus* natural dyes and bio-mordant chitosan. *Journal of Natural Fibers*, 2022, **19**(16), 13736–13752, doi: 10.1080/15440478.2022.2105469.
32. BUDDEE, S., WONGNAWA, S., SRIPRANG, P., SRIWONG, C. Curcumin-sensitized TiO<sub>2</sub> for enhanced photodegradation of dyes under visible light. *Journal of Nanoparticle Research*, 2014, **16**, 1–21, doi: 10.1007/s11051-014-2336-z.
33. ABDUL JALILL, R.D., NUAMAN, R.S., ABD, A.N. Biological synthesis of titanium dioxide nanoparticles by *Curcuma longa* plant extract and study its biological properties. *World Scientific News*, 2016, **49**(2), 204–222.
34. LIM, J., BOKARE, A.D., CHOI, W. Visible light sensitization of TiO<sub>2</sub> nanoparticles by a dietary pigment, curcumin, for environmental photochemical transformations. *RSC Advances*, 2017, **7**, 32488–32495, doi: 10.1039/c7ra05276f.
35. RUHANE, T.A., ISLAM, M.T., RAHAMAN, M.S., BHUIYAN, M.M.H., ISLAM, J.M.M., NEWAZ, M.K., KHAN, K.A., KHAN, M.A. Photo current enhancement of natural dye sensitized solar cell by optimizing dye extraction and its loading period. *Optik*, 2017, **149**, 174–183, doi: 10.1016/j.ijleo.2017.09.024.
36. DIL, M.A., HAGHIGHATZADEH, A., MAZINANI, B. Photosensitization effect on visible-light-induced photocatalytic performance of TiO<sub>2</sub>/chlorophyll and flavonoid nanostructures: kinetic and isotherm studies. *Bulletin of Materials Science*, 2019, **42**, 1–16, doi: 10.1007/s12034-019-1927-9.
37. KABIR, F., BHUIYAN, M.M.H., HOSSAIN, M.R., BASHAR, H., RAHAMAN, M.S., MANIR, M.S., ULLAH, S.M., UDDIN, S.S., MOLLAH, M.Z.I., KHAN, R.A., et al. Improvement of efficiency of dye sensitized solar cells by optimizing the combination ratio of natural red and yellow dyes. *Optik*, 2019, **179**, 252–258, doi: 10.1016/j.ijleo.2018.10.150.
38. ANOUA, R., LIFI, H., TOUHTOUH, S., EL JOUAD, M., HAJJAJI, A., BAKASSE, M., PŁOCIENNIK, P., ZAWADZKA, A. Optical and morphological properties of *Curcuma longa* dye for dye-sensitized solar cells. *Environmental Science and Pollution Research*, 2021, **28**, 57860–57871, doi: 10.1007/s11356-021-14551-9.
39. VENKATAS, J., DANIELS, A., SINGH, M. The Potential of curcumin-capped nanoparticle synthesis in cancer therapy: a green synthesis approach. *Nanomaterials*, 2022, **12**(18), 1–23, doi: 10.3390/nano12183201.
40. BERGER-SCHUNN, A. *Practical color measurement*. New York : John Wiley Sons, 1994, p. 39.
41. SIST EN 13758-1:2002. Textiles - Solar UV protective properties - Part 1: Method of test for apparel fabrics. 12 p.
42. SIRIRERKRATANA, K., KEMACHEEVAKUL, P., CHUANGCHOTE, S. Color removal from wastewater by photocatalytic process using titanium dioxide-coated glass, ceramic tile, and stainless steel sheets. *Journal of Cleaner Production*, 2019, **215**, 123–130, doi: 10.1016/j.jclepro.2019.01.037.
43. ZHAO, H., KWAK, J.H., CONRAD ZHANG, Z., BROWN, H.M., AREY, B.W., HOLLADAY, J.E. Studying cellulose fiber structure by SEM, XRD, NMR and acid hydrolysis. *Carbohydrate*

- Polymers*, 2007, **68**(2), 235–241, doi: 10.1016/j.carbpol.2006.12.013.
44. ARBUJ, S.S., HAWALDAR, R.R., MULIK, U.P., WANI, B.N., AMALNERKAR, D.P., WAGH-MODE, S.B. Preparation, characterization and photocatalytic activity of TiO<sub>2</sub> towards methylene blue degradation. *Materials Science and Engineering: B*, 2010, **168**(1–3), 90–94, doi: 10.1016/j.mseb.2009.11.010.
45. KIM, M.G., KANG, J.M., LEE, J.E., KIM, K.S., KIM, K.H., CHO, M., LEE, S.G. Effects of calcination temperature on the phase composition, photocatalytic degradation, and virucidal activities of TiO<sub>2</sub> nanoparticles. *ACS Omega*, 2021, **6**(16), 10668–10678, doi: 10.1021/acsomega.1c00043.
46. RASHID, M.M., ZORC, M., SIMONČIČ, B., JERMAN, I., TOMŠIČ, B. In-situ functionalization of cotton fabric by TiO<sub>2</sub>: the influence of application routes. *Catalysts*, 2022, **12**(11), 1–17, doi: 10.3390/catal12111330.
47. SOCRATES, G. *Infrared and raman characteristic group frequencies: tables and charts*. 3rd edition. New York : John Wiley & Sons, 2004.
48. ROHAETI, E., RAFI, M., SYAFITRI, U.D., HERYANTO, R. Fourier transform infrared spectroscopy combined with chemometrics for discrimination of *Curcuma longa*, *Curcuma xanthorrhiza* and *Zingiber cassumunar*. *Spectrochimica Acta, Part A: Molecular and Biomolecular Spectroscopy*, 2015, **137**, 1244–1249, doi: 10.1016/j.saa.2014.08.139.
49. BÖTTCHER, H., MAHLTIG, B., SARSOUR, J., STEGMAIER, T. Qualitative investigations of the photocatalytic dye destruction by TiO<sub>2</sub>-coated polyester fabrics. *Journal of Sol-Gel Science and Technology*, 2010, **55**, 177–185, doi: 10.1007/s10971-010-2230-9.
50. ZHOU, Y., TANG, R.C. Influence of fixing treatment on the color fastness and bioactivities of silk fabric dyed with curcumin. *The Journal of The Textile Institute*, 2017, **108**(6), 1050–1056, doi: 10.1080/00405000.2016.1219447.

Arzu Marmarali,<sup>1</sup> Mehmet Sevgi<sup>2</sup>

<sup>1</sup> Department of Textile Engineering, Ege University, Erzene Mahallesi Ankara Caddesi No: 172/62, 35040 Bornova, İzmir, Turkey

<sup>2</sup> MarkaLAB, Kaptanpaşa Mah. Dere Bostanı Sokak No:2/1 34440 Beyoğlu, İstanbul, Turkey

# Study on the Comfort Properties of Knitted Fabrics Produced from Conventional and Sustainable Cotton and Polyester Fibres

*Študija udobnosti pletiv, izdelanih iz konvencionalnega in trajnostnega bombaža in poliestrskih vlaken*

**Original Scientific Article/Izvirni znanstveni članek**

Received/Prispelo 8-2023 • Accepted/Sprejeto 11-2023

Corresponding author/Korespondenčni avtor:

**Prof. Dr. Arzu Marmarali**

E-mail: arzu.marmarali@ege.edu.tr

Tel: +902323111597

ORCID: 0000-0001-6251-0645

## Abstract

Recently, the production of organic fibres and the recycling of textile waste have become essential global issues due to the decrease in non-renewable resources and the increase in disposal costs. The aim of this work was to identify changes in the properties of single jersey knitwear produced from conventional and sustainable fibres after 20 washes. The samples were knitted from different conventional and sustainable yarns. The selected conventional fibres were 100% cotton, 50% cotton-50% polyester and 100% polyester, while the sustainable fibres were 100% better cotton, 100% recycled polyester, and 50% organic cotton-50% recycled polyester. Measurements were taken before and after 20 washes according to the relevant standards. It was found that fabric produced from 100% recycled polyester is suitable for active sportswear due to its high air permeability, and resistance to heat and water vapor. In addition, the fabric with 50% organic cotton-50% recycled polyester fibres was more suitable for cold environmental conditions due to its lowest water vapor resistance, good air permeability and high thermal resistance.

Keywords: organic cotton, recycled polyester, sustainable yarn, thermal comfort, comfort properties, knitted fabrics

## Izvleček

Proizvodnja organskih vlaken in recikliranje tekstilnih odpadkov sta zaradi zmanjšanja neobnovljivih surovinskih virov in povečanja stroškov deponiranja postali bistveni vprašanji po vsem svetu. Namen te raziskave je bil ugotoviti spremembe v lastnostih enojnih jersey pletiv, izdelanih iz konvencionalnih in trajnostnih vlaken. Vzorci so bili spleteni iz različnih konvencionalnih in trajnostnih prej. Izbrana konvencionalna vlakna so bila 100-odstotni bombaž, 50 % bombaž/50 % poliester in 100-odstotni poliester, medtem ko so bila trajnostna vlakna 100-odstotni boljši bombaž (better cotton™), 100-odstotni recikliran poliester in 50 % organski bombaž/50 % recikliran poliester.

Meritve so bile opravljene pred pranjem in po dvajsetih pranjih v skladu z ustreznimi standardi. Ugotovljeno je bilo, da je pletivo iz 100-odstotnega recikliranega poliestra zaradi visoke zračne prepustnosti, toplotnega upora in upora prehodu vodne pare primerno za oblačila za aktiven šport, pletivo iz 50 % organskega bombaža/50 % recikliranih poliestrskih vlaken pa je bilo zaradi najnižjega upora prehodu vodne pare, dobre zračne prepustnosti in visokega toplotnega upora primernejše za hladne okoljske razmere.

Ključne besede: organski bombaž, recikliran poliester, trajnostna preja, toplotno udobje, udobne lastnosti, pletiva

---

## 1 Introduction

Due to population growth, industrialization, rising living standards, and rapidly changing fashion trends, a significant increase in global textile consumption was inevitable. It is estimated that total textile consumption will increase by 3% by 2030 to reach 102 million tonnes [1]. Unfortunately, the use of many hazardous chemicals in garment manufacturing is also increasing [2]. The increasing environmental problems due to the size of the market and the use of chemicals in the production phase, as well as growing awareness, have led to an increasing interest in sustainable production in the textile sector [3, 4].

One of the sustainable alternatives in the textile industry is the use of environmentally friendly fibres, also known as sustainable yarns. They are materials produced from non-toxic, renewable, and biodegradable sources that have a lesser environmental impact than conventional fibres. Organic fibre production and the recycling of textile waste are widely used methods to produce sustainable fibres [5]. Organic cotton produced without chemical fertilizers and pesticides plays an important role in creating a less harmful environment [6]. The Better Cotton Initiative (BCI), which is the subject of this study, is the largest cotton sustainability programme in the world, and teaches farmers crop protection practices, water management and the importance of soil health and biodiversity, and helps them work under these conditions [7]. It is believed that when BCI cotton production increases, the environmental sustainability of the soil improves and fertilizer consumption decreases, which will eventually lead to a reduction in negative environmental impacts.

Similarly, the recycling process helps to reduce global warming and air pollution by saving energy and reducing the labour required to produce a new product [8]. The reuse and recycling of textile products could reduce the negative impact on the environment, as it could reduce the production of new textile fibres [9].

When the ecological footprint of products and materials is studied using tools such as life cycle assessment (LCA), it is found that new polyester has a larger ecological footprint compared to recycled polyester [10, 11]. Thanks to recycling, it is possible to keep waste out of landfills, reduce the need for new raw materials, save energy and water, create new jobs and reduce environmental pollution [12]. On the other hand, several researchers have found that the mechanical properties of yarn deteriorate as the percentage of recycled polyester in the blends of virgin and recycled polyester increases. This is particularly true for fine yarns, as the physical and chemical properties deteriorate due to impurities during the reprocessing of recycled polyester fibres [13, 14].

Fibres alone do not have all the necessary physical, aesthetic and serviceability properties required for ideal clothing for various applications [15]. Therefore, the blending of different fibres is a widely used method to achieve desired properties and improve weak points. The cotton-polyester blend is one of the most common blends in the textile and apparel industry. Typically, cotton-polyester blends have higher durability and better care properties than 100% cotton and less pilling, easier spinning and better uniformity than 100% polyester. The use of recycled polyester in blended yarns has opened new avenues for a sustainable future [16].

Telli [17] studied the properties of knitted fabrics made of cotton, polyester and blended yarns made of recycled polyester, and found that fabrics made of 100% polyester had the highest burst strength and the lowest abrasion resistance, followed by blended fabrics made of recycled polyester and cotton. Kurtoğlu [18] compared single jersey fabrics made from 50-50% recycled cotton-polyester and 50% cotton-50% polyester fibres. The study concluded that there was no significant difference between the quality and appearance of recycled and conventional cotton-containing fabrics. However, Utebay [19] found that the strength of yarns made from recycled cotton fibres was lower.

The fibre type, spinning technology, linear density, twist and hairiness of the yarn, as well as the thickness, cover factor, porosity and finish of the fabric, are certain factors that play an essential role in regulating the comfort properties of fabrics [20]. An ideal fabric must have high thermal resistance for protection from cold weather, low water vapor resistance for efficient heat transfer under soft thermal conditions, and fast fluid transport for heat transfer and the elimination of uncomfortable tactile sensations [21]. Celep [22] found that for single jersey fabrics made from a blend of virgin and recycled cotton fibres, thermal conductivity, heat absorbency and air permeability decreased as the percentage of recycled fibres increased, while the thermal resistance increased. Vadicherla and Saravanan [23] studied single jersey fabrics knitted with recycled polyester and cotton blend yarns. They found that the fabric became thicker, heavier and less porous as the percentage of recycled polyester blend and stitch length decreased. As the linear density increased,

the fabrics exhibited lower air permeability, lower thermal resistance and higher relative water vapor permeability. Kumar and Raja [24] found that the overall moisture management capacity (OMMC) of socks made from recycled polyester yarns was better and that the water transport capacity was greater than other fabrics. According to another study on socks produced from recycled yarns, it was found that as the percentage of recycled polyester in fibre blends increased, the thermal resistance, air permeability and relative water vapor permeability also increased, while the thermal conductivity value decreased [25].

Several researchers have studied the dimensional and mechanical properties of single jersey fabrics made from organic cotton and recycled polyesters. However, there is a lack of systematic and comparative studies focusing on the thermal comfort properties of fabrics knitted with conventional yarns and sustainable yarns, such as better cotton and recycled polyester. The aim of the present study was to investigate changes in the dimensions and thermal comfort properties of single jersey fabrics knitted from some sustainable fibres and compare them with conventional yarns after 20 washings.

## 2 Experimental

### 2.1 Materials

In this study, six different yarns with the same count and twist coefficient were produced from conventional and sustainable fibres using a ring-spinning machine. The fibre types, fibre content in the yarns, fabric codes and yarn properties are given in Table 1.

Table 1: Fibre and yarn properties

Fibre type	Fibre content in the yarn	Fabric code	Yarn count (tex)	Twist coefficient ( $\alpha_t$ )
Conventional fibres	100% cotton	C	20/1	3.8
	50% cotton/50% polyester	C-P		
	100% polyester	P		
Sustainable fibres	100% better cotton	BC		
	50% organic cotton/50% recycled polyester	OC-RP		
	100% recycled polyester	RP		

The single jersey fabrics were produced on a Mayer circular knitting machine (gauge 28, diameter 32”) with constant machine settings. The yarn feeding system was set to 14 cm yarn for 50 needles for all samples. The samples were conditioned for dry relaxation for at least 48 hours in an atmosphere with a temperature of 20 °C ± 2 °C and a relative humidity of 65% ± 5%. To observe the effect of repeated washing on fabric properties, the samples were washed 20 times in a household washing machine according to the TS EN ISO 6330:2012 standard. The washing conditions were 50 minutes at 40 °C with 20 g of commercial detergent for each wash cycle. Concerning the uniform distribution of the load in the machine, the total weight of the load was set at 3 kg, and white cotton woven fabric was used as the filling material. After each wash, the samples were hung to dry lengthwise of the fabric and then conditioned for 24 hours under standard atmospheric conditions [26].

## 2.2 Methods

Measurements were made under standard atmospheric conditions after the fabrics were dry relaxed and repeatedly washed. The codes, symbols, related

standards and instruments used in the experiments are listed in Table 2. The properties of the fabrics were measured after both dry relaxed and washed samples following the relevant standards using pre-determined instruments:

$$P = \left[ 1 - \frac{M/T}{\rho} \right] \times 100 (\%) \quad (1),$$

where  $P$  represents the porosity of the fabric (%),  $M$  represents the mass per unit area of the fabric ( $\text{g}/\text{cm}^2$ ),  $T$  represents the thickness of the fabric (cm), and  $\rho$  represents the fibre density ( $\text{g}/\text{cm}^3$ ). The fibre densities used in equation 1 are as follows:  $C = 1.53 \text{ g}/\text{cm}^3$ ,  $P = 1.38 \text{ g}/\text{cm}^3$ ,  $C-P = 1.45 \text{ g}/\text{cm}^3 = [(0.5 \times \text{fibre density of cotton}) + (0.5 \times \text{fibre density of polyester})]$ . The other important parameter is the fabric density, which is calculated according to equation 2:

$$\rho = \frac{M}{T} \quad (2),$$

where  $\rho$  represents the fabric density ( $\text{g}/\text{m}^3$ ),  $M$  represents the mass of the fabric ( $\text{g}/\text{m}^2$ ), and  $T$  represents the thickness of the fabric (m).

Table 2: Details of test methods

Test	Symbol (unit)	Method	Test device
Courses per unit length	$C_{pc}$ (courses/cm)		counted
Wales per unit length	$W_{pc}$ (wales/cm)		counted
Mass per unit area	$M$ ( $\text{g}/\text{m}^2$ )	TS EN 12127	scale
Thickness	$T$ (mm)	ASTMD 177	TESTEX TF121C
Porosity	$P$ (%)		calculated
Fabric density	$\rho$ ( $\text{g}/\text{m}^3$ )		calculated
Bursting strength	BS ( $\text{kN}/\text{m}^2$ )	ISO 13938-1	James H. Heal tru-burst
Air permeability	AP (mm/s)	TS391 EN ISO 92	MESDAN – Air Tronic
Thermal resistance	$R_{ct}$ ( $\text{m}^2\text{K}/\text{W}$ )	ISO 11092	SDL Atlas M259B
Water vapor resistance	$R_{et}$ ( $\text{m}^2\text{Pa}/\text{W}$ )	ISO 11092	SDL Atlas M259B

The Hohenstein Institute [28] developed a classification system, as shown in Table 3, to determine the rating levels of water vapor resistance. The

results were evaluated using the SPSS software to test the significance of the fibre types for the fabric properties studied.

Table 3:  $R_{et}$  comfort-rating system [28]

Rating	$R_{et}$	Description
Very good	0–6	Extremely breathable and comfortable at a higher rate of activity
Good	7–13	Very breathable and comfortable at a moderate rate of activity
Satisfactory	14–20	Breathable, but uncomfortable at a higher rate of activity
Unsatisfactory	21–30	Slight breathable, moderate comfort at a low rate of activity
Very unsatisfactory	31+	Not breathable and uncomfortable, with a short tolerance time

### 3 Results and discussion

The dimensions and thermal comfort characteristics of the dry relaxed fabrics and the washed fabrics are shown in Tables 4 and 5, respectively. In these tables,

the mean values are indicated by the letters “a”, “b” and “c” (where “a” represents the lowest value and “c” represents the highest value). If the mean values of the different fibre materials do not differ significantly according to statistical analyses, they are marked with the same letter.

Table 4: Dimensional characteristics of the samples after dry relaxation and 20 washes

Fabric code	$C_{pc}$ (course/cm)		$W_{pc}$ (wale/cm)		Mass per unit area (g/m <sup>2</sup> )		Thickness (mm)		Porosity (%)		Fabric density (kg/m <sup>3</sup> )	
	D <sup>1)</sup>	W <sup>2)</sup>	D	W	D	W	D	W	D	W	D	W
C	15	15	18	17	141.3 <sup>a)</sup>	140.7 <sup>a)</sup>	0.67 <sup>a)</sup>	0.66 <sup>a)</sup>	86	86	210.9	210.0
C-P	16	16	19	18	147.7 <sup>b)</sup>	148.3 <sup>b)</sup>	0.75 <sup>b)</sup>	0.74 <sup>b)</sup>	86	86	196.9	200.4
P	16	16	18	17	145.7 <sup>b)</sup>	142.0 <sup>a)</sup>	0.81 <sup>c)</sup>	0.79 <sup>b)</sup>	87	87	186.8	184.4
BC	16	15	18	18	140.3 <sup>a)</sup>	138.7 <sup>a)</sup>	0.68 <sup>a)</sup>	0.67 <sup>a)</sup>	86	86	206.3	207.0
OC-RP	16	16	18	17	146.7 <sup>b)</sup>	141.3 <sup>a)</sup>	0.77 <sup>b)</sup>	0.76 <sup>b)</sup>	87	87	190.5	185.9
RP	16	16	18	17	149.0 <sup>b)</sup>	150.0 <sup>b)</sup>	0.85 <sup>c)</sup>	0.83 <sup>c)</sup>	87	87	175.3	180.7

<sup>1)</sup> dry relaxation, <sup>2)</sup> after 20 washes

<sup>a)</sup> the lowest level of mean values according to statistical analyses

<sup>b)</sup> the second level of mean values according to statistical analyses

<sup>c)</sup> the maximum level of mean values according to statistical analyses

Table 5: Thermal comfort characteristics of the samples after dry relaxation and 20 washes

Fabric code	Bursting strength (kN/m <sup>2</sup> )		Air permeability (mm/s)		Thermal resistance (m <sup>2</sup> K/W)		Water vapor resistance (m <sup>2</sup> Pa/W)	
	D <sup>1)</sup>	W <sup>2)</sup>	D	W	D	W	D	W
C	575.4 <sup>a)</sup>	442.2 <sup>a)</sup>	695.1 <sup>a)</sup>	567.8 <sup>a)</sup>	0.019 <sup>a)</sup>	0.017 <sup>a)</sup>	3.17 <sup>c)</sup>	2.74 <sup>a)</sup>
C-P	602.0 <sup>b)</sup>	574.9 <sup>b)</sup>	667.1 <sup>a)</sup>	764.6 <sup>c)</sup>	0.027 <sup>c)</sup>	0.022 <sup>b)</sup>	3.05 <sup>b)</sup>	2.83 <sup>b)</sup>
P	661.5 <sup>b)</sup>	676.1 <sup>c)</sup>	1635.0 <sup>d)</sup>	1558.8 <sup>f)</sup>	0.027 <sup>c)</sup>	0.031 <sup>c)</sup>	3.06 <sup>b)</sup>	3.47 <sup>c)</sup>
BC	572.1 <sup>a)</sup>	447.7 <sup>a)</sup>	751.6 <sup>b)</sup>	617.4 <sup>b)</sup>	0.025 <sup>b),c)</sup>	0.016 <sup>a)</sup>	3.12 <sup>c)</sup>	2.80 <sup>a)</sup>
OC-RP	629.3 <sup>b)</sup>	599.4 <sup>b)</sup>	717.9 <sup>b)</sup>	897.8 <sup>d)</sup>	0.025 <sup>b),c)</sup>	0.022 <sup>b)</sup>	2.83 <sup>a)</sup>	2.88 <sup>b)</sup>
RP	648.9 <sup>b)</sup>	657.0 <sup>c)</sup>	1254.2 <sup>c)</sup>	1206.4 <sup>e)</sup>	0.032 <sup>d)</sup>	0.033 <sup>c)</sup>	3.19 <sup>c)</sup>	3.48 <sup>c)</sup>

<sup>1)</sup> dry relaxation, <sup>2)</sup> after 20 washes

<sup>a)</sup> the lowest level of mean values according to statistical analyses

<sup>b)</sup> the second level of mean values according to statistical analyses

<sup>c)</sup> the maximum level of mean values according to statistical analyses

<sup>d)</sup> the fourth level of mean values according to the statistical analyses

<sup>e)</sup> the fifth level of mean values according to the statistical analyses

<sup>f)</sup> the maximum level of mean values according to the statistical analyses

### 3.1 Dimensional characteristics

Statistical analysis showed that the fibre material had no significant effect on the values of course/cm, wale/cm and porosity in dry relaxation and after repeated washings. The results show that as the polyester fibre content increases, the thickness of the samples increases linearly, and there is no significant difference between the thicknesses of the fabrics made from conventional and sustainable fibres (Figure 1). In addition, the fabric mass per unit area of the fabrics made from sustainable fibres shows a similar trend to the fabric thickness. 100% cotton (C) and 100% better cotton (BC) fabrics have the lowest mass per unit area values, while the difference in mass per unit area for fabrics containing polyester is usually negligible. However, when examining fabric density,

it was noted that 100% polyester (P) fabrics have minimum values and 100% cotton (C) fabrics have maximum values after dry relaxation and after 20 washes. When investigating the effect of repeated washings on dimensional properties, it was found that there was no significant difference in wale/cm, course/cm, fabric thickness or fabric porosity after 20 washings. In general, the fabric mass values decreased after repeated washing for the different materials. Although it was expected that fabric mass would increase due to shrinkage that may occur in the fabric after washing, the fact that the fabric mass value remained constant and even decreased for some samples after 20 washes suggests that fibre detachment occurs in the fabric.

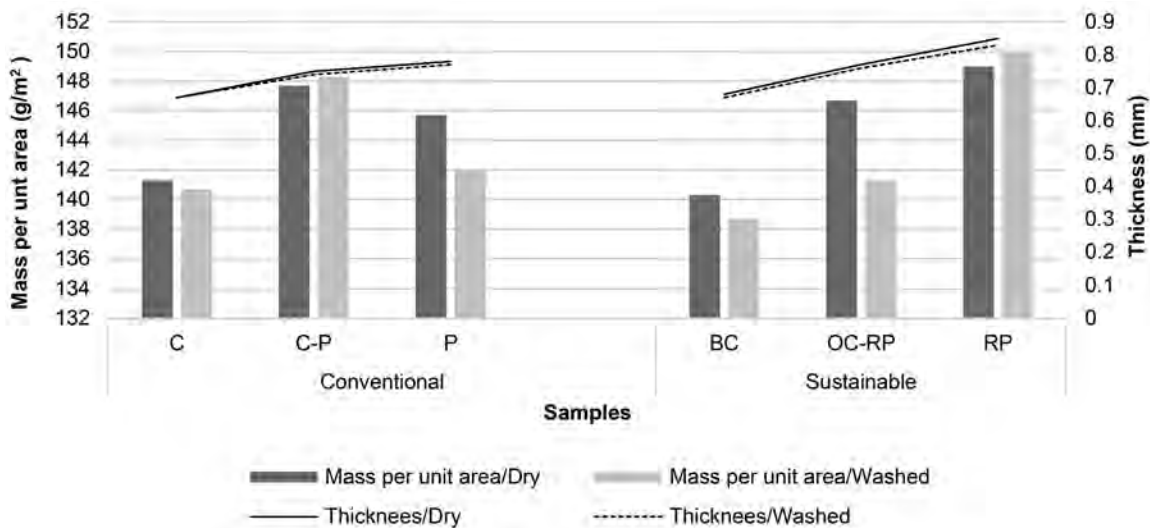


Figure 1: Mass per unit area and fabric thickness values for before and after the washing processes.

### 3.2 Bursting strength

Bursting strength is a measure of the strength and durability of a fabric, and depends largely on the fabric structure, fibre type, blend ratio and yarn properties [29]. This value is important in certain situations where durability and tensile strength are critical.

Statistical analysis showed that the bursting strength values of the samples with polyester fibres were significantly higher for both relaxation states (Figure 2). As mentioned by previous researchers,

this result is related to the high bursting strength value of polyester fibres [30, 31] and the lower mass per unit area and thickness values of these specimens. According to the results, the difference between the bursting strength values of samples containing the same amount of conventional and sustainable fibres was insignificant. On the other hand, 100% polyester (P) and 100% recycled polyester (RP) samples have significantly higher bursting strength than 50% cotton-50% polyester (C-P) samples after the

20 washings. The results show that higher thickness values lead to higher strength values, as mentioned by Herath [32]. However, the bursting strength of

recycled polyester specimens is significantly lower than that of conventional polyester specimens in both relaxation states.

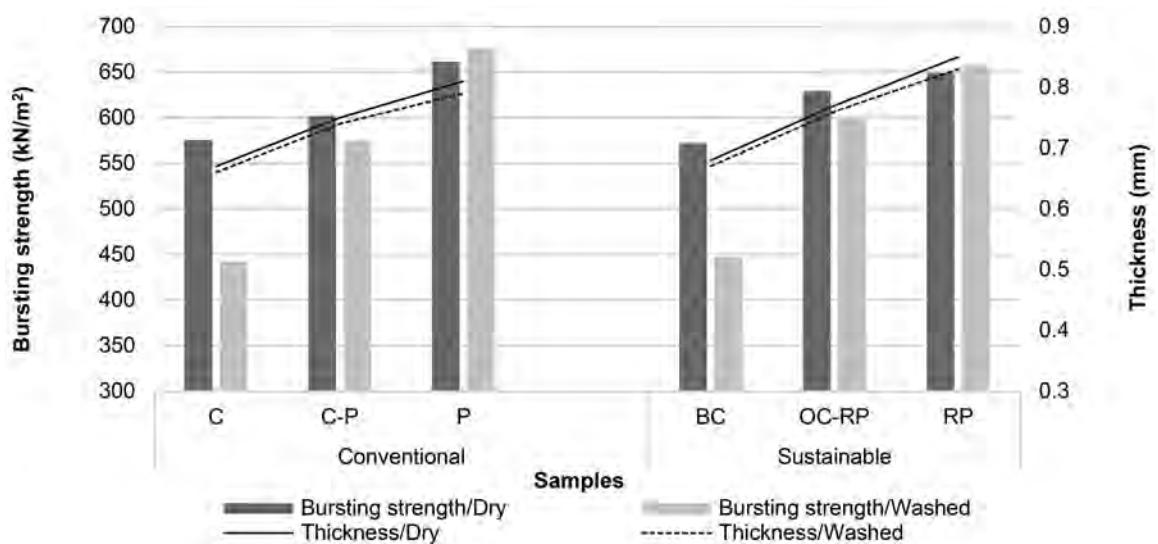


Figure 2: Bursting strength and fabric thickness values for before and after the washing processes

### 3.3 Air permeability

Garments with good air permeability allow air to pass through the fabric, which improves ventilation and moisture transfer. Higher air permeability is generally preferred to allow better air circulation and cooling during high-intensity activities or in hot climates. However, for colder or windy conditions a balance between air permeability and thermal insulation is required.

When investigating the influence of material type on air permeability, it was found that the 100% polyester (P) and recycled polyester (RP) samples had significantly higher values than the 100% cotton (C) samples in both relaxation states due to their low fabric density and high porosity (Figure 3). The difference in air permeability values of the 100% cotton

(C) and 50% cotton-50% polyester (C-P) samples before and after repeated washings is not statistically significant. When comparing the air permeability values of conventional and sustainable fibres, it was found that the 100% better cotton (BC) sample had a higher value than the conventional cotton sample. Similarly, the air permeability value of the 50% organic cotton-50% recycled polyester (OC-RP) sample was higher than that of the 50% cotton-50% polyester (C-P) sample. On the other hand, recycled polyester has lower air permeability than conventional polyester fabric. When the effect of washing was examined, it was observed that the permeability generally decreased after 20 washes, except for the 50% cotton-50% polyester (C-P) and 50% organic cotton-50% recycled polyester (OC-RP) samples.

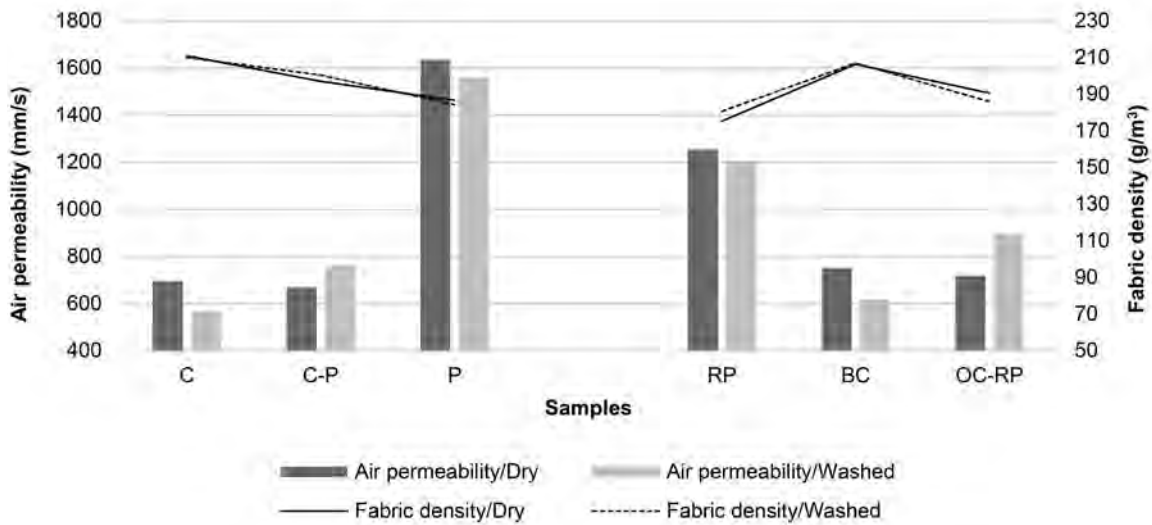


Figure 3: Air permeability and fabric density values for before and after washing processes

### 3.4 Thermal resistance

The thermal resistance of sportswear refers to the ability of the fabric to insulate and warm the wearer in cold environments or outdoor activities. When investigating the influence of fibre type, it was found that fabrics produced from conventional and sustainable 100% polyester fibres had the highest thermal resistance values before and after washing. The samples knitted from 100% cotton (C) and 100% better cotton (BC) for conventional and sustainable fibres, respectively, had the highest thermal resistance values (Figure 4). This result can be explained by fabric density, which is a function of fabric mass and thickness. 100% recycled polyester (RP) fabrics had the lowest fabric density value

before and after the washing process, which can be attributed to the highest thickness values and mass. As found in previous studies [33, 34], fabrics with lower fabric density have higher thermal resistance, which is due to the larger amount of stagnant air in their structure. When comparing conventional and sustainable fibres, it was found that sustainable fibres generally had higher thermal resistance values than conventional fibres. The results indicate that all samples, except the 100% polyester (P) and 100% recycled polyester (RP) samples, showed a decrease in thermal resistance after 20 washes. This is because the fabric density of these samples decreased after repeated washings.

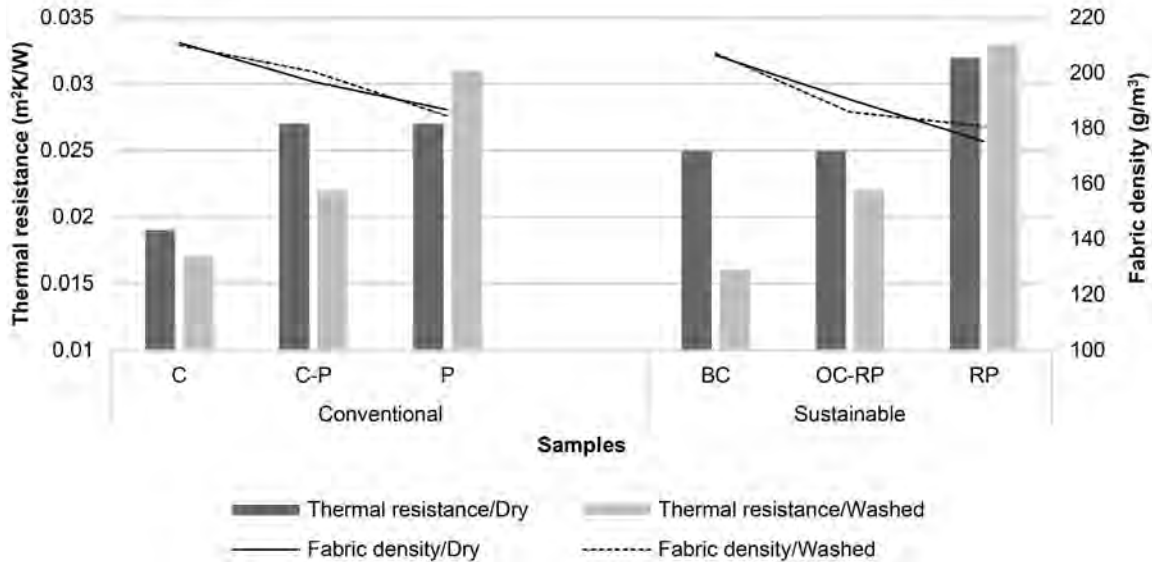


Figure 4: Thermal resistance and fabric density results in dry relaxation and after 20 washings.

### 3.5 Water vapor resistance

The water vapor resistance of a material is a measure of how reluctant it is to let water vapor through. This

value is an important characteristic of sportswear because it affects breathability and the ability to manage moisture during physical activity.

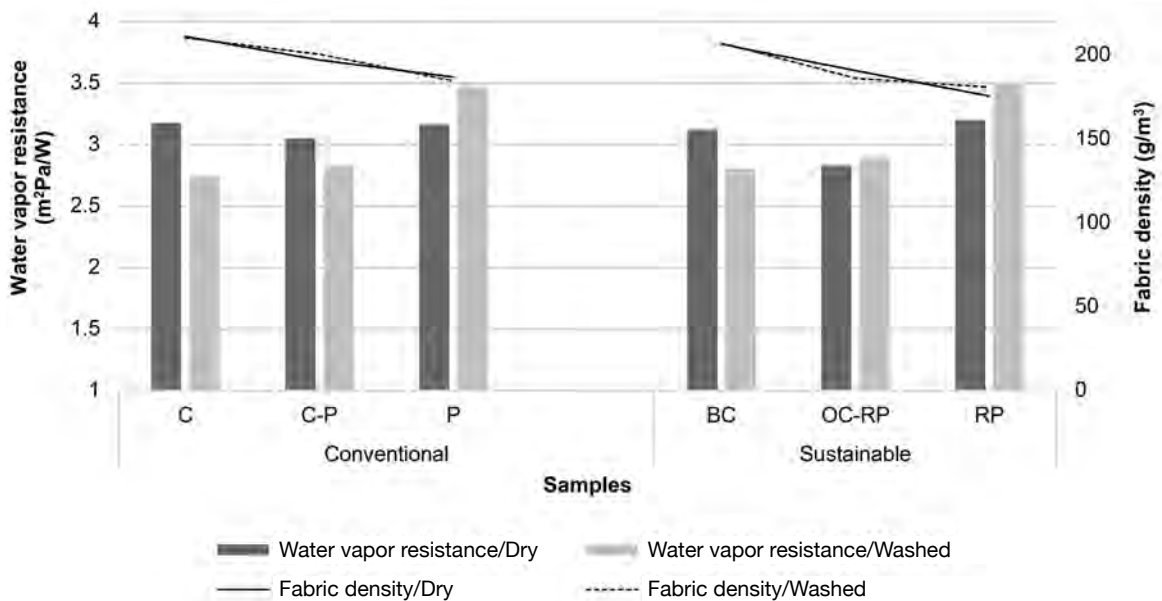


Figure 5: Water vapor resistance and fabric density results in dry relaxation and after 20 washings

The results show that the lowest value for water vapor resistance was found in 50% organic cotton-50% recycled polyester (OC-RP) fabric in dry relaxation situations. However, after 20 washes, the 100% cotton (C) and 100% better cotton (BC) sam-

ples had the lowest value, as can be seen in Figure 5. On the other hand, as the polyester content in the fabric structure increased, the water vapor resistance also increased. This value is crucial for sportswear, especially for high-intensity activities such as running

or cycling. This is because, when the water vapor resistance of a fabric is high, it prevents the water vapor from evaporating and cooling the skin, so that the stored heat cannot be dissipated from the body. In this case, the wearer does not feel comfortable [35]. Hydrophobic polyester fibres, on the other hand, practically do not absorb moisture but can release it into the atmosphere by diffusion, so that the moisture is transported away from the skin surface and the wearer feels comfortable. According to the Hohenstein Institute classification criterion listed in Table 2, it can be concluded that all the fabric samples developed in this study had “very good” water vapor resistance. In comparisons between dry relaxed samples and samples that were subjected to 20 washes, the water vapor resistance increased for the 100% polyester (P) and 100% recycled polyester (RP) samples by increasing number of washes, as mentioned by Reljic [28]. Considering the difference between the water vapor resistance values of conventional yarns and their sustainable versions, it was found that the samples produced from sustainable fibres had similar water vapor resistance values. This result shows that sustainable and recycled fibres can be used instead of conventional fibres.

## 4 Conclusion

In this study, the dimensional and thermal comfort properties of single jersey fabrics produced from different conventional and sustainable fibres were measured, compared and statistically evaluated. In this context, fabric samples were produced using 100% cotton, 100% better cotton, 100% polyester and 100% recycled polyester, 50% cotton-50% polyester and 50% organic cotton-50% recycled polyester yarns. As evident from the results, the fabric mass, thickness and thus bursting strength of the 100% cotton and 100% better cotton samples are significantly lower than the samples containing polyester fibre for both relaxation states. In terms of statistical results, it can be concluded that fabric density and fibre type

generally have a significant influence on the studied properties of single jersey fabrics. It is evident that, as the fabric density increased, the fabric became heavier, resulting in poorer air permeability, thermal resistance and water vapor resistance. No significant difference was found between the properties of conventional fibres (100% cotton, 100% polyester, and 50% cotton-50% polyester) and sustainable fibres (100% better cotton, 100% recycled polyester, and 50% organic cotton-50% recycled polyester) in terms of dimensions and thermal comfort. It can thus be said that sustainable fibres could be used instead of conventional fibres to protect the environment. Moreover, it was found that fabric produced using 100% polyester and 100% recycled polyester had higher air permeability, thermal resistance and water vapor resistance than the other types of fibres. This indicates that the fabric knitted with 100% recycled polyester fibre is suitable for active sportswear applications. On the other hand, the fabric produced using 50% organic cotton-50% recycled polyester fibres with satisfactory air permeability and thermal resistance and the lowest water vapor resistance values was found to be more suitable for cold environmental conditions. The use of sustainable fibres makes textile products more environmentally friendly. It is therefore recommended to increase the use of sustainable fibres in the textile industry.

## References

1. Pulse of the fashion industry [online]. Global Fashion Agenda [accessed 20. 11. 2023]. Available on World Wide Web: <<https://globalfashionagenda.org/impact-initiatives/pulse-of-the-industry>>.
2. PARMAKOĞLU, Emire Ülkü. *Color removal from textile wastewater using activated carbons produced from textile wastes: M.Sc. Thesis*. Izmir : Ege University, 2020, <https://tez.yok.gov.tr/UlusalTezMerkezi/tezSorguSonucYeni.jsp>.

3. ANGUELOV, Nikolay. The changing face of fast fashion. In *The Sustainable Fashion Quest*. London : Taylor & Francis, 2021, 1–22, doi: 10.4324/9781003153344-3.
4. PARAS, Manoj Kumar, CURTEZA, Antonela. Revisiting upcycling phenomena: a concept in clothing industry. *Research Journal of Textile and Apparel*, 2018, **22**(1), 46–58, doi: 10.1108/RJTA-03-2017-0011.
5. ESER, B., ÇELİK, P., ÇAY, A., AKGÜMÜŞ, D. Sustainability and recycling opportunities in the textile and apparel sector. *Tekstil ve Mühendis*, 2016, **23**(101), 43–60, doi: 10.7216/1300759920162310105.
6. RAMASAMY, Karthikeyan M. Comparative study of organic and regular cotton knitted fabrics. *Research Journal of Textile and Apparel*, 2015, **19**(3), 45–51, doi: 10.1108/RJTA-19-03-2015-B006.
7. Introducing better cotton traceability [online]. Better Cotton [accessed 4 June 2023]. Available on World Wide Web: <bettercotton.org>.
8. SHAH, Pragnesh, BANSAL, Abhishek, SINGH, Rajesh Kumar. Life cycle assessment of organic, BCI and conventional cotton: a comparative study of cotton cultivation practices in India. In *Designing Sustainable Technologies, Products, and Policies*. Edited by Benetto E, Gericke K and Gupton M. Cham : Springer, 2018, 67–78.
9. JUANGA-LABAYEN, Jeaner P., LABAYEN, Ildefonso V., YUAN, Qiuyan. A review on textile recycling practices and challenges. *Textiles*, 2022, **2**(1) 174–188, doi: 10.3390/textiles2010010.
10. SAYGILI, Ebru, SAYGILI, Arıkan Tarık, GOREN YARGI, Seher. An analysis of the sustainability disclosures of textile and apparel companies in Turkey. *Tekstil ve Konfeksiyon*, 2019, **29**(3), 189–196, doi: 10.32710/tekstilvekonfeksiyon.471049.
11. RADHAKRISHNAN, Shanti, VETRIVEL, Preethi, VINODKUMAR, Aishwarya, PALANI-SAMY, Hareni. Recycled polyester – tool for savings in the use of virgin raw material. In *Environmental Footprints of Recycled Polyester*. Edited by Subramanian Senthilkannan Muthu. Singapore : Springer, 2019, 49–83, doi: 10.1007/978-981-13-9578-9\_3.
12. 5 reasons to recycle – and how you can recycle right [online]. San Jose Recycles [accessed 20. 11. 2023]. Available on World Wide Web: <[sanjose-recycles.org/5-reasons-to-recycle](http://sanjose-recycles.org/5-reasons-to-recycle)>.
13. UYANIK, Seval. A study on the suitability of which yarn number to use for recycle polyester fibre. *Journal of The Textile Institute*, 2019, **110**(7), 1012–1031, doi: 10.1080/00405000.2018.1550889.
14. KIRIS, Gul, YILMAZ, Demet. The effect of recycled polyester (rPET) filament fibre properties on various woven fabric performance properties. *Tekstile and Apparel*, 2021, **31**(3), 171–182, doi: 10.32710/tekstilvekonfeksiyon.767428.
15. AHMAD, Shehbaz Hafiz, JAMSHAD, Hafsa. Development of thermo-physiologically comfortable knit structure for sports application. *Tekstile and Apparel*, 2019, **29**(2), 105–112, doi: 10.32710/tekstilvekonfeksiyon.570700.
16. VADICHERLA, Thilak, SARAVANAN, Dhandapani. Effect of blend ratio on the quality characteristics of recycled polyester/cotton blended ring spun yarn. *Fibres & Textiles in Eastern Europe*, 2017, **25**(2), 48–52, doi: 10.5604/12303666.1227875.
17. TELLI, Abdurahman, OZDIL, Nilgun, BABAARSLAN, Osman. Usage of PET bottle wastes in textile industry and contribution to sustainability. *Journal of Textiles and Engineer*, 2012, **9**(86), 47–55, doi: 10.7216/130075992012198607.
18. KURTOGLU, Necem Ozlem, SEVENTEKIN, Necdet, PAMUK, Masuk. A study on recycling the fabric scraps in apparel manufacturing industry. *Tekstile and Apparel*, 2013, **23**(3), 286–289.
19. UTEBAY, Burcin, ÇELİK, Pinar, CAY, Ahmet. Effects of cotton textile waste properties on recycled fibre quality. *Journal of Cleaner Production*, 2019, **222**, 29–35, doi: 10.1016/j.jclepro.2019.03.033.
20. MOHAPATRA, Sradhanji, VIDYA, Thangavelu, KUMAR, Vasath, RAJWIN, A. Jebastin, BABU, V. Ramesh, PRAKASH, C., SHAH, B. Anas, ROY,

- Reetuparna. Study of thermal comfort properties of different kinds of polyester knitted fabrics. *Fibres & Textiles in Eastern Europe*, 2021, **29**(5), 50–55, doi: 10.5604/01.3001.0014.9297.
21. MARTI, Meritxell, GISBERT-PAYA, Jaime, BONET-ARACIL, Angeles, JOVANČIĆ, Petar, LIS, Manuel J., CODERCH, Luisa. Increased comfort of polyester fabrics. *Polymers*, 2021, **13**(17), 1–12, doi: 10.3390/polym13173010.
  22. CELEP, Gizem, DOGAN, Gamze, YUKSEK-KAYA, M. Emin, TERCAN, Mevlut. An investigation of thermal comfort properties of single jersey fabrics including recycled fibres. *Düzce Üniv Bilim ve Teknoloji Dergisi*, 2016, **4**, 104–112.
  23. VADICHERLA, Thilak, SARAVANAN, D. Thermal comfort properties of single jersey fabrics made from recycled polyester and cotton blended yarns. *Indian Journal of Fibre & Textile Research*, 2017, **42**(3), 318–324, doi: 10.56042/ijfr.v42i3.10713.
  24. KUMAR, Vasanth D., RAJA, D. Influence of moisture management properties on socks made from recycled polyester. *Fibres & Textiles in Eastern Europe*, 2020, **28**, 4(142), 76–81, doi: 10.5604/01.3001.0014.0939.
  25. KUMAR, Vasanth D., RAJA, D. Study of thermal comfort properties on socks made from recycled polyester/virgin cotton and its blends. *Fibres and Polymers*, 2021, **22**(3), 841–846, doi: 10.1007/s12221-021-0471-6.
  26. SEVGI, Mehmet. *A study on the effects of repeated household washing and drying on dimensional and thermal comfort properties of fabrics knitted from sustainable yarns: M.Sc. Thesis*. Izmir : Ege University, 2022, <https://tez.yok.gov.tr/Ulusal-TezMerkezi/tezSorguSonucYeni.jsp>.
  27. ERTEKIN, Mustafa, ERTEKIN, Gozde, MARMARALI, Arzu. Analysis of thermal comfort properties of fabrics for protective applications. *Journal of The Textile Institute*, 2017, **109**(8), 1091–1098, doi: 10.1080/00405000.2017.1402425.
  28. RELJIĆ, Mirjana, STEPANOVIĆ, Jovan, LAZIĆ, Branislava, ĆIRKOVIĆ, Nenad, CEROVIĆ, Dragana. The change of water vapour resistance of materials used for the clothing production during exploitation. *Advanced Technologies*, 2016, **5**(2), 73–78, doi: 10.5937/savteh1602073R.
  29. SITOTAW, Dereje. An investigation on the dependency of bursting strength of knitted fabrics on knit structures. *Industrial Engineering & Management*, 2017, **6**(3), 2–4, doi: 10.4172/2169-0316.1000221.
  30. DEGIRMENCI, Zuleyha, CORUH, Ebru. Comparison of the performance and physical properties of plain, pique, double-pique and fleeced knitted fabrics. *Textile and Apparel*, 2016, **26**(2), 159–165.
  31. KUNDU, S. Kumar, CHOWDHURY, Usha. Comparison of comfort properties of jersey and interlock knits in polyester, cotton/spandex, and polyester/rayon/spandex. *SSRG International Journal of Polymer and Textile Engineering*, 2020, **7**(1), 6–22, doi: 10.14445/23942592/IJPTE-V7I1P102.
  32. HERATH, Chathura N. Bursting strength of core spun cotton/spandex single jersey and 1×1 rib knitted fabrics. *Fibres and Polymers*, 2021, **22**(4), 1160–1169, doi: 10.1007/s12221-021-9383-8.
  33. BEDEZ ÜTE, Tuba, ÇELİK, Pinar, KADOĞLU, Hüseyin, ÜZÜMCÜ, M. Bünyamin, ERTEKİN, Gözde, MARMARALI, Arzu. An investigation on the use of different natural fibres in undergarments in terms of comfort properties. *Journal of Textiles and Engineer*, 2018, **25**(112), 335–343, doi: 10.7216/1300759920182511207.
  34. HAVENITH, George. Interaction of clothing and thermoregulation. *Exogenous Dermatology*, 2002, **1**(5), 221–230, doi: 10.1159/000068802.
  35. KAKVAN, Ali, NAJAR, S. Saeed, PSIKUTA, Agnes. Study on effect of blend ratio on thermal comfort properties of cotton/nylon-blended fabrics with high-performance Kermel fibre. *Journal of The Textile Institute*, 2015, **106**(6), 674–682, doi: 10.1080/00405000.2014.934045.

# SHORT INSTRUCTIONS FOR AUTHORS OF SCIENTIFIC ARTICLES

## Scientific articles categories:

- **Original scientific article** is the first publication of original research results in such a form that the research can be repeated and conclusions verified. Scientific information must be demonstrated in such a way that the results are obtained with the same accuracy or within the limits of experimental errors as stated by the author, and that the accuracy of analyses the results are based on can be verified. An original scientific article is designed according to the IMRAD scheme (Introduction, Methods, Results and Discussion) for experimental research or in a descriptive way for descriptive scientific fields, where observations are given in a simple chronological order.
- **Review article** presents an overview of most recent works in a specific field with the purpose of summarizing, analysing, evaluating or synthesizing information that has already been published. This type of article brings new syntheses, new ideas and theories, and even new scientific examples. No scheme is prescribed for review article.
- **Short scientific article** is original scientific article where some elements of the IMRAD scheme have been omitted. It is a short report about finished original scientific work or work which is still in progress. Letters to the editor of scientific journals and short scientific notes are included in this category as well.

**Language:** The manuscript of submitted articles should be written in UK English and it is the authors responsibility to ensure the quality of the language.

**Manuscript length:** The manuscript should not exceed 30,000 characters without spacing.

**Article submission:** The texts should be submitted only in their electronic form in the format \*.doc (or \*.docx) and in the format \*.pdf (made in the computer program Adobe Acrobat) to the address: [tekstilec@a.ntf.uni-lj.si](mailto:tekstilec@a.ntf.uni-lj.si). The name of the document should contain the date (year-month-day) and the surname of the corresponding author, e.g. 20140125Novak.docx. The articles proposed for a review need to have their figures and tables included

in the text. The article can also be submitted through a cloud-based file transfer service, e.g. "WeTransfer" ([www.wetransfer.com](http://www.wetransfer.com)).

**Publication requirements:** All submitted articles are professionally, terminologically and editorially reviewed in accordance with the general professional and journalistic standards of the journal Tekstilec. Articles are reviewed by one or more reviewers and are accepted for publication on the basis of a positive review. If reviewers are not unanimous, the editorial board decides on further proceedings. The authors can propose to the editorial board the names of reviewers, whereas the editorial board then accepts or rejects the proposal. The reviewers' comments are sent to authors for them to complete and correct their manuscripts. The author is held fully responsible for the content of their work. Before the author sends their work for publication, they need to settle the issue on the content publication in line with the rules of the business or institution, respectively, they work at. When submitting the article, the authors have to fill in and sign the Copyright Statement ([www.tekstilec.si](http://www.tekstilec.si)), and send a copy to the editors by e-mail. They should keep the original for their own personal reference. The author commits themselves in the Copyright Statement that the manuscript they are submitting for publication in Tekstilec was not sent to any other journal for publication. When the work is going to be published depends on whether the manuscript meets the publication requirements and on the time reference the author is going to return the required changes or corrections to the editors.

**Copyright corrections:** The editors are going to send computer printouts for proofreading and correcting. It is the author's responsibility to proofread the article and send corrections as soon as possible. However, no greater changes or amendments to the text are allowed at this point.

**Colour print:** Colour print is performed only when this is necessary from the viewpoint of information comprehension, and upon agreement with the author and the editorial board.

**More information on:** [www.tekstilec.si](http://www.tekstilec.si)

